

**STUDIES ON THE ADSORPTION OF SURFACTANTS AND POLYMERS
TO SURFACES AND THEIR EFFECTS ON
COLLOIDAL FORCES**

Ayşen Tulpar

Dissertation submitted to the Faculty of Virginia Polytechnic Institute and State University in
partial fulfillment of the requirements for the degree of

Doctor of Philosophy

IN

CHEMISTRY

Professor William A. Ducker, Chairman

Professor Alan Esker

Professor Timothy E. Long

Professor Brian M. Tissue

Professor Thomas C. Ward

September 8, 2004

Blacksburg, Virginia

Keywords: Surface Charge, Self-Assembled Monolayer, Atomic Force Microscopy,
Surface Plasmon Resonance

Copyright 2004, Aysen Tulpar

STUDIES ON THE ADSORPTION OF SURFACTANTS AND POLYMERS TO SURFACES AND THEIR EFFECTS ON COLLOIDAL FORCES

Ayşen Tulpar

ABSTRACT

Surfactants, polymers, and their mixtures are widely used in commercial formulations of paints, water-based adhesives, detergents, food, and other products. This thesis describes measurements of the forces acting on colloidal particles in surfactant and polymer solutions. The change in force on addition of surfactants and polymers is usually caused by adsorption to an interface. In this thesis, I also describe the effect of surface charge density, surface crystallinity, surface heterogeneity, and preadsorbed polymer on surfactant adsorption.

A new method for the stabilization of colloidal particles is introduced via the synthesis and adsorption of unnatural proteins. Unnatural proteins can be synthesized using the natural ‘machinery’ of a bacterial cell with almost any primary sequence, and provide an environmentally friendly route to colloidal stabilization. As a model system, we study the stabilization of alumina, because alumina has a high Hamaker constant and is therefore difficult to stabilize. An unnatural protein with the sequence, thioredoxin-Pro₃₉Glu₁₀ is used. The Glu₁₀ is anionic (pH > 3) and is designed to adsorb to positively charged alumina (pH < 9). The thioredoxin-Pro₃₉ is hydrophilic so it should remain in solution, thereby providing a steric barrier to the approach of two particles in a range of salt and pH conditions. Ellipsometry experiments show that thioredoxin-Pro₃₉Glu₁₀ adsorbs to alumina. Force measurements with the Atomic Force Microscopy (AFM) colloid probe technique show that adsorption of the unnatural protein leads to repulsive forces that decay exponentially with the separation between the surfaces, and are independent of salt concentration. The loss of a salt-dependent force shows that adsorption of the unnatural protein has effectively neutralized the charge on the alumina. Thus, I have shown that an unnatural protein can be used to control the stability of a colloidal system. In general, the same hydrophilic block can probably be added to a variety of anchoring blocks to stabilize different colloidal particles.

Electrostatic forces are frequently responsible for the stabilization of colloidal particles. The decay length of these forces is dictated by the electrolyte concentration. The relationship between the decay length and the concentration is well understood for fully dissociated 1:1 electrolytes. Here, I examine the decay-length in solutions where the ions associate strongly. The forces are measured between silica surfaces in aqueous carboxylic acid and surfactant solutions. The decay lengths of the electrostatic double-layer force in both these solutions are well described by the usual expression for decay length when the concentration of ions is obtained from an activity measurement.

The effect of the surface properties of the solid substrate on surfactant adsorption is also described in this thesis. The adsorption characteristics of a charged surfactant onto fixed charged surfaces as a function of surface charge density is reported. This is the first time that a method has been introduced for making a series of known fixed charged surfaces. Investigating surfactant adsorption to these surfaces has improved our understanding of the role of charge density in surfactant adsorption and desorption. The desired surface charge density is achieved by the use of gold-thiol self-assembled monolayers (SAMs) of different ω -groups ($-\text{OH}$ and $-\text{N}^+(\text{CH}_3)_3$). The mole fraction of $-\text{N}^+(\text{CH}_3)_3$ on the mixed SAM dictates the surface charge density. The charge on $-\text{N}^+(\text{CH}_3)_3$ is fixed and does not self-regulate. The adsorption of sodium dodecyl sulfate (SDS) to the interface between these model surfaces and aqueous solutions of SDS is investigated. Atomic Force Microscopy (AFM) of the adsorbed surfactant reveals no surface micelles above the critical micelle concentration, cmc, over a wide variety of $-\text{N}^+(\text{CH}_3)_3$ densities. This shows that the lateral mobility of ions other than surfactant at the interface is important for the formation of surface micelles of ionic surfactants. Adsorption isotherms of SDS (with no added salt) measured by Surface Plasmon Resonance (SPR) show a plateau region in which the surface excess of SDS is equal to the known fixed surface charge. This demonstrates that the adsorption is electrostatically driven. There is no critical surface charge density at which adsorption rises rapidly. Thus there appears to be no ‘hemimicelle concentration’. My work suggests that the formation of hemimicelles depends on the lateral mobility of the surface ions. Desorption experiments starting above the cmc show rapid desorption of SDS into water until the surface excess is equal to the surface charge density. The rapid desorption is followed by a much slower desorption. The elucidation of this fast-slow desorption pattern based on charge density is made possible by the preparation of a set of constant charge surfaces.

To My Parents
Cahide Tulpar and Prof. Semih S. Tulpar

ACKNOWLEDGEMENTS

I would like to express my sincere gratitude and appreciation to my advisor, Professor William A. Ducker for teaching me how to think critically, how to write scientifically, how to approach problems systematically, and for letting me be, and for supporting me, and for always trusting in me, and for making it fun to work with him. I will always value his scientific insight and friendship. Thank you Professor Ducker!

I would like to thank my committee members for reviewing my dissertation and giving valuable suggestions. I wish to express my gratitude to Professor Thomas Ward, for his support and guidance from my first day in Blacksburg. I would like to thank Professor Alan Esker, for loving the Turkish food so much; Professor Timothy Long, for his encouragement and for sharing his scientific insight with me; Professor Brian Tissue, for his understanding and for his help in the use of his equipments. I also would like to thank Professor Hervé Marand for serving in my committee in my final defense and for his trust in me as a tutor.

I wish to express my thanks to Professor Richey Davis and Professor Allan Shultz for their valuable discussions, to Professor David Kingston, Professor James Tanko, and Professor Neal Castagnoli, Jr., for allowing me to work in their lab for my synthetic work, to Professor Mark Anderson and Professor Felicia Etzkorn for providing access to the equipment of their research group, to Professor Raymond Dessy for his help with SPR and simulation programs, to Professor Richard Gandour for attending my talk in the ACS conference 2003 and for his constant support, to Professor James Wightman for always greeting me in Turkish and for supporting the international events, to Professor Larry Taylor, Professor Harold McNair, Professor James Glanville, Dr. Barbara Bunn and Dr. Jeannine Eddleton for their sincere support of the international students in the Chemistry Department.

I would like to thank the Ducker group for their companionship and stimulating scientific discussions. I especially would like to thank the former postdoctoral members, Dr. Vivek Subramanian and Dr. Jung-Fu Liu, for their help, support and amity during the first stages of my graduate studies. I also wish to thank Dr. Luke Mosley and Dr. Robert Cain for their friendship and help. I am thankful to fellow graduate students Chang Jang and Spencer Clark, Min Mao and Weslyn Ward. I wish to express my sincere thanks to William Lokar, 3rd for being there with me and by me in the same lab for the past five years of my graduate life in Blacksburg. I also wish to

express my sincere thanks to Clayton McKee for his humorous remarks, our interesting scientific and world discussions, and for being my “best buddy”.

I would also like to thank fellow graduate students in the Chemistry Department, who have helped me through the years. Some of them are: Dr. Francisco Cavadas, Dr. John Struss, Dr. Erkan Baloğlu, Dr. Belhu Metaferia, Dr. Bekir Karlığa, Dr. Jianli Wang and the Ward group. I also would like to acknowledge Ayça Özol from the Statistics Department, who has helped me in the analysis of some of my results.

I would also like to acknowledge the financial support of the Department of Chemistry at Virginia Tech in the form of teaching assistantship and in the form of tuition funds, and National Science Foundation in the form of research funds.

I would also like to acknowledge the Chemistry Department staff: Frank Cromer, Bill Bebout, Jan McGinty, Ronna Cadorette, Joey Fagan, Mike Johnson, Melvin Shaver, John Miller, Fred Blair, Scott Allen, Larry Jackson, Vicki Hutchison, Thomas Bell, Agness Chandler, Jane Waugh, Debbie Davis, Vicky Simpkins, Andy Grubb, Steve Whitaker and Sue Connor for her smiling face and the coins.

Throughout the years that I have been to Blacksburg, I have also met some wonderful people, whose love and support I have always felt in my heart. Iris Stadelmann (Dadone) and Paolo Dadone, Erkan and Simge Baloğlu, Bekir Karlığa, Egemen Özbek, Ritu Paul, Sheila Gradwell, Alice Harper, Kim Mitchell, Ella Chow, Charles Tchatchoua, Nazan and İrfan Gündüz, Özdemir Özarslan, Gülaçtı Topçu, and all of the staff at Cranwell International Center. I am thankful to my roommates Didem Durmaz, Ayça Özol, Ekin Atilla, Pınar Ömür, and Tuğba Tunalı for being great friends and sharing their life with me. I would also like to express my sincere thanks to Serkan Ünal and Ufuk Karabıyık for their understanding and for making me feel welcome in their home during the final stages of my dissertation. I also wish to acknowledge the staff at PK’s and at Mill Mountain Café for providing a comfortable atmosphere. Thank you all...

I would also wish to thank William Ducker, Suzanne Ducker, Thomas Ducker, Matthew Ducker, Franz van Damme, Elian van Damme, Donald McKeon, Evelyn McKeon, Kay Castagnoli and Neal Castagnoli, who have opened their homes and hearts to me. They have been a second family to me and I wish to keep my bonds tight with them forever. I love you very much!

I feel indebted to my professors in Turkey without whom I would not have come this far. I wish to express my sincere gratitude to Melahat Özey for teaching me English and for being there for me since 1987, Hülya Kordel for teaching me Chemistry, and Nursel Denizöz for teaching me Physics at Kadıköy Anatolian High School.

I wish to express my sincere appreciation and gratitude to my professors at Koç University; Professor İskender Yılgör and Mrs. Emel Yılgör who have always been there for me like my parents and who have encouraged me to come to Virginia Tech, Professor Ersin Yurtsever who has put the seeds of love of Physical Chemistry in me, and Professor Attila Aşkar who has shown me the beauty of Mathematics as a language. I also wish to express my gratitude to Professor Atilla Güngör at Marmara University for his constant support.

I cannot thank enough my family members in Turkey, who have supported me in this long journey. I wish to thank my aunts, my uncles and my cousins who have been supportive of me and my parents: Gülsen, Işık, Ali, Uğur, Acar, Fatih and Çağatay Uluç, Leylifer, Haluk, Tolga and Semih Aşkın, Mesut, Belgin and Müge Avşar, Jale and Şule Öge, İlhan and Nimet Özkök, Melahat and Deniz Akagül, Özge and Ayhan Saraç, Ural Feyzoğlu, Oya and Necip Süerkan, Gülsen Koçer and Sevin Engin. You all have a special place in my heart. I am forever grateful to my uncle Işık Uluç for teaching me in two days how to read, Ali Uluç for discussing science with me since I was a little girl and Deniz Akagül for being a role model for me as an academician.

I also wish to express my sincere appreciation to İnci Işın, who has supported me and made me feel at home during her stays in Blacksburg and Nashville. I would like to thank her for her understanding, for her young heart and for her calmness.

I am the person I am today because of my parents, Semih Servet Tulpar and Cahide Tulpar. Their joy of living, their love of nature, people, music, art and science, their dedication to their work, their honesty, their wisdom and their life experience has shaped my life. I have learned a lot from them until now and I am still learning...I am very much grateful to them for letting their only daughter go to a country far away to follow her dreams. You are always on my mind and in my heart!

There is also another person, who has shaped my life since I came to Blacksburg: Emre Işın, who has been with me since day one. He has been my friend, my family, my brother, my teacher, my inspiration, my strength, my weakness and my love. I could not do it without him.

For all the days we have spent together and we will spend together and, for all the journeys we have taken together and we will take together, I thank him with all my heart.

TABLE OF CONTENTS

| | |
|---|-----------|
| CHAPTER 1: INTRODUCTION..... | 1 |
| 1.1. Introduction..... | 1 |
| 1.2. Adsorption | 2 |
| 1.3. Surfactant Adsorption to Solid–Aqueous Interfaces | 3 |
| 1.3.1. Adsorption Isotherms | 4 |
| 1.3.2. Mechanism of Adsorption and Implied Orientation of Adsorbed Surfactants | 10 |
| 1.3.2.1. Adsorption of Ionic Surfactants | 11 |
| 1.3.2.2. Adsorption of Non-ionic Surfactants | 13 |
| 1.3.3. Molecular Organization (Self-Assembly) of Surfactants on the Surface | 13 |
| 1.4. Polymer Adsorption on Solid Surfaces | 16 |
| 1.4.1. Homopolymers | 16 |
| 1.4.2. Diblock Copolymers..... | 18 |
| 1.4.2.1. Theoretical Calculations | 20 |
| 1.4.2.2. Experimental Measurements..... | 26 |
| 1.4.2.3. Charged Block Copolymers..... | 30 |
| 1.4.3. Proteins | 32 |
| 1.5. Polymer-Surfactant Interactions..... | 35 |
| 1.5.1. Polymer-Surfactant Solutions..... | 36 |
| 1.5.1.1 Binding Isotherms..... | 36 |
| 1.5.1.2. Change in Surfactant Solution Properties | 38 |
| 1.5.2. Microstructure of the Polymer-Surfactant Complexes | 40 |
| 1.5.3. Polymer-Surfactant Mixtures on Solid Surfaces | 42 |
| 1.6. Forces between Particles and Surfaces | 45 |
| 1.6.1. Van der Waals Forces..... | 47 |
| 1.6.2. Electrostatic Double Layer Forces | 49 |
| 1.6.3. DLVO Theory..... | 51 |
| 1.6.4. Steric-Polymer Forces | 53 |
| 1.6.4.1. Forces between Polymer Brushes | 55 |
| 1.6.4.1a. Measurements with Surface Forces Apparatus | 55 |

| | |
|---|----|
| 1.6.4.1b. Measurements with Atomic Force Microscopy | 56 |
|---|----|

| | |
|---|-----------|
| CHAPTER 2: DECAY LENGTHS OF DOUBLE-LAYER FORCES IN SOLUTIONS OF PARTLY-ASSOCIATED IONS | 58 |
| 2.1. Introduction..... | 58 |
| 2.2. Experimental Section..... | 61 |
| 2.2.1. Materials | 61 |
| 2.2.2. Surface Tension Measurements..... | 62 |
| 2.2.3. Force–Distance Measurements..... | 62 |
| 2.2.4. pH Measurements | 63 |
| 2.3. Analysis of Raw Data..... | 63 |
| 2.3.1. Force–Separation..... | 63 |
| 2.4. Results | 64 |
| 2.5. Discussion..... | 68 |
| 2.6. Conclusion | 69 |

| | |
|--|-----------|
| CHAPTER 3: SURFACTANT ADSORPTION AT SOLID-AQUEOUS INTERFACES CONTAINING FIXED CHARGES | 70 |
| 3.1. Introduction..... | 70 |
| 3.2. Experimental Section..... | 75 |
| 3.2.1. Materials | 75 |
| 3.2.2. Atomic Force Microscopy (AFM)..... | 76 |
| 3.2.3. Surface Plasmon Resonance (SPR)..... | 77 |
| 3.2.4. X-ray Photoelectron Spectroscopy (XPS) | 77 |
| 3.2.5. Cyclic Voltammetry | 78 |
| 3.2.6. Contact Angles | 78 |
| 3.3. Analysis of Raw Data..... | 79 |
| 3.3.1. Analysis of XPS Data | 79 |
| 3.3.2. Calculation of Adsorbed Amount from SPR Experiments..... | 79 |
| 3.4. Results and Analysis | 81 |
| 3.4.1. Determination of Covalently-Bound Surface Charge Density | 81 |

| | |
|---|------------|
| 3.4.2. Adsorption Isotherms of SDS..... | 84 |
| 3.4.3. Structure of Adsorbed SDS Aggregates | 91 |
| 3.5. Discussion..... | 93 |
| 3.5.1. Mechanism of SDS Adsorption on Fixed-Charge Surfaces | 93 |
| 3.5.2. Morphology of Surfactants on Fixed-Charge Surfaces | 94 |
| 3.6. Conclusions..... | 98 |
| | |
| CHAPTER 4: UNNATURAL PROTEINS FOR THE CONTROL OF SURFACE FORCES | 100 |
| 4.1. Introduction..... | 100 |
| 4.2. Experimental Section..... | 109 |
| 4.2.1. Biosynthesis..... | 109 |
| 4.2.2. Materials for Adsorption Experiments..... | 109 |
| 4.2.3. Solutions..... | 109 |
| 4.2.4. Ellipsometry..... | 110 |
| 4.2.5. Atomic Force Microscopy (AFM)..... | 110 |
| 4.3. Analysis of Raw Data..... | 111 |
| 4.3.1. Calculation of Adsorbed Amount from Ellipsometry..... | 111 |
| 4.3.2. Force Analysis..... | 112 |
| 4.4. Results and Discussion..... | 112 |
| 4.4.1. Characterization of the Alumina Surfaces..... | 112 |
| 4.4.2. Adsorption and Forces in the Presence of Trx-Pro ₃₉ Glu ₁₀ | 114 |
| 4.5. Conclusions..... | 118 |
| | |
| CHAPTER 5: POLYMER-SURFACTANT INTERACTIONS AT THE SILICA-WATER INTERFACE..... | 120 |
| 5.1. Introduction..... | 120 |
| 5.2. Experimental Section..... | 121 |
| 5.2.1. Materials and Solutions | 121 |
| 5.2.2. AFM Measurements | 121 |
| 5.3. Analysis of Raw Data..... | 122 |

| | |
|--|----------------|
| 5.4. Results and Discussion..... | 122 |
| 5.4.1. AFM Images | 122 |
| 5.4.2. Force Measurements..... | 122 |
| 5.5. Conclusions..... | 126 |
| | |
| CHAPTER 6: SURFACTANT ADSORPTION ON HYDROPHOBIC SURFACES: EFFECT OF SURFACE CRYSTALLINITY | 127 |
| 6.1. Introduction..... | 127 |
| 6.2. Experimental Section..... | 129 |
| 6.2.1. Materials and Solutions | 129 |
| 6.2.2. AFM Measurements | 129 |
| 6.3. Results and Discussion..... | 129 |
| 6.4. Conclusions..... | 132 |
| | |
| CHAPTER 7: SURFACE CONFINEMENT EFFECTS ON SURFACTANT ADSORPTION..... | 133 |
| 7.1. Introduction..... | 133 |
| 7.2. Experimental Section..... | 134 |
| 7.2.1. Materials and Solutions | 134 |
| 7.2.2. AFM Measurements | 134 |
| 7.3. Results and Discussion..... | 135 |
| 7.3.1. C ₁₄ TAB Adsorption on COOH–SAM and OH–SAM..... | 135 |
| 7.3.2. Lithography and C ₁₄ TAB Adsorption on the Heterogeneous SAM..... | 136 |
| 7.4. Conclusions..... | 138 |
| VITA..... | 139 |

LIST OF FIGURES

| | | |
|--------------|--|----|
| Figure 1.1. | Comparison of adsorption isotherms: Langmuir vs. Surfactant..... | 6 |
| Figure 1.2a. | The adsorption isotherm of SDS on alumina..... | 7 |
| Figure 1.2b. | The zeta potential of alumina particles in SDS solutions..... | 8 |
| Figure 1.3. | Conformation of a physisorbed homopolymer on a surface | 17 |
| Figure 1.4. | The stages of adsorption of diblock copolymers onto a surface | 20 |
| Figure 1.5. | Polymer segment density profiles for the tail block..... | 23 |
| Figure 1.6. | The binding isotherm of SDS onto PEO | 37 |
| Figure 1.7. | Surface tension of PVP/SDS solutions..... | 39 |
| Figure 1.8. | Effect of SDS on PEO adsorption | 44 |
| Figure 1.9. | Surface charge and diffuse part of the double-layer..... | 49 |
| Figure 1.10. | DLVO theory..... | 52 |
| Figure 2.1. | Forces between a glass sphere and a silica sheet in acetic acid solutions | 64 |
| Figure 2.2. | Forces between a glass sphere and a silica sheet in SDS solutions..... | 65 |
| Figure 2.3. | Decay lengths in SDS and C ₁₂ TABr solutions..... | 66 |
| Figure 2.4. | Ratio of Experimental:Calculated values of decay lengths for SDS..... | 67 |
| Figure 2.5. | Ratio of Experimental:Calculated values of decay lengths for C ₁₂ TABr..... | 67 |
| Figure 3.1. | Model for surface charge density and surfactant adsorption..... | 73 |
| Figure 3.2. | SPR data for SDS solutions..... | 80 |
| Figure 3.3. | Cyclic voltammogram for S(CH ₂) ₁₁ OH | 82 |
| Figure 3.4. | Control of surface charge density..... | 84 |
| Figure 3.5. | SAM density vs. surface charge density..... | 84 |
| Figure 3.6. | Adsorption of SDS to a series of SAMs of fixed surface charge | 85 |
| Figure 3.7. | Adsorbed density of SDS vs. surface charge density..... | 86 |
| Figure 3.8. | Adsorption isotherms of SDS adjusted for ω-OH groups | 87 |
| Figure 3.9. | Comparison of SDS adsorption in the first and second plateaus regions..... | 88 |
| Figure 3.10. | Desorption isotherms of SDS..... | 89 |
| Figure 3.11. | The surface excess of SDS remaining vs. surface charge density..... | 90 |

| | |
|--|-----|
| Figure 3.12a. AFM image of SAM–16mM SDS solution interface | 92 |
| Figure 3.12b. AFM image of SAM–16mM SDS solution interface in 0.1M NaCl..... | 92 |
| Figure 3.13. Effect of surface charge distribution on surfactant adsorption..... | 97 |
| Figure 4.1. The generic unnatural protein design. | 104 |
| Figure 4.2a. Target unnatural protein structure. | 108 |
| Figure 4.2b. Target adsorbed layer structure. | 108 |
| Figure 4.3. Forces between alumina surfaces as a function of pH | 113 |
| Figure 4.4a. Forces between Trx-Pro ₃₉ Glu ₁₀ covered alumina surfaces in KNO ₃ | 116 |
| Figure 4.4b. Semi-log plot of forces between Trx-Pro ₃₉ Glu ₁₀ covered alumina surfaces . | 116 |
| Figure 4.5. Forces between Trx covered alumina surfaces in KNO ₃ | 117 |
| Figure 5.1a. Forces between silica surfaces in water and in PEO solutions..... | 123 |
| Figure 5.1b. Forces between silica surfaces in water and in PEO solutions at pH~2..... | 123 |
| Figure 5.2. Effect of SDS on forces between silica surfaces in PEO solution | 124 |
| Figure 5.3. Force between silica surfaces in PEO and 40 mM SDS solutions | 125 |
| Figure 6.1. Forces between a silicon tip and a C ₈ SAM surface in CTAB solutions..... | 130 |
| Figure 6.2. Comparison of forces in SDS, C ₁₆ TAB and C ₁₂ E8 solutions at the cmc. | 131 |
| Figure 7.1. Is organization of surfactants a function of patch dimension? | 134 |
| Figure 7.2a. AFM image of the COOH–SAM–14 mM C ₁₄ TAB solution interface..... | 136 |
| Figure 7.2b. AFM image of the COOH–SAM–14 mM C ₁₄ TAB solution interface..... | 136 |
| Figure 7.3. AFM image of the patterned surface in ethanol. | 137 |

LIST OF TABLES

| | |
|---|-----|
| Table 2.1. Decay lengths in acetic acid solutions | 65 |
| Table 2.2. Decay lengths in formic acid solutions..... | 65 |
| Table 3.1. Normalized XPS photopeak area ratios for SAM surfaces..... | 83 |
| Table 3.2. Contact angles of aqueous SDS solutions on SAM surfaces..... | 88 |
| Table 3.3. Tip-SAM separation for the jump-in in AFM force measurements..... | 93 |
| Table 4.1. Decay lengths of measured forces between Trx-coated alumina surfaces | 118 |
| Table 5.1. Decay lengths in PEO solutions as a function of SDS concentration..... | 125 |

CHAPTER 1: INTRODUCTION

1.1. Introduction

Surfactants, polymers, and their mixtures are widely used in commercial formulations of paints, water-based adhesives, detergents, food, and other products. In all these processes, the primary effect of the surfactants and polymers is achieved by adsorption to an interface, which modifies the surface properties, including the forces between surfaces. Both the *surface forces* and the *surface modification* depend on the amount adsorbed on the surface and how these molecules “self-assemble” at the solid-liquid interface.

Most of my studies focus on the surface modification through the adsorption of surfactants and polymer-surfactant mixtures at the solid-liquid interface. The nature of the substrate, the type of the solvent and temperature affect the adsorption characteristics of these molecules. I set aside the effects of the solvent and the temperature; the solvent used is always water and the temperature is always 22 ± 2 °C. I investigate the influence of the surface properties of the substrate on surfactant adsorption (Chapters 3, 6 and 7). In Chapter 3, studies on the adsorption of a charged surfactant onto surfaces with *fixed* surface charge densities as a function of surface charge density are described. In Chapter 5, I report on my results on the effect of a preadsorbed polymer on the adsorption of a surfactant. In Chapter 6, I describe my work on the investigation of the surface morphology of a wide range of surfactants onto hydrophobic surfaces as a function of surfactant concentration. In Chapter 7, studies on the adsorption of a surfactant on a heterogeneous surface are reported.

The second focus of my work is on the surface forces. The surface forces are important in the control of the stability of colloidal suspensions. A colloidal suspension is stable when the force between the colloidal particles is repulsive. This repulsive force is present naturally for charged particles (electrostatic double-layer force), however for some particles addition of polymers is necessary to induce a repulsive force (steric force). In Chapter 2, I summarize my results on measurements of decay lengths of electrostatic double-layer forces in the presence of surfactants and other partially associated ions. In

Chapter 4, I report on my studies on the repulsive steric forces caused by the adsorption of unnatural proteins, a new method for colloidal stabilization.

The common theme in my thesis is the adsorption of molecules on surfaces. Therefore in the next section, I give an overall introduction of adsorption in general. In later sections, the adsorption of surfactants, polymers, their mixtures and surface forces are reviewed.

1.2. Adsorption

The term adsorption is first introduced by Kayser in 1881 to describe his observations of the condensation of gases on free surfaces, a phenomenon discovered independently both by Scheele and Fontana¹ some years earlier.² Adsorption is said to occur if the concentration of the molecules in the fluid-adsorbent boundary is higher than that in the bulk. Adsorption may occur at any interface, liquid-gas, liquid-liquid, solid-gas, solid-liquid. My focus is on the adsorption of molecules (surfactants, polymers and proteins) at the solid-aqueous interface, where the adsorption of one molecule is always accompanied by desorption of one (or more) other molecule.

Adsorption of molecules can only occur if the Gibbs energy, G , of the system decreases:

$$\Delta_{ads}G = \Delta_{ads}H - T \Delta_{ads}S < 0 \quad (1.1)$$

where H , S , and T are the enthalpy, entropy and absolute temperature respectively, and Δ_{ads} is the change in G , H , and S resulting from the adsorption process. If the absolute value of $\Delta_{ads}G$ is large, “high-affinity” adsorption isotherms are observed.

Adsorption of molecules at the solid-liquid interface can be reversible or irreversible. For reversible adsorption to occur, the adsorption and desorption isotherms should coincide. Therefore, when the chemical potential is reduced by dilution of the molecules in bulk, there should be spontaneous desorption to reach to the new equilibrium state. In an irreversible adsorption process, although there is a driving force

¹ Fontana, F. *Memorie Mat. Fis. Soc. Ital. Sci.* **1777**, *1*, 679.

² McBain, J.W. *The Sorption of Gases and Vapors by Solids*, Routledge:London, 1932; Tien, C. *Adsorption Calculations and Modeling*; Butterworth-Heinemann: Newton, 1994.

for desorption upon dilution, the system reaches a metastable state (where there is a high energy barrier for further desorption) and there is no or little desorption.³

Adsorption is driven by the following interactions at the solid–aqueous interface.

1. *Ionic Interactions*: Coulomb attraction or repulsion between charges.
2. *Lifshitz van der Waals (vdW)*: Dispersion, orientation, induction forces.
3. *Hydrophobic interactions*: Entropically driven interaction due to the effect of the water structure near hydrophobic interfaces.
4. *Hydrogen bonding*: A strong dipole-dipole interaction.

Water is used as the solvent for all adsorption studies in my work. Liquid water is characterized by a high dielectric constant that screens the coulombic forces, and by a high boiling point indicating the strength of intermolecular forces. One single water molecule, on average, forms 3.5 H-bonds with other water molecules.⁴ It is the presence of H-bonds that give water a relatively open and ordered structure. This structure can be disrupted by the presence of foreign molecules. In the case of apolar molecules⁵ and small, highly charged ions there is excess ordering and in the case of large monovalent ions⁶ there is disordering of the water molecules. These unique properties suggest that water and local changes in water structure (which affect local dielectric properties) play an important role in adsorption.

1.3. Surfactant Adsorption to Solid–Aqueous Interfaces

The dual nature (polar head and non-polar tail) of surfactants is responsible for the adsorption of these molecules at interfaces, and for the formation of micelles in their bulk solutions. The driving force for a surfactant to adsorb at an interface is to lower the free energy of the whole system. In this review, the main focus will be on surfactant adsorption behavior at the solid-liquid interface.

Solution properties of the surfactant and properties of the solid-liquid interface

³ Haynes, C. A.; Norde, W. *Colloids Surf., B* **1994**, 2, 517–566.

⁴ Israelachvili, J. *Intermolecular and Surface Forces*; Academic Press: San Diego, 1992; p.127.

⁵ Tanford, C. *The Hydrophobic Effect: Formation of Micelles and Biological Membranes*; John Wiley & Sons: New York, 1980.

⁶ Burgess, J. *Ions in Solution*; Halsted Press: New York, 1988.

govern the adsorption of surfactants at the solid-liquid interface.⁷ Three factors that control the adsorption of surfactants are:⁸

- 1) The chemistry of the hydrophilic section (head group), and the hydrophobic section (tail group). The length of the tail is usually 8–12 carbons.
- 2) The nature of the solid surface.
- 3) The nature of the liquid.

Adsorption of the surfactants onto solid surfaces causes a surface modification of the solid surface. For example, a positively charged surface can be made negatively charged or a hydrophobic surface can be made hydrophilic by the adsorption of surfactants. These modifications depend on the amount of adsorbed surfactant, the orientation and the organization of surfactant molecules on the surface. The rest of this section reviews research on the determination of the adsorbed amount, mechanism and molecular organization of surfactants at the solid–liquid interface.

1.3.1. Adsorption Isotherms

The most fundamental measurement is the determination of the adsorbed amount of the surfactant as a function of concentration at a fixed temperature, i.e. adsorption isotherm. An adsorption isotherm relates the surface excess of adsorbate to its equilibrium concentration in the liquid phase.⁹ The surface excess of a component is defined as the excess amount of this component in the system over a hypothetical standard (the amount that would occur if the bulk phase continued up to the interface), free of adsorption. Surface excess amounts are usually normalized by the surface area of the substrate (number of moles of adsorbate per unit area of solid) to create an intensive property. The most common method of determining the adsorbed amount is by depletion of that component when a solid is added to the solution.

For surfactant solutions, the number of moles of surfactant adsorbed per unit area of solid, Γ , is

⁷ Ananthapadmanabhan, K.P. In *Interactions of Surfactants with Polymers and Proteins*, Goddard, E. D., Ananthapadmanabhan, K. P., Eds.; CRC: Boca Raton, 1993; p. 5.

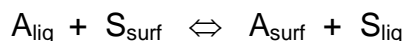
⁸ Myers, D. *Surfactant Science and Technology*; VCH: New York, 1992, p. 275.

⁹ Clunie, J. S; Ingman, B. T. In *Adsorption from Solution at the Solid/Liquid Interface*, Parfitt, G.D.; Rochester, C.H., Eds.; Academic Press: New York, 1983; p. 105.

$$\Gamma = \frac{(C_0 - C)V}{ma_{sp}} \quad (1.2)$$

where C_0 is the concentration of solution before adsorption and C is the equilibrium concentration of solution after adsorption, m is the mass of insoluble adsorbent, V is the solution volume and a_{sp} is the particle specific surface area.¹⁰ C_0 can be controlled by the initial concentration of surfactant solution, m and V can be easily measured and a_{sp} can be determined experimentally. The most difficult quantity to obtain is C . C has been determined by surface tension measurements, titration techniques and direct spectroscopic studies^{11,12} of the adsorbed species after the solid substrates are centrifuged.

The experimentally determined adsorption isotherms are compared with theoretical isotherms to obtain information about the mechanism of adsorption and orientation of the surfactant molecules. The simplest theoretical isotherm is the Langmuir adsorption isotherm, which is based on the following equilibrium,



where A represents the adsorbate, S represents the solvent. The subscripts show the liquid and surface phases. K is the dimensionless equilibrium constant for the process.

The Langmuir equation is:

$$\Gamma_A = \Gamma_{\text{max}} \left(\frac{C_A K}{1 + C_A K} \right) \quad (1.3)$$

where Γ_A is the amount of solute adsorbed per unit area at concentration C (C_A is the concentration C normalized by C^θ , C/C^θ , to keep the dimensions correct), Γ_{max} is the maximum adsorbed amount per unit area.

The derivation of the Langmuir adsorption isotherm assumes that there is a monolayer of adsorbate, and that ΔG_{ads} of a molecule at each site is independent of the

¹⁰ Chatteraj, D. K.; Mahapatra, P.; Biswas, S. In *Surfactants in Solution*, Chattopadhyay, A. K.; Mittal, K. L., Eds.; Marcel Dekker: New York, 1996; p. 83.

¹¹ Wangerud, P; Olofsson, G. *J. Colloid Interface Sci.* **1992**, *153*, 392–398.

¹² Lijour, Y.; Calves, J.; Saumagan, P. *J. Chem. Soc., Faraday Trans. 1* **1987**, *83*, 3283–3293.

occupancy of each of the neighboring sites. Therefore it is assumed that there are no intermolecular forces among the molecules at neighboring sites. A classic Langmuir adsorption isotherm is shown in Figure 1.1 with the red curve. However, the adsorption isotherm for an ionic surfactant onto an oppositely charged substrate is typically S-shaped (the blue curve in Figure 1.1), not Langmuirian. This means that there is a large increase of the surface excess at a certain concentration due to the aggregation of surfactant molecules on the surface.

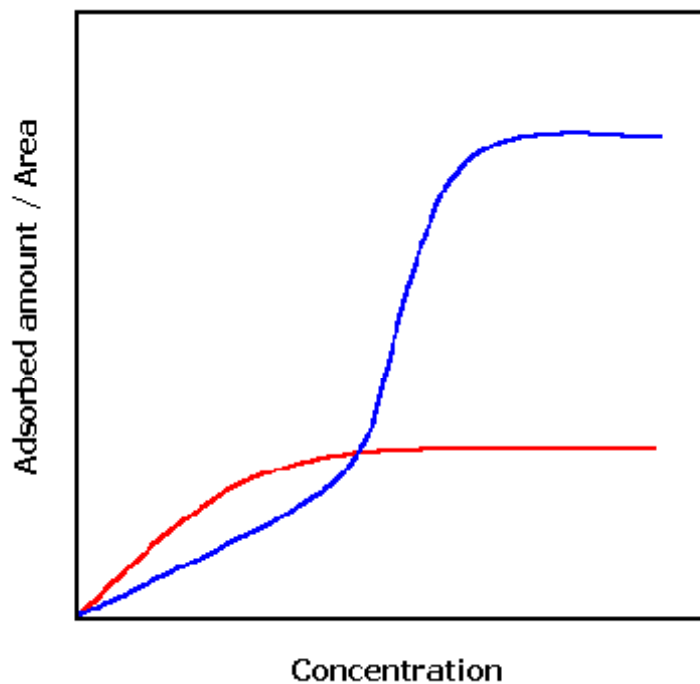


Figure 1.1 The red curve is a Langmuir adsorption isotherm and the blue curve is a typical adsorption isotherm for an ionic surfactant onto an oppositely charged surface.

Adsorption of sodium dodecyl sulfate (SDS) on alumina at neutral pH provides a good model system to analyze. Alumina at this pH is positively charged. Chandar et al. have used 2-phase titration technique to determine the adsorption isotherm of this system.¹³ The typical adsorption isotherm is shown below:

¹³ Chandar, P; Somasundaran, P; Turro, N. J. *J. Colloid Interface Sci.* **1987**, *117*, 31–46.

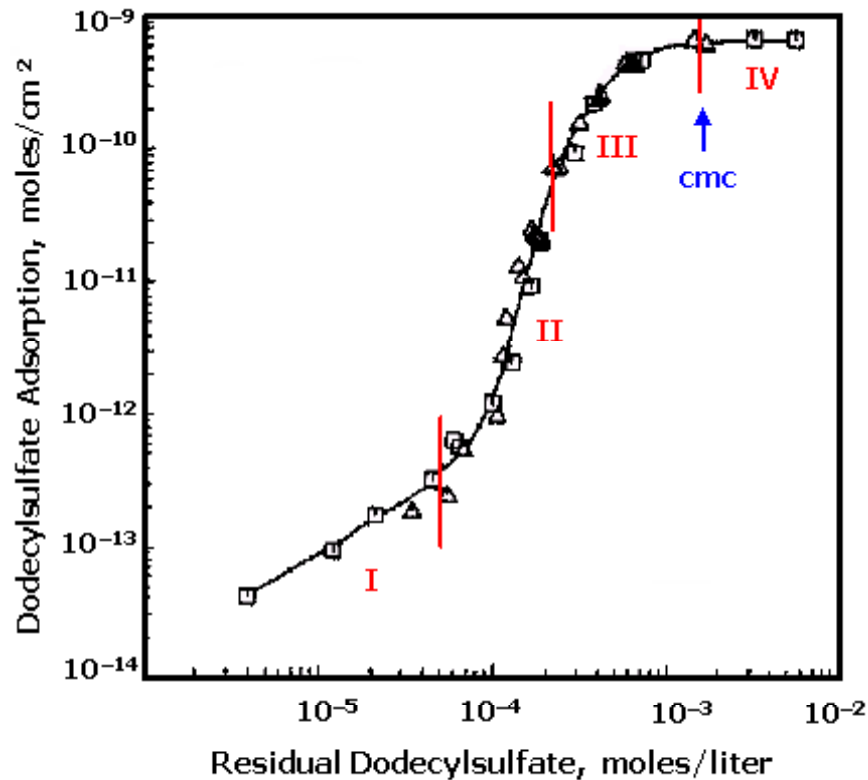


Figure 1.2a The adsorption isotherm of SDS on alumina in 0.1M NaCl at pH=6.5. The critical micelle concentration of SDS in 0.1M NaCl is marked as cmc. Reprinted from *J. Journal Colloid Interface Sci.* **1987**, 117, 31–46, with permission from Elsevier.

From this adsorption isotherm, the orientation and mechanism of surfactant adsorption is deduced as follows:¹⁴

1) In Region 1, the isotherm has a slope of unity under constant ionic strength conditions. The slope of unity can be explained through the differentiation of the logarithmic form of the Graham equation with respect to the logarithm of the bulk concentration of the surfactant.¹⁵ When there are only electrostatic interactions between the alumina surface and the surfactant, and the potential of the surface is independent of surfactant concentration, the differential is equal to 1. Therefore, the surfactant adsorbs “individually” in this region through electrostatic interactions between the anionic surfactant and the positively charged mineral. The almost constant zeta potential of

¹⁴ Somasundaran, P.; Kunjappu, J. T. *Colloids Surf.* **1989**, 37, 245–268.

¹⁵ Somasundaran, P.; Healy, T.W.; Fuerstenau, D.W. *J. Phys. Chem.* **1964**, 68, 3562–3566.

alumina (See Figure 1.2b.) supports the idea that the charge characteristics of the surface do not change significantly and the adsorption occurs as the exchange between the charged surfactant, and chloride ions. The increase in adsorption in Region 2 marks the onset of surfactant association at the surface through lateral interaction between hydrocarbon chains (hemimicelle formation). By the end of this region, the surface charge is neutralized as it can be seen from Figure 1.2b.

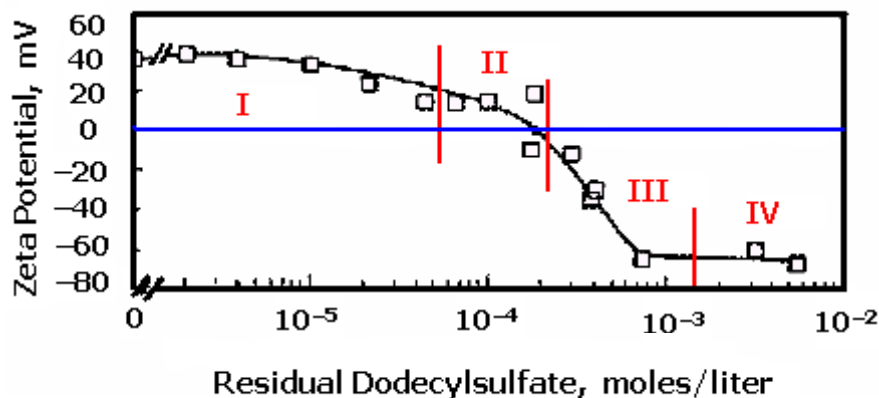


Figure 1.2b The zeta potential of alumina particles as a function of SDS concentration in 0.1M NaCl at pH=6.5. Reprinted from *J. Journal Colloid Interface Sci.* **1987**, 117, 31–46, with permission from Elsevier.

2) Region 3 is marked by a decrease in the slope of the adsorption isotherm, which is ascribed to the increasing electrostatic hindrance to the surfactant process following interfacial charge reversal. Since the surface and the surfactant are now both negatively charged, the electrostatic repulsion allows less surfactant to adsorb on to the surface. The negative zeta potential of alumina in this region proves that the surface is negatively charged.

3) The plateau adsorption in Region 4 corresponds to maximum surface coverage. This means that further increase in surfactant bulk concentration alters neither the surface excess nor the zeta potential. Chander et al. attribute this to the micelle formation in the bulk. However, this may not necessarily be true. The constant surface excess can be achieved even below the micelle formation in the bulk if the solid–liquid interfacial surface tension changes linearly with the surfactant chemical potential.

This explanation is just hypothetical. However, point 2 has been proven to be true by calorimetric studies, which gave thermodynamic evidence that hydrophobic interactions are the driving force of aggregative adsorption process, just like it is the case in micelle formation in solution.¹⁶

The adsorption isotherm of an ionic surfactant onto a hydrophobic surface is quite different. Greenwood et al. studied the adsorption of SDS on graphite.¹⁷ They have observed two plateaus on the adsorption isotherm, one at the half-maximum density and one at the maximum density. The presence of the first plateau is different than the case of SDS adsorption on alumina. The hydrophobic interactions between the SDS tail and the hydrophobic graphite cause the surface to be covered by the surfactants in this region. The alumina, being hydrophilic, did not have this effect on the adsorption of SDS. The passage between the plateaus was explained by the transition of the surfactant molecule's orientation from horizontal to perpendicular to the surface. The change in molecular organization has been proven to be incorrect by Wanless and Ducker by AFM images.¹⁸ According to AFM results, the transition is due to a change in the spacing of the hemicylinders of SDS adsorbed on graphite.

The adsorption of non-ionic surfactants onto hydrophilic surfaces differs from that of ionic surfactants because of the absence of electrostatic interactions. Non-ionic surfactants usually adsorb by hydrogen bonding and hydrophobic interactions. Since hydrogen bonding is relatively weak in comparison with electrostatic and chemical bonding, the *nature of water structure* at the solid-liquid interface will be of particular importance for the adsorption of non-ionic surfactants.

The most common type of nonionic surfactant favored in the adsorption isotherm studies is that comprising a polyethylene glycol group, $(\text{CH}_2\text{CH}_2\text{O})_n$, linked to either an alkyl or an alkylphenyl hydrocarbon chain (C_mE_n).^{19,20,21,22,23,24} Harris et al. have used

¹⁶ Kiraly, Z.; Findenegg, G. H. *J. Phys. Chem. B* **1998**, *102*, 1203–1211.

¹⁷ Greenwood, F. G.; Parfitt, G. D.; Picton, N. H.; Wharton, D. G. In *Adsorption from Aqueous Solution*; Weber, W. J., Matijevic, E., Eds.; ACS: Washington DC, 1968; p. 135.

¹⁸ Wanless, E. J.; Ducker, W. A. *J. Phys. Chem.* **1996**, *100*, 3207–3214.

¹⁹ Levitz, P.; Drake, J. M.; Klafter, J. *J. Chem. Phys.* **1988**, *89*, 5224–5236.

²⁰ Partyka, S.; Lindheimer, M.; Zaini, S.; Keh, E.; Brun, B. *Langmuir* **1986**, *2*, 101–105.

²¹ Lindheimer, M.; Keh, E.; Zaini, S.; Partyka, S. *J. Colloid Interface Sci.* **1990**, *138*, 83–91.

²² Denoyel, R.; Rouquerol, J. *J. Colloid Interface Sci.* **1991**, *143*, 555–572.

²³ Bohmer, M. R.; Koopal, L. K. *Langmuir* **1990**, *6*, 1478–1484.

small angle neutron scattering to determine the adsorption isotherm of non-ionic surfactants on PS latex particles.²⁵ Bee et al. have used surface tension measurements to study the adsorption of non-ionic surfactants to Teflon latex particles.²⁶

Non-ionic ethoxylated alcohols exhibit strong adsorption on silica but not on some other minerals such as alumina. Somasundaran et al. have determined the adsorption isotherm of dodecyloxyhepta-ethoxyethyl alcohol(C₁₂E₈) on silica.²⁷ In this adsorption isotherm, Region 3 in Figure 1.2a is absent, because the surfactant does not inhibit its own adsorption by reversing the surface charge. Recently, Portet et al. have also determined adsorption isotherms of C_mE_n type of non-ionic surfactants on silica using a HPLC method.²⁸

The adsorption isotherms of non-ionic surfactants onto hydrophobic surfaces have also been studied.^{29,30} C₈E₄ adsorption isotherms on graphite had no inflection points but had continuous rise with negative curvature until a plateau was reached at the cmc. The absence of an inflection point shows that there is no cooperative aggregation of surfactant molecules on the surface. The surfactant forms a monolayer structure on the surface. Note the similarity of this type of adsorption isotherm to the Langmuir adsorption isotherm.

1.3.2. Mechanism of Adsorption and Implied Orientation of Adsorbed Surfactants

Rosen³¹ classifies the adsorption mechanisms of ionic and nonionic surfactants onto solid surfaces as follows:

- 1) Ion Exchange: This mechanism involves replacement of counterions adsorbed onto the substrate from the solution by similarly charged surfactant ions.

²⁴ Van Den Boomgard, T. H.; Tadros, T. H. F.; Lyklema, J. *J. Colloid Interface Sci.* **1987**, *16*, 8–16.

²⁵ Harris, N. M; Ottewill, R. H.; White, J. W. In *Symposium on Adsorption from Solution*; Ottewill, R. H., Rochester, C. H.; Smith, A. L., Eds.; Academic Press, 1987; p. 139.

²⁶ Bee, H. E., Ottewill, R. H.; Rance, D. G.; Richardson, R. A. In *Symposium on Adsorption from Solution*; Ottewill, R. H., Rochester, C. H.; Smith, A. L., Eds.; Academic Press, 1987; p. 155.

²⁷ Somasundaran, P.; Krishnakumar, S. *Colloids Surf., A* **1997**, *123*, 491–513.

²⁸ Portet, F.; Desbene, P. L.; Treiner, C. *J. Colloid Interface Sci.* **1997**, *194*, 379–391.

²⁹ Gellan, A.; Rochester, C. H. *J. Chem. Soc., Faraday Trans. 1* **1985**, *81*, 1503–1512.

³⁰ Hey, M. J.; MacTaggart, W. J. *J. Chem. Soc., Faraday Trans. 1* **1984**, *80*, 699–707.

³¹ Rosen, M. J. *Surfactants and Interfacial Phenomena*; Wiley: New York, 1989; p. 39.

- 2) Ion Pairing: This mechanism involves adsorption of surfactant ions from solution onto oppositely charged surface sites unoccupied by counterions.
- 3) Hydrogen Bonding.
- 4) Polarization of Pi-electrons: This mechanism involves the adsorption of surfactants onto surfaces because of the attraction between electron-rich aromatic groups of the surfactants and positive sites on the substrate.
- 5) Van der Waals Dispersion Forces.
- 6) Hydrophobic Bonding: This mechanism occurs when the tendency of the hydrophobic groups of the surfactant molecules or the hydrophobic solid surface to escape from an aqueous environment (or the water molecules' tendency to keep maximum hydrogen bonding) becomes large enough to permit the surfactant molecules to adsorb on hydrophobic surfaces or to adsorb onto solid adsorbent by aggregating their chains.

The above classification is based on the experimental findings of 1960s–1970s,^{32,33,34,35} which basically focus on the adsorption isotherms and zeta potential changes of the substrates. However, to get a better insight into the mechanism by which surfactants adsorb and how this mechanism changes with concentration, knowledge on the orientation and the microenvironment of the adsorbed surfactants is needed.

1.3.2.1. Adsorption of Ionic Surfactants

Photoluminescence emission (fluorescence and phosphorescence) of a molecule is capable of reporting the changes in its microenvironment and has been used to explore the solution behavior of surfactants. The molecule that is used generally is pyrene. By comparing the intensity of the highest energy vibrational bond (I1) to the third highest energy vibrational bond (I3), the polarity of the medium can be determined. Somasundaran et al. have used this technique to determine the microstructure of SDS on alumina.³⁶ At full surface coverage the ratio of bond intensities was characteristic of a hydrocarbon environment, and not of water. So, the alkyl chains of the surfactant must be

³² Wakamatsu, T.; Fuersteneau, D. W. In *Adsorption from Aqueous Solution*, Weber, W. Matijeric, J. E., Eds.; ACS: Washington DC, 1968; p. 161.

³³ Rupprecht, H; Liebl, H. *Kolloid Z.Z. Polym.* **1972**, *250*, 719–723.

³⁴ Snyder, L. R. *J. Phys. Chem.* **1968**, *72*, 489–494.

³⁵ Giles, C. H.; D'Silva, A. P.; Easton, I. A. *J. Colloid Interface Sci.* **1974**, *47*, 766–768.

³⁶ Somasundaran, P; Kunjappu, J. T. *Colloids Surf., A* **1989**, *37*, 245–268.

aggregating on the surface. The same technique has been used to study the adsorption of tetradecyltrimethylammonium chloride (C₁₄TAC) on alumina at pH 10.³⁷ In a recent study by Strom et al.³⁸ fluorescent probes have been used to investigate the aggregate sizes of cationic surfactants at the silica-water interface. However, the uncertainty in the determination of the aggregate sizes was large in this study. One problem with the use of pyrene may be the perturbation of the “structure” of surfactant aggregates because of the pyrene. That is, the structure may be different in the absence of pyrene.

For SDS-alumina system, NMR spectroscopy has been used to determine the microstructure of the adsorbed SDS.³⁹ The fundamental feature of the NMR method is the strong variation of the quadruple coupling with the curvature of the surfactant-water interface. According to the results of Quist and Soderlind only ribbons, oblate micelles or a porous bilayer structure could account for the NMR spectrum.

For another system, n-decylbenzene sulfonate on alumina, ²H NMR spectra of adsorbed surfactants showed more restricted motion of molecules at low surface coverage than at high coverages and a single resonance for adsorbed surfactants, which meant a fast molecular exchange between the solution and the surface phase.⁴⁰

Polarized infrared attenuated reflection (IR-ATR) or attenuated total reflection-Fourier transform-infrared technique (ATR-FT-IR) can be used to investigate the average molecular chain orientation of adsorbed surfactant at the solid-liquid interface.⁴¹ Jeon et al.⁴² have studied the adsorption of an alkyl phosphate anionic surfactant on alumina by this technique. It was found that, as the adsorption density approached the maximum value, the average orientation of the surfactant molecules became more perpendicular to the surface. The same technique has been applied to study the adsorption of hexadecyltrimethylammonium bromide (C₁₆TAB) on silica.⁴³ Neivandt et al. have also concluded that as the surface excess of surfactant increased with pH, there was a trend toward increased alignment of the surfactant normal to the surface.

³⁷ Huang, L.; Somasundaran, P. *Colloids Surf., A* **1996**, *117*, 235–244.

³⁸ Strom, C.; Hansson, P.; Jonsson, B.; Soderman, O. *Langmuir* **2000**, *16*, 2469–2474.

³⁹ Quist, P. O.; Soderlind, E. *J. Colloid Interface Sci.* **1995**, *172*, 510–517.

⁴⁰ Nagashima, K.; Blum, F. D. *J. Colloid Interface Sci.* **1999**, *214*, 8–15.

⁴¹ Ulman, A. *ACS Symp. Ser.* 447, ACS: Washington DC, 1990; p. 144.

⁴² Jeon, J.S.; Sperline, R.P.; Raghavan, S.; Hiskey, J.B. *Colloids Surf., A* **1996**, *111*, 29–38.

⁴³ Neivandt, D. J.; Gee, M. L.; Hair, M. L.; Tripp, C. P. *J. Phys. Chem. B* **1998**, *102*, 5107–5114.

1.3.2.2. Adsorption of Non-ionic Surfactants

Ellipsometric measurements provide valuable information for the understanding of adsorption mechanisms and molecular orientation of adsorbed layers in the direction normal to the surface. Tiberg⁴⁴ has used this technique to study the adsorption of polyethylene glycol monoalkyl ethers (C_mE_n) at hydrophobic and hydrophilic surfaces. It was deduced from the adsorbed-layer thickness measurements that at hydrophilic surfaces, the adsorbed surfactants appeared tilted towards the surface at low coverage and this tilt decreased continuously with increasing surface coverage. However, these results could not discriminate among different aggregate topologies.

Neutron reflectivity can provide information about the orientation of surfactant molecules normal to the surface. Fragneto et al.⁴⁵ have used a hydrophobic Self-Assembled Monolayer (SAM) on silicon as a substrate to study the adsorption of $C_{12}E_4$ with this technique. The use of separate deuterium labels for the alkyl chains and ethylene glycol chains has shown that the surfactant molecule was oriented with the ethylene glycol chains pointing toward the solution.

1.3.3. Molecular Organization (Self-Assembly) of Surfactants on the Surface

A characteristic feature of surfactant adsorption at concentrations starting from slightly below the critical micelle concentration (cmc) is that adsorbed surfactants form local aggregates on the surface. These aggregates have been referred to as hemimicelles, admicelles, surface micelles or more generally solloids.

The organization of these aggregates also gives information on the mechanism and orientation of the surfactants on solid surfaces. In 1994, Manne et al.⁴⁶ have started the pioneering work of applying Atomic Force Microscopy (AFM) to image the aggregates of adsorbed surfactants at the solid-liquid interface. The power of this technique comes from the fact that information about the surface structures is learned directly, independent of models, and with no need to put additional probes into the

⁴⁴ Tiberg, F. *J. Chem. Soc., Faraday Trans.* **1996**, 92, 531–538.

⁴⁵ Fragneto, G.; Lu, J. R.; McDermott, D. C.; Thomas, R. K., *Langmuir* **1996**, 12, 477–486.

⁴⁶ Manne, S.; Cleveland, J. P.; S.; Gaub, H. E.; Stucky, G. D.; Hansma, P. K. *Langmuir* **1994**, 10, 4409–4413.

system. This study provided clear evidence that the surfactants form hemi-cylindrical micelles on graphite.

Following this study, in 1995, Manne et al.⁴⁷ studied adsorption of tetradecyltrimethylammonium bromide (C₁₄TAB) on silica. The images showed spherical aggregates adsorbed on silica. The same molecule forms full cylinders on mica. Here the importance of the structure of the solid substrate is observed. Although both substrates are hydrophilic and negatively charged, the molecular organization is different on each of them. On graphite, which is a hydrophobic solid, AFM images revealed half-cylindrical aggregates of surfactants. These observations showed that the earlier models, which predict a uniform layer on hydrophobic substrates and a uniform bilayer on hydrophilic ones, were wrong.

Following this work, anionic, cationic and non-ionic surfactant layers adsorbed at solid surfaces have been studied with AFM. AFM not only gives images of these layers but also provides information about the thickness of adsorbed layers.

Wanless and Ducker⁴⁸ have studied SDS adsorption on graphite and observed structures that are ordered in one dimension (hemicylinders) following the steps on the graphite structure. It has been found that the solution medium had no effect on the shape of the surface aggregates. The solution medium has been changed by either adding salt (NaCl) or by increasing SDS concentration. However, the periodicity of the aggregates was found to increase with the addition of more SDS or salt into system.

Lamont and Ducker⁴⁹ have studied the adsorption of C₁₆TAB and hexadecyltrimethylammonium chloride (C₁₆TAC) on mica. At concentrations above the cmc, the surface structures went from cylinders to flat bilayers with time. This supported the mechanism by ion exchange. To check the effect of ions on the adsorption, LiCl and CsBr were used. The presence of ions changes the density of charges on the surface, moreover they can bind to surfactant aggregates. As the salt concentration increased, the structures went from bilayers to cylindrical micelles to globular micelles. A similar study was performed by Ducker and Wanless in 1999.⁵⁰

⁴⁷ Manne, S.; Gaub, H. E. *Science* **1995**, *270*, 1480–1482.

⁴⁸ Wanless, E. J.; Ducker, W. A. *J. Phys. Chem.* **1996**, *100*, 3207–3204.

⁴⁹ Lamont, R. E.; Ducker, W. A. *J. Am. Chem. Soc.* **1998**, *120*, 7602–7607.

⁵⁰ Ducker, W. A.; Wanless, E. J. *Langmuir* **1999**, *15*, 160–168.

Adsorption of non-ionic surfactants (C_mE_n) on graphite, silica and hydrophobic silica were studied by Grant et al.⁵¹ Globular micelles were observed on silica, while continuous layers were observed on hydrophobic silica and graphite. The continuous layer formation is due the fact that the surfactant covers the surface to reduce the water-exposed hydrophobic area. Since both water and the $-OH$ groups on silica can form hydrogen bonding with the ethyleneoxide head group, this is maximized in the case of globular micelle formation on the surface.

Grant et al.⁵² have studied how the interfacial organization of adsorbed non-ionic surfactant molecules ($C_{12}E_8$) is affected by varying surfactant-surface interactions. They have used thiol-modified gold surfaces to change the hydrophobicity of the surface. They have found that organization of $C_{12}E_8$ aggregates at the solid-liquid interface was strongly influenced by the hydrophobicity of the interface. As the hydrophobicity of the surfaces was increased, the surface micelles got denser. This implies the importance of hydrophobic interaction when micelles adsorb on the surface. At more hydrophobic surfaces, the surfactants formed a homogeneous layer on the surface in agreement with the previous studies.

In a recent work by Dong et al.,⁵³ the aggregate structure of the non-ionic surfactant, $C_{12}E_5$, adsorbed on mica has been studied as a function of temperature with AFM. It was found that there was a phase transition temperature (21 °C) where the surfactant surface aggregates changed their structure abruptly. In an earlier study by Liu and Ducker⁵⁴ on cationic surfactant ($C_{16}TAB$) adsorption on silica, mica and graphite, it was shown that there was no significant effect of temperature on the surface aggregate structures on graphite. However, for mica and silica the aggregate structure of $C_{16}TAB$ changed as the temperature was increased above the Krafft temperature, T_K , the temperature above which, micelles of $C_{16}TAB$ form in bulk solution. Specifically, $C_{16}TAB$ formed a flat layer at $T < T_K$ and spherical micelles at $T > T_K$ on silica; and a flat layer at $T < T_K$ and cylinders at $T > T_K$ on mica in 10 mM KBr solutions.

⁵¹ Grant, L. M.; Tiberg, F.; Ducker, W. A. *J. Phys. Chem.* **1998**, *102*, 4288–4294.

⁵² Grant, L. M.; Ederth, T.; Tiberg, F. *Langmuir* **2000**, *16*, 2285–2291.

⁵³ Dong, J.; Mao, G. *Langmuir* **2000**, *16*, 6641–6647.

⁵⁴ Liu, J. F.; Ducker, W. A. *J. Phys. Chem. B* **1999**, *103*, 8558–8567.

1.4. Polymer Adsorption on Solid Surfaces

Polymers have been used as stabilizers for colloidal particles since 2500 BC when the ancient Egyptians used casein and gum Arabic to stabilize carbon black fibers for use as ink.⁵⁵ Today polymers adsorbed on solid surfaces are used in a large number of products including adhesives, coatings, paint and ink. The properties of these materials are governed by the adsorbed amount of the polymer and the conformation of the adsorbed polymer at the solid–liquid interface. The adsorbed amount and the conformation of an adsorbed polymer are influenced by the molecular weight of the polymer used and the interaction energy of the polymer segments with each other, with the surface and with the solvent. These interaction energies may be small in magnitude, but when the overall energy for all segments is taken into account, the result may be a significant driving force for adsorption leading to high affinity adsorption isotherms for polymer adsorption.

The adsorption of polymers onto surfaces is rarely an equilibrium process and most of the time it is irreversible; the polymer cannot desorb off the surface once it is adsorbed onto the surface. The reason for this can be viewed in two ways. The first one is the very low probability of all segments desorbing simultaneously. If each segment is treated independent of one another, then the probability of the desorption of a polymer chain is $(P_{\text{des}})^N$, where P_{des} is the probability of desorption of a segment and N is the number of segments in a polymer. The second one is the conformational adaptability of polymers. In a desorption experiment, when a few polymer segments are detached from the surface, the conformational entropy of the adsorbed polymer chain is going to increase, which will decrease the driving force for further segment desorption.⁵⁶

1.4.1. Homopolymers

The Flory-Huggins lattice theory of homogeneous solutions⁵⁷ has been extended by Scheutjens and Fleer^{58,59} to describe the adsorption of flexible polymers at surfaces.⁶⁰

⁵⁵ Napper, D.H. *Polymeric Stabilization of Colloid Dispersions*; Academic Press: London, 1983.

⁵⁶ Cheng, Y-L.; Lok, B. K.; Robertson, C. R. In *Surface and Interfacial Aspects of Biomedical Polymers: Protein Adsorption*; Andrade, J., Eds.; Plenum Press: New York, 1985; p.121–150.

⁵⁷ Flory, P. J. *Principles of Polymer Chemistry*; Cornell University Press: Ithaca, New York, 1953.

⁵⁸ Scheutjens, J. M. H. M.; Fleer, G. J. *J. Phys. Chem.* **1979**, *83*, 1619–1635.

⁵⁹ Scheutjens, J. M. H. M.; Fleer, G. J. *J. Phys. Chem.* **1980**, *84*, 178–190.

The conformation of an adsorbed flexible polymer molecule can be best described in terms of three parts as it can be seen from Figure 1.3:⁶¹

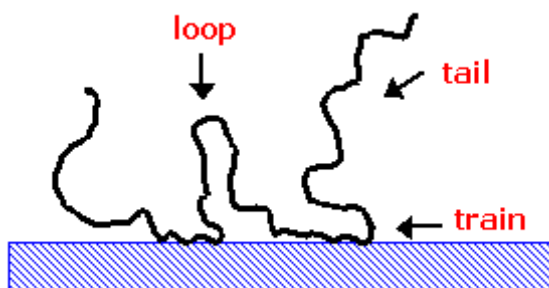


Figure 1.3 Conformation of a physisorbed homopolymer on a surface.

- 1) the trains, segments of consecutive monomers adsorbed at the interface
- 2) the loops, segments of the chain that extend into the adjacent bulk phase in between two trains
- 3) the tails, two segments at the end of the polymer chain; these generally have lower free energies of adsorption than other segments and thus tend to extend into the bulk phase.

The distribution of trains, loops, and tails depends on the free energy of adsorption of segments of the polymer molecule, the flexibility of the chain and the concentration of the polymer solution. The importance of the tail segments decreases with increase of molecular weight.⁶² However, at high polymer concentrations, the importance of tails increases, because the chains compete for surface sites and form much thicker layers (2/3 of chain length), with tails dominating in the periphery of the adsorbed layer.⁶³

The molecular weight of polymers and therefore the length of polymer chains have effects on polymer adsorption. Theoretical calculations show preferential adsorption

⁶⁰ Schillén, K.; Claesson, P. M.; Malmsten, M. *J. Phys. Chem. B* **101**, 4238–4252.

⁶¹ Fleer, G. J.; Scheutjens, J. M. H. M. *Adv. Colloid Interface Sci.* **1982**, *16*, 341–359.

⁶² Macritchie, F. In *Advances in Protein Chemistry*; Anfinsen, C.B. and Edsall, J.T., Eds.; Academic Press: New York, 1978; p.283–326.

⁶³ Scheutjens, J. M. H. M.; Fleer, G. J. *J. Phys. Chem.* **1980**, *84*, 178–190.

of polymers with different chain lengths in certain solution conditions at equilibrium.⁶⁴ From dilute and moderately concentrated solutions, long chains adsorb preferentially because of the higher translational entropy of the short chains in the solution. From very concentrated solutions, the reverse is true. A weak preferential adsorption of short chains is found, caused by conformational entropy effects (a short chain has relatively more ends).

Above, I have given a brief overview of the general adsorption characteristics of homopolymers at the solid–liquid interface. My work in Chapter 4 utilizes a complex unnatural protein that contains blocks of homopolymers (homopolyaminoacids). We have used the structure of a diblock copolymer for the unnatural protein, because when homopolymers *strongly* adsorb onto surfaces, they have a flattened configuration with a segment density profile that decays rapidly from the surface.^{65,66} This flattened conformation results in a thin adsorbed polymer layer, which is not suitable for steric stabilization of colloidal particles.⁶⁷ When homopolymers *weakly* adsorb onto surfaces, then the thickness of the adsorbed layer increases, but this time the polymers are attached loosely to the surface, which may lead to even more destabilization due to the bridging of polymer chains between particles, especially at low surface coverage. Therefore, homopolymers are not very good stabilizers for colloidal systems. So, here I will focus on block copolymers.

1.4.2. Diblock Copolymers

The adsorption of diblock copolymers at the solid–liquid interface plays an important role in the stabilization of colloidal particles in inks, paints, coatings and pharmaceuticals.⁵⁵ Block copolymers often behave like surfactant molecules at the solid–liquid interface. Usually they contain a block that adsorbs to the surface, the anchor, and another block that does not have any affinity for the surface, the buoy. When the buoy block has a more extended conformation on the surface than in bulk, the adsorbed layer is

⁶⁴ Scheutjens, J. M. H. M.; Fleer, G. J. In *The Effect of Polymers on Dispersion Properties*, Tadros, T. F., Eds.; Academic Press: London, 1982; p.145.

⁶⁵ Cosgrove, T.; Crowley, T. L.; Vincent, B.; Barnett, K. G.; Tadros, T. F. *Faraday Symp. Chem. Soc.* **1981**, *16*, 101–108.

⁶⁶ de Gennes, P. G. *Adv. Colloid Interface Sci.* **1987**, *27*, 189–209.

⁶⁷ Munch, M. R.; Gast, A. P. *J. Chem. Soc., Faraday Trans.* **1990**, *86*, 1341–1348.

called a *brush*,⁶⁸ which is also called an extended *buoy* layer. The buoy block can extend into the solution up to as much as 10 times⁶⁹ its normal radius of gyration in solution, and it is this brush layer that provides the thick steric stabilization.

The solvent plays an important role in the adsorption of block copolymers. If both blocks of the diblock copolymer are soluble, the solvent is called nonselective. If only one of the blocks dissolves, the solvent is selective, and the block copolymers may form micelles in solution.⁷⁰ The adsorption of block copolymers may be complicated by the presence of micelles in solution.^{71,72} In this review, I am going to discuss the adsorption behavior of diblock copolymers from nonselective solvents and from selective solvents below the critical micelle concentration.

The relative length of the blocks is of great importance for the structure of the adsorbed polymer layers on surfaces. When the anchor block is long, the adsorption is governed by the adsorption energy of this block to the surface and the lateral repulsion between the buoy blocks is then relatively weak. For diblock copolymers of the same total length, decreasing the relative length of the anchor block enhances the adsorbed amount because the relative contribution of the buoy segments to the adsorbed amount increases. When the anchor block is short, the lateral repulsion between the buoy blocks becomes important. In this case, the total adsorbed amount decreases with decreasing anchor length for diblock copolymers of fixed total length.⁷³

The process of the adsorption of diblock copolymers onto surfaces occurs in two stages.⁷⁴ In the first stage, any molecule that is in close proximity to the surface adsorbs and the transport of the molecules to the surface is due to diffusion. The adsorbed molecules are widely separated and the conformation of the buoy blocks is almost the same as that in solution. As more chains adsorb to the surface, the average distance between anchored chains gets smaller than the size of the buoy blocks in solution and the

⁶⁸ Milner, S. T. *Science* **1991**, *251*, 905–914.

⁶⁹ Hadziioannou, G.; Patel, S.; Granick, S.; Tirrel, M. *J. Am. Chem. Soc.* **1986**, *108*, 2869–2876.

⁷⁰ Bijsterbosch, H. D.; Cohen Stuart, M. A.; Fleer, G. J. *Macromolecules* **1998**, *31*, 9281–9294.

⁷¹ Van Lent, B.; Scheutjens, J. M. H. M. *Macromolecules* **1989**, *22*, 1931–1937.

⁷² Johner, A.; Joanny, J. F. *Macromolecules* **1990**, *23*, 5299–5311.

⁷³ Bijsterbosch, H. D.; Stuart, M. A. C.; Fleer, G. J.; Van Caeter, P.; Goethals, E. J. *Macromolecules* **1998**, *31*, 7436–7444.

⁷⁴ Motschmann, H.; Stamm, M.; Toprakcioglu, C. *Macromolecules* **1991**, *24*, 3681–3688.

buoy blocks start stretching (See Figure 1.4). Monte Carlo simulations⁷⁵ have shown this two-stage process.

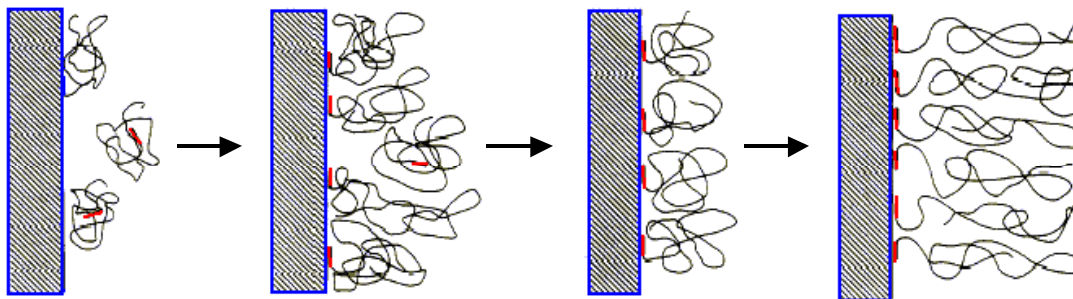


Figure 1.4 The stages of adsorption of diblock copolymers from a selective solvent onto a surface. Reprinted with permission from *Macromolecules* 1991, 24, 3681–3688. Copyright [1991] American Chemical Society.

Theoretical calculations and models play a key role in the investigation of polymer adsorption characteristics. In fact, in polymer science theory usually precedes the experimental findings. This is generally not the case for surfactant science probably because of the ease with which experimental conditions can be controlled systematically. For this reason, a thorough background on the theoretical aspects of polymer brush formation is given in the next section.

1.4.2.1. Theoretical Calculations

The first modeling of the adsorption characteristics of polymers end-anchored to surfaces was done by Alexander-de Gennes; this approach can be applied to the adsorption of diblock copolymers because of the extended brush characteristics of adsorbed diblock copolymers.^{76,77,78,79} The analysis of Alexander-de Gennes considers two contributions to the free energy of the end-anchored polymer chains in an athermal

⁷⁵ Zhan, Y.; Mattice, W. L.; Napper, D. H. *J. Chem. Phys.* **1993**, 98, 7502–7507.

⁷⁶ de Gennes, P. G. *Macromolecules* **1980**, 13, 1069–1075.

⁷⁷ de Gennes, P. G. *J. Phys. (Paris)* **1976**, 37, 1445–1452.

⁷⁸ Alexander, S. J. *J. Phys. (Paris)* **1977**, 38, 983–987.

⁷⁹ Dolan, A. K.; Edwards, S. F. *Proc. R. Soc. London A* **1974**, 337, 509–516.

solvent: osmotic and elastic. The osmotic contribution is due to the change in concentration of the adsorbed layer, while the elastic contribution is related to the entropy of a chain when it is stretched or compressed from its equilibrium dimensions. Minimizing the total energy gives an equation for the brush height, h , of the adsorbed polymer. In bulk solution, the size of the polymer chain is characterized by the radius of gyration, R_g :

$$R_g = aN^\nu \quad h = Nas^{1-\nu/2\nu} \quad (1.4)$$

where ν depends on the solution conditions, N is the number of segments in the non-adsorbing part of the chain, a is the size of a segment of the chain and s is a dimensionless surface density of chains, $s = a^2/d^2$, where d is the average spacing between chains on the surface. As N becomes large, $h \gg R_g$ and the chains in the brush are strongly stretched. In a good solvent, $\nu = 3/5$, so h scales with $s^{1/3}$. However, these scaling arguments do not provide an explicit form for the equilibrium segment density profile as a function of distance from the surface. They assume a step-function density profile in which all chains have identical behavior.

Mean field theory was used to predict the segment density profiles of polymer brushes by Milner, Witten and Cates.^{80,81,82} They took into account the excluded volume interactions among polymer chains. Their results showed a parabolic polymer segment density rather than the step function assumed by Alexander and de Gennes.

All the theoretical models described till now are for polymer brushes formed from an end-attachment of a homopolymer chain onto a surface. The following sections give theoretical modeling of the adsorption of diblock copolymers on surfaces.

1.4.2.1.a. Mean field approach

Munch and Gast⁸³ were the first to theoretically study the adsorption of diblock copolymers on a surface. In their work, they have focused on the adsorption of a diblock copolymer consisting of a large soluble extending block A and a small insoluble anchoring block B. They have introduced the concept of critical adsorption concentration,

⁸⁰ Milner, S. T.; Witten, T. A.; Cates, M. E. *Europhys. Lett.* **1988**, *5*, 413–418.

⁸¹ Milner, S. T.; Witten, T. A.; Cates, M. E. *Macromolecules* **1988**, *21*, 2610–2619.

⁸² Milner, S. T.; Witten, T. A.; Cates, M. E. *Macromolecules* **1989**, *22*, 853–861.

⁸³ Munch, M. R.; Gast, A. P. *Macromolecules* **1988**, *21*, 1366–1372.

cac, concentration below which no adsorption occurs and above which all the diblock copolymer adsorbs onto the surface. The value of cac decreased as the attraction energy between the surface and block B increased, as the copolymer-solvent compatibility decreased and as the length of block A decreased. They have also given scaling relations for the thickness of the adsorbed polymer layer, L_A : $L_A \sim N_B^{0.17}$, $L_A \sim N_A^{0.7}$, where N_A and N_B are the degrees of polymerization of block A and B, respectively.

Evers, Scheutjens and Fler^{84,85} have extended the Scheutjens and Fler theory^{86,87,88} for the adsorption of homopolymers from a binary mixture to study the adsorption of AB block copolymers. Block A segments had a high affinity for the surface and block B segments had the same affinity for the surface as the solvent. Their self-consistent-field theory did not make a priori assumptions about the conformations of the adsorbed molecules. They derived the equations for the conformation probabilities, the segment density profiles, and the free energy.⁸⁴ From the segment density profiles, they concluded that the A segments were mainly found in trains and loops, while the B segments contributed mainly to the density profile of tails.

They also analyzed the effect of the surface affinity of the A and B segments and that of the solvent quality for the B segments on the segment density profiles. When the surface affinity was high for the A segments and the solvent quality was good for the B segments, more extended adsorbed layers and higher segment densities were found due to a higher adsorbed amount. When the solvent quality was poor for the B segments, the density in the tail region increased and the segment density profile was less extended.

Evers, Scheutjens and Fler have also determined the dependence of the adsorbed amount and the hydrodynamic thickness on the internal composition of block copolymers.⁸⁵ They found that the adsorbed amount linearly increased with the block-length ratio, N_B/N_A , for chain lengths above 50 and for not too low fractions of A segments. The hydrodynamic layer thickness was found to depend on the adsorbed amount.

⁸⁴ Evers, O. A.; Scheutjens, J. M. H. M.; Fler, G. J. *Macromolecules* **1989**, *22*, 1931–1937.

⁸⁵ Evers, O. A.; Scheutjens, J. M. H. M.; Fler, G. J. *J. Chem. Soc., Faraday Trans.* **1990**, *86*, 1333–1340.

⁸⁶ Scheutjens, J. M. H. M.; Fler, G. J. *J. Phys. Chem.* **1979**, *83*, 1619–1635.

⁸⁷ Scheutjens, J. M. H. M.; Fler, G. J. *J. Phys. Chem.* **1980**, *84*, 178–190.

⁸⁸ Scheutjens, J. M. H. M.; Fler, G. J. *Macromolecules* **1985**, *18*, 1882–1900.

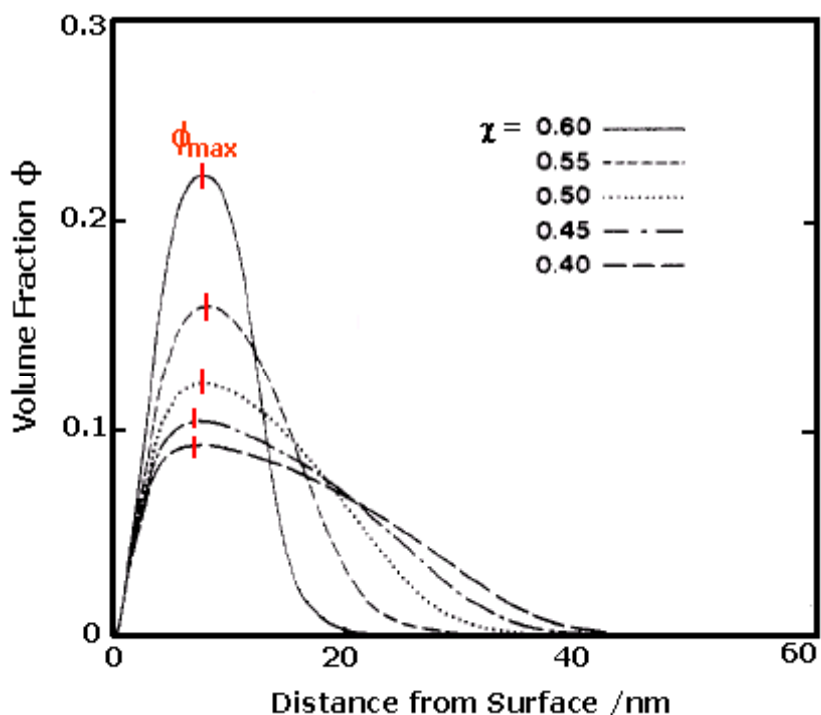


Figure 1.5 Polymer segment density profiles as a function of solvent quality, $\chi = 0.6 - 0.4$, from poor solvent to better solvents for the tail block. Reprinted with permission from *Macromolecules* 1990, 23, 3321–3339. Copyright [1991] American Chemical Society.

Whitmore and Noolandi⁸⁹ have studied the adsorption of diblock copolymers in systems where the solvent was bad for one of the blocks and either good, theta, or poor solvent for the second block. They have done calculations of the polymer density profiles above a surface. (See Figure 1.5.) The polymer density profiles (volume fraction of the polymer segments vs. distance from surface) were qualitatively the same for good, theta, and poor solvents, for polymers with low to high molecular weights, and for low to high surface coverage. As it can be seen from Figure 1.5, they all rise from zero to a maximum value, ϕ_{\max} , (similar to Alexander and de Gennes) and then decrease toward (similar to Milner, Witten and Cates) zero in a smooth and extended “tail-like” fashion. The ϕ_{\max}

⁸⁹ Whitmore, M. D.; Noolandi, J. *Macromolecules* 1990, 23, 3321–3339.

becomes smaller and the layer thickness increases as the solvent quality is changed from being poor to good for the tail block.

1.4.2.1.b. Scaling theory approach

Marques et al.⁹⁰ were the first to study the adsorption of a diblock copolymer on a surface in a highly selective solvent using scaling arguments taking into account possible aggregation formation in the solution in equilibrium with the adsorbed layer. From their calculations, they have found four adsorption regimes depending on the value of the external chemical potential of the polymer chains (the chemical potential of the polymer chains in solution). In extremely dilute solutions, there was a threshold for adsorption depending on the strength of the vdW energy of a film of the anchor block in contact with the surface. After this threshold, the adsorption was controlled by the vdW energy (Rollin Regime). At higher concentrations, micellization occurred in solution and there were two adsorption regimes depending on the asymmetry ratio of the copolymer; vdW-Buoy regime and buoy-dominated regime. At even higher concentrations where the solution was in a lamellar phase, and when the vdW forces were small, the structure of the adsorbed layer was the same as that of lamella. As a general conclusion, their theory predicts an adsorption in the vdw-buoy regime as long as the anchor block has a much lower degree of polymerization than the buoy block, in a wide range of solution concentrations and independent of copolymer organization in solution.

Marques and Joanny⁹¹ have also studied the adsorption of a diblock copolymer on a surface from a nonselective solvent. In a nonselective solvent (contrary to a highly selective solvent), the vdW interaction between the polymer and the surface was of no importance and the solutions were isotropic and homogeneous in the dilute solution regime. Their theory predicts that the structure of the adsorbed copolymer depends on the asymmetry of the copolymer at thermodynamic equilibrium. The asymmetry ratio of the copolymer, β , was defined as the ratio of the natural radii of gyration of the tail block B to the anchor block A, R_B/R_A . When β was smaller than $N_A^{1/2}$, the block A was a fluffy continuous layer on the surface and its concentration profile decayed in the same way as in an adsorbed homopolymer. The adsorbed amount and the thickness of this layer were

⁹⁰ Marques, C.; Joanny, J. F.; Leibler, L. *Macromolecules* **1988**, *21*, 1051–1059.

⁹¹ Marques, C. M.; Joanny, J. F. *Macromolecules* **1989**, *22*, 1454–1458.

smaller than those of a layer formed from the adsorption of a homopolymer with the same number of segments. The buoy layer had a thickness that scaled linearly with the molar mass of the B block. When β was larger than $N_A^{1/2}$, the anchor layer formed a quasi-two-dimensional polymer solution on the surface.

1.4.2.1.c. Monte Carlo Simulations

Shih et al.⁹² were the first to use Monte Carlo simulations to study the adsorption of diblock copolymers from a *good* solvent on surfaces. They did simulations not only for the adsorption of diblock copolymers but also for homopolymers. Their results showed that the segment density profiles of the adsorbed diblock copolymers were more uniform and that the adsorbed diblock copolymer layers could extend much farther into the solution, as compared to the homopolymer. At high surface coverage, the thickness of the adsorbed copolymer layer, h , increased with increasing length of the tail block, N_1 , as $N_1^{0.6}$ for small N_1 and as $N_1^{1.0}$ for $N_1 > 30$ with the length of the adsorbing block kept constant at $N_2=10$.

Zhan et al.⁹³ have also simulated the adsorption of diblock copolymers onto surfaces from a *good* solvent. Their results on the adsorption isotherms had a Langmuir character when the surface coverage of the anchor block was small. The fraction of coverage of the surface with the anchor block increased as the concentration of the polymer increased, as the length of the anchor block increased, and as the surface affinity of the segments in the anchor block increased. The anchor block did not form a dense homogeneous layer (there were some unoccupied surface sites available) even when the attractive interaction was strong and concentration was high. The adsorption isotherms deviated from a Langmuir character when the length of the anchor block became large and when the surface affinity of the segments in the anchor block was strong. The adsorbed amount decreased with increasing length of the buoy block and increased with increasing length of the anchor block.

Wang et al.⁹⁴ have carried out Monte Carlo simulations to study the adsorption of block copolymers from a *selective* solvent onto surfaces. They have determined the

⁹² Shih, W. Y.; Shih, W.-H.; Aksay, I. A. *Mat. Res. Soc. Symp. Proc.* **1989**, *140*, 431–436.

⁹³ Zhan, Y.; Mattice, W. L.; Napper, D. H. *J. Chem. Phys.* **1993**, *98*, 7502–7507.

⁹⁴ Wang, W.; Lin, Z.-Z.; Ebner, C. *Physical Review E* **1993**, *48*, 4622–4631.

distribution of the buoy block as it was stretched away from the surface. They have carried out calculations for both a homopolymer anchored at one end onto a surface, and a block copolymer, with an A adsorbing block and a B buoy block, adsorbed on a surface. The nonadsorbed block behaved the same way in both of the systems; a parabolic segment density with a long tail at farther distances from the surface. The thickness of this layer scaled as $N_B^{0.6}$ in a good solvent. In a bad solvent, the chain was collapsed close to the surface with no depletion region so that the maximum in the density was almost adjacent to the surface. As the quality of solvent increased, the mean distance of a segment from the surface increased smoothly as the polymer changed conformation from collapsed to an extended one.

1.4.2.2. Experimental Measurements

Experimental measurements have been carried out to understand the adsorption behavior of block copolymers. Adsorbed amount of the polymer, the thickness of the adsorbed layer and the microstructure of the adsorbed polymer (conformation and the segment density profile) have been determined by the utilization of spectroscopic techniques, ellipsometry, neutron reflectivity, neutron scattering, surface forces apparatus and atomic force microscopy.

1.4.2.2.a. Adsorbed Amount

Parsonage et al.⁹⁵ have studied the effect of the sizes of the blocks in PVP-PS on the adsorption of this block copolymer from toluene onto mica and polished silicon wafers. For this system, toluene is a *selective solvent* for PS. They have used scintillation counting (using tritium-labeled polymers) and XPS to measure the adsorbed amount of a series of copolymers with different block sizes and molecular weights. They have found that the surface density of the polymer depended primarily on the molecular weight of PVP for polymers with moderate asymmetry ($10 < \beta < 100$) while for polymers with high asymmetry ($\beta > 100$), the surface density was determined by the molecular weight of the non-adsorbing PS block. Their results agree well with the model of Marques et al.⁹¹

⁹⁵ Parsonage, E.; Tirrell, M.; Watanabe, H.; Nuzzo, F. G. *Macromolecules* **1991**, *24*, 1987–1995.

Guzonas et al.⁹⁶ have also studied the effect of the sizes of the blocks in PS-PEO on the adsorption of this block copolymer in toluene onto mica. However, this time toluene is a *non-selective solvent*. They have performed IR measurements to determine the adsorbed amount of a series of PS-PEO copolymers. When their results are compared with those of Parsonage et al., the adsorbed amounts are lower. This shows that there is more adsorbed amount when adsorption is from a selective solvent than from a nonselective solvent. Their results agree well with the model of Marques et al. except for copolymers with high asymmetry.

A very similar system has been studied by Dorgan et al.⁹⁷ who have investigated the adsorption of PEO-PS block copolymers from toluene onto silicon wafers with ellipsometry. They have observed drastic changes in adsorption behavior with time and concentration. At low copolymer concentrations, there was an overshoot of the adsorbed amount and the adsorbed amount did not reach an equilibrium value over time (1.4 days). This happened when the block size was large; for small adsorbing block sizes, this phenomenon was not present. They had a few hypotheses for the explanation of the overshoot and time effect at low concentrations: a rearrangement of the adsorbed chains on the surface, a replacement process of initially adsorbed chains with an unfavorable conformation by chains from solution, and polydispersity (chains with a more favorable β value may replace already existing ones).⁹⁸

Wu et al.⁹⁹ have investigated the adsorption of poly(dimethyl amino ethyl methacrylate)-poly(n-butyl methacrylate), DMAEM-BMA, onto silica in 2-propanol, a *nonselective solvent*. DMAEM adsorbs onto silica. They have measured the adsorbed amount with solution depletion technique and confirmed their results with gravimetric analysis of silica with adsorbed polymer. They have also determined the hydrodynamic thickness by photon correlation spectroscopy. With constant degrees of polymerization, both the adsorbed amount and the hydrodynamic thickness exhibited steep maximums as the adsorbing block composition was varied, in agreement with the theory of Evers,

⁹⁶ Guzonas, D. A.; Boils, D.; Tripp, C. P.; Hair, M. L. *Macromolecules* **1992**, *25*, 2434–2441.

⁹⁷ Dorgan, J. R.; Stamm, M.; Toprakcioglu, C.; Jerome, R.; Fetters, L. J. *Macromolecules* **1993**, *26*, 5321–5330.

⁹⁸ Stamm, M.; Dorgan, J. R. *Colloids Surf., A* **1994**, *86*, 143–153.

⁹⁹ Wu, D. T.; Yokoyama, A.; Setterquist, R. L. *Polymer Journal* **1991**, *23*, 709–714.

Scheutjens and Fleer. The hydrodynamic layer thickness scaled on the order of 0.53 with the degree of polymerization of the non-adsorbing block, contrary to 0.7 as predicted by Munch and Gast.¹⁰⁰ The difference was attributed to the nonselective nature of the solvent used in this study.

Bijsterbosch et al.¹⁰¹ have described the adsorption of diblock copolymers of poly(vinyl methyl ether) and poly (2-ethyl-2-oxazoline) and PEO-poly(2-methyl-2-oxazoline) at the silica-water interface. They have measured the adsorbed amount with optical reflectometry and the hydrodynamic thickness with dynamic light scattering. Their system has both a *nonselective solvent* and a *nonselective adsorption*. The adsorbed amount and hydrodynamic thickness as a function of block copolymer composition showed a shallow maximum. At this maximum, the longest block was also the strongest adsorbing block. They have also compared the adsorbed amounts with homopolymers. The nonselectively adsorbed block copolymers showed a higher adsorbed amount and a higher hydrodynamic thickness as compared to the homopolymers of similar molecular weight.

There have been also studies done on the adsorption of triblock copolymers on surfaces.^{102,103,104} However, due to the presence of the *same* blocks at the two ends of the polymer, these types of copolymers do not really parallel our studies. Therefore, no information on the adsorption behavior of these types of polymers will be given in this review.

1.4.2.2.b. Microstructure of the Adsorbed Polymer

Conformation

Neutron reflection experiments provide information on the neutron refractive index profile normal to the reflecting interface. Therefore they are widely used to probe the composition of surfaces and interfaces. The conformation or the polymer segment density profiles of adsorbed polymers on surfaces can be obtained with this method.

¹⁰⁰ Munch, M. R.; Gast, A. P. *Polymer Comm.* **1989**, *30*, 324–326.

¹⁰¹ Bijsterbosch, H.D.; Stuart, M. A. C.; Fleer, G. J.; Van Caeter, P.; Goethals, E. J. *Macromolecules* **1998**, *31*, 7436–7444.

¹⁰² Tiberg, F.; Malmsten, M.; Linse, P.; Lindman, B. *Langmuir* **1991**, *7*, 2723–2730.

¹⁰³ Ou-Yang, H. D.; Gao, Z. *Journal de Physique II* **1991**, *1*, 1375–1385.

¹⁰⁴ Griffiths, P. C.; Cosgrove, T.; Shar, J.; King, S. M.; Yu, G-E.; Booth, C.; Malmsten, M. *Langmuir* **1998**, *14*, 1779–1785.

Cosgrove et al.¹⁰⁵ have used neutron reflectivity to study the conformation of PS-PVP adsorbed onto mica from cyclohexane, in toluene. They have fitted their experimental data with segment density profiles assuming an exponential profile, a Gaussian profile, a parabolic fit and Scheutjens-Fleer model. Gaussian and SF profiles were virtually superimposable. Gaussian, SF and parabolic fits gave equally good fits. This means that the buoy blocks of the adsorbed block copolymers have segment density profiles that have a maximum or are parabolic.

Field et al.¹⁰⁶ have also used neutron reflectivity to study the conformation of PS-PVP block copolymers on quartz from toluene. They have investigated the effect of the PVP block size (PS block size kept constant) on the adsorbed conformation of the polymer. Their results showed that the polymer density profile normal to the surface for the larger anchor blocks was well-described by the mushroom type profile, which is predicted by the scaling theories at low surface coverages, where the distance between the anchor points is greater than the radius of gyration of the nonadsorbing block. As the molecular weight of the anchor block increased, the distance between the anchor points of the mushrooms increased. As the molecular weight of PVP was reduced, there was a crossover from mushrooms to brushes.

Satija et al.¹⁰⁷ used the same technique to investigate symmetric diblock copolymers of PS-PMMA adsorbed on a quartz surface from carbon tetrachloride. Their results showed that the PMMA block strongly adsorbed onto quartz forming a PMMA rich layer of thickness comparable to its radius of gyration. The PS blocks were so extended into the solution that PS density was undetectable by neutron reflectivity.

Extended length of the brush layers from Force Measurements

When two surfaces bearing polymer brushes approach each other, they start exerting a repulsive force. This force arises because of the build-up of an osmotic pressure, generated by overlap of the tail segments of the adsorbed polymer. The distance

¹⁰⁵ Cosgrove, T.; Heath, T. G.; Phipps, J. S.; Richardson, R. M. *Macromolecules* **1991**, *24*, 94–98.

¹⁰⁶ Field, J. B.; Toprakcioglu, C.; Dai, L.; Hadziioannou, G.; Smith, G.; Hamilton, W. *J.Phys.II France* **1992**, *2*, 2221–2235.

¹⁰⁷ Satija, S.K.; Majkrzak, C. F.; Russell, T. P.; Sinha, S. K.; Sirota, E. B.; Hughes, G. J. *Macromolecules* **1990**, *23*, 3860–3864.

where the force is observed initially can therefore be approximated as twice the extended length of the polymer chain into solution.

Tirrell's group^{108,109,110,111,112} has used the Israelachvili surface forces apparatus^{113,114} to determine the layer thicknesses of adsorbed diblock copolymers and the force profiles between such surfaces. They have studied the adsorption of poly(2-vinylpyridine)-polystyrene (PVP-PS) block copolymers on mica from solution in toluene, a selective solvent for PS. They have found that the forces were detectable at many multiples of the unperturbed dimensions (R_g) of the tail blocks, in contrast to the 2-3 R_g separation where forces were first observed between adsorbed homopolymer layers.¹¹⁵ Additional information on the application of the surface forces apparatus to study the adsorption of diblock copolymers is given in Section 1.5.

1.4.2.3. Charged Block Copolymers

In more recent years, there has been interest in the study of the adsorption of charged diblock copolymers on surfaces. Hoogeveen et al.^{116,117} were the first to study the adsorption properties of diblock copolymers consisting of a charged and an uncharged block. They have measured the adsorbed amount of poly(dihydroxypropyl methacrylate)-poly(dimethylaminoethylmethacrylate), PHMA-PAMA, on silica and titania as a function of pH, salt concentration and copolymer composition using reflectometry. PAMA is positively charged below pH~8 and PHMA is neutral.

When the composition of the block copolymer was varied, a maximum was observed in the adsorbed amount. In the first region (high PAMA), the adsorption was governed by the charge compensation and in the second region (low PAMA), the adsorption was governed by the electrostatic attraction of the PAMA block to the surface.

¹⁰⁸ Hadziioannou, G.; Patel, S.; Granick, S.; Tirrell, M. *J. Am. Chem. Soc.* **1986**, *108*, 2869–2876.

¹⁰⁹ Tirrell, M.; Patel, S.; Hadziioannou, G. *Proc. Natl. Acad. Sci. USA* **1987**, *84*, 4725–4728.

¹¹⁰ Parsonage, E. E.; Tirrell, M.; Watanabe, H.; Nuzzo, R. G. *Macromolecules* **1991**, *24*, 1987–1995.

¹¹¹ Patel, S.; Tirrell, M.; Hadziioannou, G. *Colloids Surf.* **1988**, *31*, 157–179.

¹¹² Watanabe, H.; Tirrell, M. *Macromolecules* **1993**, *26*, 6455–6466.

¹¹³ Israelachvili, J. N.; Adams, G. E. *Nature* **1976**, *262*, 773–776.

¹¹⁴ Israelachvili, J. N.; Adams, G. E. *J. Chem. Soc., Faraday Trans. 1* **1978**, *74*, 975–1001.

¹¹⁵ Israelachvili, J. N.; Tirrell, M.; Klein, J.; Almog, Y. *Macromolecules* **1984**, *17*, 204–209.

¹¹⁶ Hoogeveen, N. G.; Cohen Stuart, M. A.; Fler, G. J. *Faraday Discuss.* **1994**, *98*, 161–172.

¹¹⁷ Hoogeveen, N. G.; Cohen Stuart, M. A.; Fler, G. J. *Colloids Surf., A* **1996**, *117*, 77–88.

In their sequential adsorption experiments, they have found that there was no absolute preference for either PAMA or PHMA on the surface. However, they have not used PHMA but polysaccharide dextran for this study due to the fact that homopolymer PHMA was hydrolyzed in solution and was negatively charged at $\text{pH} > 4$. PHMA was not hydrolyzed when it was a part of the block copolymer. From these results, they suggested a mixed layer for the adsorption of the block copolymer. At low adsorbed amounts, the PHMA block could adopt a relatively flat conformation, while at high adsorbed amounts, it might be forced to form loops and tails.

Amiel et al.¹¹⁸ have studied the adsorption of PtBS-NaPSS (poly(tert-butylstyrene)-poly(styrene sulfonate)) on silica surfaces from aqueous solutions using ellipsometry. The PSS block is negatively charged in solution and hydrophilic while the PtBS block is uncharged and hydrophobic. The PSS block was bigger than the PtBS block. In a salt free solution, they have not found any adsorbed polymer on silica. In 1M salt, the adsorbed amount of the copolymer was greater than the adsorbed amount of the homopolymer NaPSS of similar molecular weight. The hydrophobic block played a significant role in the anchoring of the diblock at silica. The adsorbed amount increased two times if the polyelectrolyte block size was reduced by half.

Walker and Grant¹¹⁹ have carried out a study on the investigation of the conformation of DNA block copolymers adsorbed on latex particles by hydroxyl radical footprinting.¹²⁰ They have synthesized DNA molecules with different ratios of phosphodiester (one charge per nucleotide) and ethylphosphonate (no charge) linkages. Since at neutral pH, all four bases (A, C, G, T) are uncharged, the charge characteristics of single-stranded DNA is dictated solely by the type of linkage employed. Therefore monodisperse solutions of DNA with precisely known electrostatic properties were used in their study. When the particles were positively charged, all nucleotides adsorbed with their sugar moieties in direct contact with latex surface, as no significant cleavage was

¹¹⁸ Amiel, C.; Sikka, M.; Schneider, J. W.; Tsao, Y-H.; Tirrell, M.; Mays, J. W. *Macromolecules* **1995**, *28*, 3125–3134.

¹¹⁹ Walker, H. W.; Grant, S. B. *Langmuir* **1995**, *11*, 3772–3777.

¹²⁰ In hydroxyl radical footprinting, a hydroxyl radical attacks on the sugar moiety in the DNA backbone and results in strand scission, cutting the DNA molecules into two pieces at the site of attack. Regions of a DNA molecule, which are less accessible to hydroxyl radical, are cut less frequently. Therefore the DNA segments away from the surface are cut more frequently than segments directly adjacent to the surface.

observed at any position of the molecule. When the surface was negatively charged, a fraction of the molecules appeared to adsorb with their sugar off the surface, and increasing the surface density of the adsorbed DNA caused a greater fraction of the molecules to adsorb with their sugar moieties in solution.

Walter et al.¹²¹ have studied the adsorption of a zwitterionic block copolymer PMMA-PDMAEMA on silicon. At the isoelectric point of the block copolymer (iep), the copolymers were insoluble in water. They have observed a substantial adsorption at the iep of the polymer due to macroscopic precipitation of the neutral polymer chains.

1.4.3. Proteins

The building blocks of proteins are 20 naturally occurring amino acids, which have cationic, anionic, hydrogen bonding or hydrophobic side chains. The reaction of amino acids with each other forms peptides. If a peptide has fewer than ten amino acids, it is known as an oligopeptide; if it has more than ten amino acids, it is known as a polypeptide.¹²² Proteins are composed of polypeptides and there may be more than one polypeptide in a protein's structure. My work in Chapter 4 utilizes a protein synthesized by using the machinery of a bacterial cell; Thioredoxin-Pro₃₉Glu₁₀. This protein has a block copolymer structure and may be called a polypeptide, but we call it an unnatural protein because of the presence of thioredoxin in its structure and because it is not naturally found in nature.

Protein adsorption is important in biological processes like “cell adhesion, biocompatibility of synthetic polymers and blood coagulation”.¹²³ Proteins are surface active because of their polymeric structure and, amphoteric and amphiphilic nature.¹²⁴ The wide variety of amino acids with positively/negatively charged, hydrophilic and hydrophobic side chains induce the adsorption of proteins to many surfaces. When a protein is in the vicinity of an interface, its microenvironment is altered as well as its

¹²¹ Walter, H.; Harrats, C.; Muller-Buschbaum, P.; Jerome, R.; Stamm, M. *Langmuir* **1999**, *15*, 1260–1267.

¹²² Conn, E.C.; Stumpf, P.K. *Outlines of Biochemistry*; John Wiley & Sons: New York, 1976; Chapter 4.

¹²³ Horbett, T. A. In *Biomaterials: Interfacial Phenomena and Applications*, Cooper, S.L. and Peppas, N.A., Eds.; 1982, ACS: Washington, DC, p.233–244.

¹²⁴ Macritchie, F. *Adv. Protein Chem.* **1978**, *32*, 283–326.

equilibrium structure. Thus the protein conformation may change upon adsorption.¹²⁵ For example, hydrophobic residues that are usually hidden in the core of a protein in the native state of the protein¹²⁶ may be exposed in the vicinity of a hydrophobic surface.¹²⁷ The adoption of an unnatural conformation is called “denaturation” or “unfolding”.

The following variables are important in the study of protein adsorption:

- 1) pH of the solution. The charged side chains have pK_a values of ~10, 7, 4 so changes in pH will affect the charge and will determine where the experiment is done relative to the isoelectric point of the protein.
- 2) The ionic strength of the solution. The ionic strength affects the pK_a of the side chains and the charge distribution near the protein.
- 3) The concentration of the protein and the equilibration time it takes for the protein to adsorb onto a surface.

Despite the long history of study on protein adsorption, the fundamental mechanisms of adsorption remain partly to be understood, and research on protein adsorption is very active. This is probably due to the diversity of systems studied (the type of the protein and the characteristics of the interface) and of the methodologies employed in this interdisciplinary research area. The main aim in my studies concerning protein adsorption is the stabilization of colloidal particles through the adsorption of an unnatural protein, which has a diblock copolymer nature. However, due to biosynthetic difficulties, my unnatural diblock protein has also a His-patch thioredoxin (a mutant form of natural thioredoxin) attached to the tail block. I have not carried out a comprehensive study on the characteristics of protein adsorption in my work, therefore only a brief outline of the properties of adsorbed proteins on surfaces will be given in this section. To my knowledge, there have not been any studies on the adsorption properties of His-patch thioredoxin on surfaces.

Thioredoxin was first isolated in 1964 from *Escherichia coli*.¹²⁸ Depending on the chemical environment, thioredoxin can catalyze reduction of a protein disulfide bond or

¹²⁵ Andrade, J.D. In *Surface and Interfacial Aspects of Biomedical Polymers*, Vol 2. Protein Adsorption, Andrade, J. D., Ed.; Plenum Press: New York, 1985; p.1–80.

¹²⁶ Wertz, D. H.; Scheraga, H. A. *Macromolecules* **1978**, *11*, 9–15.

¹²⁷ Hoffman, A. S. *Biomed. Mater. J. Res. Symp.* **1974**, *8*, 77–83.

¹²⁸ Laurent, T. C.; Moore, E. C.; Reichard, P. *J. Biol. Chem.* **1964**, *239*, 3436–3444.

oxidation of a dithiol to a disulfide.¹²⁹ Its three-dimensional structure was determined by X-ray diffraction¹³⁰ and multidimensional NMR spectroscopy¹³¹. These studies show that the 108-residue polypeptide chain folds into a compact globular conformation with a central twisted, five-stranded β -sheet forming a hydrophobic core surrounded by the four α -helices on the external surface observed in solution by NMR. Compact globular proteins are densely packed molecules of roughly spherical shape containing a considerable amount and variety of internal architecture.¹³² Insulin, lysozyme, cytochrome c, myoglobin and ribonuclease fall into this category. Hydrophobic side-groups tend to be buried in the interior of the molecule and the charged groups are almost always located in the aqueous periphery of the protein, making the protein soluble in aqueous environment.¹³³

General Features of Protein Adsorption

The adsorption isotherms generally show an “overshoot” in adsorbed amount as a function of time and a kink or inflection in the isotherm at about half-saturation.¹³⁴ Within the first minute of contact, adsorption is rapid and reversible. Given sufficient time, the adsorbed proteins undergo conformational changes, which lead to increased surface interactions. Proteins less optimally adsorbed undergo desorption, hence overshoot in the time curve. The protein is adsorbed in a random arrangement at coverages less than 50%. At coverages greater than 50%, ordering may develop which leads to more efficient packing and an increase in adsorbed amount, hence the kink in the isotherm.¹³⁴

These are regarded as rules of thumb for protein adsorption although each surface-protein-solution system is unique and may not exhibit all of these features.

Structure and Microenvironment of Adsorbed Proteins

Walton has pioneered the study of protein conformational changes upon adsorption using fluorescence and circular dichroism spectroscopies.^{134,135,136} The degree

¹²⁹ Holmgren, A. *Thioredoxin. Annu. Rev. Biochem.* **1985**, 54, 237–271.

¹³⁰ Katti, S.; LeMaster, D. A.; Eklund, H. *J. Mol. Biol.* **1990**, 212, 167–184.

¹³¹ Dyson, H. J.; Holmgren, A.; Wright, P. E. *Biochemistry* **1989**, 28, 7074–7087.

¹³² Haynes, C. A.; Norde, W. *Colloids Surf., B: Biointerfaces* **1994**, 2, 517–566.

¹³³ Creighton, T.E. *Proteins: Structures and Molecular Principles*, W.H. Freeman: NY, 1984.

¹³⁴ Soderquist, M. E.; Walton, A. G. *J. Colloid Interface Sci.* **1980**, 75, 386–392.

¹³⁵ Walton, A. G.; Meanpa, F. C. *J. Colloid Interface Sci.* **1979**, 72, 265–278.

of conformational changes is directly related to the contact time, and it is now generally accepted that protein conformational change can be a rather slow event.

The intrinsic UV fluorescence of tryptophan (Trp) is generally used to follow adsorption of proteins. The shifts in the wavelength give information about the microenvironment. However, if there is more than one Trp, the signal is the sum and it is difficult to deduce the microenvironment of each Trp. For example, for bovine albumin adsorbed on hydrophilic quartz, the fluorescence maximum is 342 nm in bulk solution and shifts to 333 nm upon adsorption showing that adsorption changes the conformation of the molecule.¹³⁶ FTIR^{137,138} is also used for direct determination of conformational changes during adsorption process due to shifts in infrared absorption bands.

After compiling data from a variety of sources and experimental techniques, Norde¹³⁹ concludes that layer thicknesses of proteins adsorbed to solids are usually comparable to the dimensions of the native protein in aqueous solution. This suggests that although structural rearrangements may occur upon adsorption, the internal coherence (stability) of globular proteins prevents them from completely unfolding on a surface into loose “loop and tail” like structures.

1.5. Polymer-Surfactant Interactions

Polymers and surfactants in solution are extensively used together in both biological and industrial processes to take advantage of the wider variety of properties that mixtures can produce compared to individual components.¹⁴⁰ For example, the addition of a surfactant to a polymer solution can either increase or decrease the solubility of the polymer. Similarly, the presence of a polymer on a solid surface can either promote or inhibit the adsorption of surfactant. The main characteristic of these mixed solutions is that the polymer and the surfactant molecules associate via van der Waals forces,

¹³⁶ McMillin, C. R.; Walton, A. G. *J. Colloid Interface. Sci.* **1974**, *48*, 345–349.

¹³⁷ Gendreau, R. M.; Leininger, R. I.; Winters, S.; Jakobsen, R. J. *In Biomaterials, Adv. Chem. Ser.* **199**, 1982, p. 371–394.

¹³⁸ Sakurai, Y., Akaike, T. Kataoka, K., Okano, T. In *Biomedical Polymers*, Goldberg, E. P., Nakajima, A., Eds.; Academic Press: NY, 1980; p. 335–379.

¹³⁹ Norde, W. *Adv. Colloid Interface Sci.* **1986**, *25*, 267–340.

¹⁴⁰ Tirrel, M. In *Interaction of Surfactants with Polymers and Proteins*, CRC Press: Boca Raton, 1993; p. 59.

hydrogen bonding, electrostatic forces or hydrophobic forces. The possibilities of interaction range with the different kinds of polymers and surfactants available:

- 1) Non-ionic polymers with anionic, cationic or non-ionic surfactants
- 2) Polyelectrolytes with anionic, cationic or non-ionic surfactants

The emphasis on this review will be on the systems with an uncharged synthetic water-soluble polymer and a synthetic surfactant. The focus is on the adsorption properties of polymer-surfactant solutions at the solid-liquid interface, and an overview of the bulk properties and local/micro structure of the complexes will also be given.

1.5.1. Polymer-Surfactant Solutions

1.5.1.1 Binding Isotherms

Surfactants often associate with polymers in solution. The binding isotherm expresses the amount of “bound” surfactant as a function of the free surfactant concentration. These isotherms are similar to the adsorption isotherms of surfactants on solid surfaces. Therefore, they also give information about the nature of the binding process and indirectly about the structure of aggregates.

In order to determine the binding isotherm, the equilibrium free surfactant concentration needs to be determined in the solution containing both polymer and surfactant.¹⁴¹ Changes in viscosity and surface tension, surfactant selective electrodes and dialysis methods¹⁴² have been used to measure the binding. It should be noted that although the early studies^{143,144} on polymer-surfactant binding studies present good experimental data, the model based on the large set of experimental data (conductivity, surface tension, and viscosity) is wrong.

A typical binding isotherm for a non-ionic polymer and an anionic surfactant is shown in Figure 1.6.¹⁴²

¹⁴¹ Rodenheiser, A.P.; Kwak, J.C.T. In *Polymer-Surfactant Systems*, Marcel Dekker, New York, 1998; p. 1.

¹⁴² Shirahama, K. *Colloid and Polymer Sci.*, **1974**, 252, 978–981.

¹⁴³ Jones, M. N. *J. Colloid Interface Sci.* **1967**, 23, 36–42.

¹⁴⁴ Schwuger, M. J. *J. Colloid Interface Sci.* **1973**, 43, 491–498.

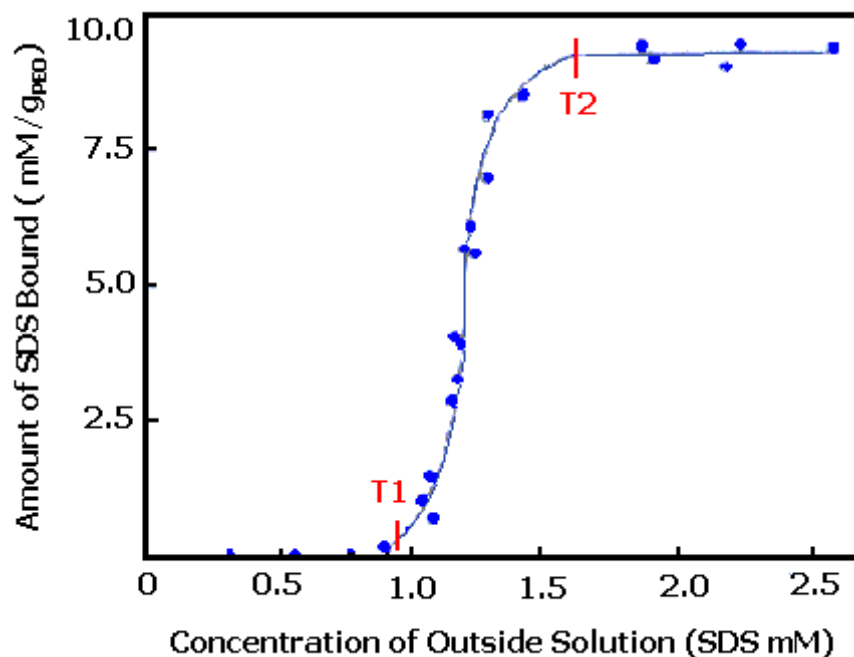


Figure 1.6 The binding isotherm of SDS onto PEO in 0.1M NaCl at 30 °C. Reprinted with permission from *Colloid. Polym. Sci.* 1974, 252, 978–981. Copyright [1974] Springer-Verlag.

There are two critical concentrations: T1 for the onset of cooperative interactions between the polymer and the surfactant (also called the critical association concentration, cac), T2 for the saturation of the polymer with the surfactant. This association is best viewed as a polymer-induced micellization, because cac is lower than the cmc, which is 1.5 mM in 0.1M NaCl.¹⁴⁵ Polymer-induced micellization is generally seen in the case of ionic surfactant binding to non-ionic polymers.

Shirahama et al.¹⁴⁶ have used surfactant-selective electrodes to study the binding of cationic surfactants to non-ionic polymers, polyethylene oxide (PEO), polyvinylalcohol (PVA) and polyvinylpyrrolidone (PVP). They found that binding to PVA was slightly cooperative, whereas binding to PEO lacked cooperativity. PVP did not

¹⁴⁵ Hansson, P.; Lindman, B. *Current Opinion in Colloid and Interface Science* **1996**, 1, 604–613.

¹⁴⁶ Shirahama, K.; Himura, A.; Takisawa, N., *Colloid Polym. Sci.*, **1987**, 265, 96–100.

bind to the surfactants at all. Their results show that there is not much interaction between cationic surfactants and non-ionic polymers.

Few researchers have studied the binding of non-ionic surfactants to non-ionic polymers. Anthony and Zana found that the cmc of the surfactant did not change in the presence of the polymer.¹⁴⁷ From this, they concluded that there was no significant binding of the surfactant to the polymer.

The outcome of binding isotherm studies is the fact that polymer-surfactant binding happens in a cooperative way. Since the presence of a bound surfactant induces the binding of others, there has to be aggregate formation.

1.5.1.2. Change in Surfactant Solution Properties

Determining the bulk properties of polymer-surfactant solutions and comparing them with the bulk surfactant solution properties, gives insight into the binding process of the surfactant to the polymer. Free surfactant ion concentration is the major bulk property that relates to the binding of the surfactant to the polymer. Several methods have been used for this purpose.

Surface tension:

Although surface tension is a surface property, it depends on the free surfactant ions present in the bulk solution. In order to measure the binding of a surfactant to a polymer in solution, one needs to measure the concentration of free surfactant in the presence of the polymer-surfactant complex. This is difficult because the polymer-surfactant complex may also have some surface-active properties. However, when a slightly surface active polymer capable of binding to the surfactant, is present in the surfactant solution, changes in surface tension are observed compared with the surfactant-only surface tension.

Chari et al.¹⁴⁸ have determined the surface tension behavior of sodium dodecyl sulfate (SDS) in the presence of polyvinylprolydine (PVP). They have observed the two critical concentrations: T1, the beginning of the polymer-surfactant binding, and T2, the saturation of the polymer with the surfactant aggregates. T2' marks the formation of free

¹⁴⁷ Anthony, O.; Zana, R. *Langmuir* **1994**, *10*, 4048–4052.

¹⁴⁸ Chari, K.; Hossain, T. *Z. J. Phys. Chem.*, **1991**, *95*, 3302–3305.

micelles in the bulk solution (See Figure 1.7). In a similar study by Sesta et al.¹⁴⁹ lithium perfluoronanoate, LiPFN, has been used instead of SDS. This system also revealed the T1, T2 and T2' stages.

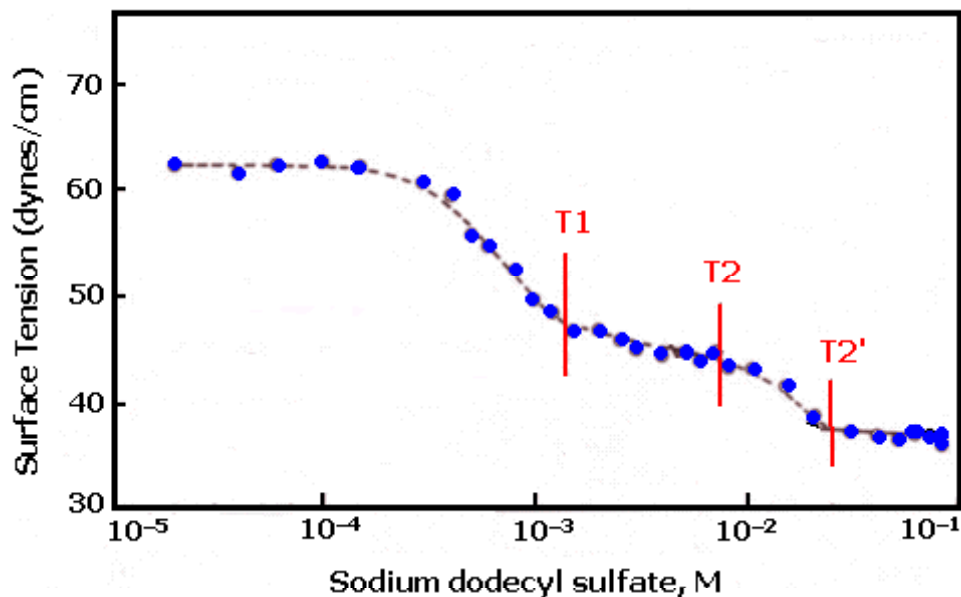


Figure 1.7 Surface tension of PVP/SDS solutions in 0.001 M NaCl at pH=6 and 25 °C. Reprinted with permission from *J. Phys. Chem.*, 1991, 95, 3302–3305. Copyright [1991] American Chemical Society.

Surfactant-Ion Selective Electrodes:

Studies with surfactant electrodes offer the advantage of fast in situ determination of non-bound surfactant ions in solution.¹⁵⁰ Therefore, they are ideal to study the polymer-surfactant solutions. The activity of the surfactant is calculated from the emf using the Nerst Equation. Comparison of the emf in surfactant solutions with the emf in polymer-surfactant solutions gives the degree of association with the polymer.

Both Kresheck et al.¹⁵¹ and Wan-Badhi et al.¹⁵² have measured the emf of a DS⁻ ion selective electrode in PVP/SDS solution. Two critical concentrations are observed, T1 and T2, similar to those in surface tension measurements.

¹⁴⁹ Sesta, B.; Segre, A.L.; D'Aprano, A.; Proiette, N. *J.Phys. Chem.B* **1997**, 101, 198–204.

¹⁵⁰ Birch, B. J.; Clarke, D. E.; Lee, R. S.; Oakes, J. *Analytica Chimica Acta* **1974**, 70, 417–423.

¹⁵¹ Kresheck, G. C.; Constantinidis, I. *Anal. Chem.* **1984**, 56, 152–156.

The properties of polymers in solution also change on addition of surfactants. The change in viscosity^{153,154,155,156,157} and cloud points of polymer solutions¹⁵⁸ can be used to determine surfactant binding. Usually, binding of surfactants to a polymer chain decreases the viscosity of the polymer. The cloud point of a non-ionic polymer generally increases with the addition of surfactant.

1.5.2. Microstructure of the Polymer-Surfactant Complexes

NMR:

The first use of NMR to detect the microenvironment of PEO/SDS systems dates back to 1970s. Smith et al.¹⁵⁹ have used ¹⁹F NMR with F₃SDS/PEO and found similar values of chemical shift for the polymer-bound surfactant and micellized surfactant. This proved the presence of micelle type aggregates in the presence of the polymer at cac. Another important result was the fact that there was only one ¹⁹F NMR signal, which meant a rapid exchange of surfactant ions between all possible sites.

Cabane¹⁶⁰ studied the PEO/SDS system using ¹³C, ¹H, and ²³Na NMR. He found that only the first three carbon atoms of SDS (counted from the SO₄ head-group) exhibit ¹³C chemical shifts consistent with the presence of PEO. The other carbon atoms of SDS had the same chemical shifts as they had in SDS micelles. This showed that the major part of the alkyl chain of SDS was in an environment similar to a normal micelle, in the polymer-surfactant complex. Therefore, the polymer binds to the surfaces of the surfactant micelles. This means that only a small fraction of the polymer chain is involved in this binding and the rest of the polymer chain is present as loops in the solution. However, the polymer chain may also wrap around the micelle. Indeed, Gao et al.¹⁶¹ have found that 50% of the PEO segments adsorbed to the micelles at PEO/SDS

¹⁵² Wan-Badhi, W. A.; Wan-Yunus, M. Z.; Bloor, D. M.; Hall, D. G.; Wynjones, E. *J. Chem. Soc. Faraday Trans.* **1993**, *89*, 2737–2742.

¹⁵³ Francois, J.; Dayantis, J.; Sabbadin, J. *Eur. Polym. J.* **1985**, *21*, 165–174.

¹⁵⁴ Tam, K.C. In *Hydrophilic Polymers: Performance with Environmental Acceptability*, eds. J. Edward Glass, ACS, Washington DC, **1996**, p. 205.

¹⁵⁵ Jiang, W. H.; Han, S. J. *J. Colloid Interface Sci.* **2000**, *229*, 1–5.

¹⁵⁶ Saito, S.; Kitamura, K. *J. Colloid Interface Sci.* **1971**, *35*, 346–353.

¹⁵⁷ Mya, K. Y.; Jamiesson, A. M.; Sirivat, A. *Langmuir* **2000**, *16*, 6131–6135.

¹⁵⁸ Karlstrom, G.; Carlsson, A.; Lindman, B. *J. Phys. Chem.* **1990**, *94*, 5005–5015.

¹⁵⁹ Smith, M. L.; Muller, N. *J. Colloid Interface Sci.* **1975**, *52*, 507–515.

¹⁶⁰ Cabane, B. *J. Phys. Chem.* **1977**, *81*, 1639–1645.

¹⁶¹ Gao, Z.; Wasyliston, R.; Kwak, J. C. *J. Phys. Chem.* **1991**, *95*, 462–467.

concentration ratio of 3.3. This finding is more reasonable than Cabane's according to the viscosity changes in polymer solutions in the presence of surfactant micelles at cac.¹⁵³

¹³C is not very sensitive to study polymer-surfactant complexes, due to the low natural abundance of ¹³C isotope. Ramachandran et al.¹⁶² have improved Cabane's experiments by using ¹³C labeling of the first carbon bonded to SO₄. Their results showed that a higher chemical shift was observed in the presence of polymer. This suggests that PEO penetrates to the first carbon.

Aggregation number of surfactants:

From the NMR studies it has been concluded that surfactant micelles form a complex with the polymer. If this is the case, a change in the aggregation number, N , of surfactants in the micelles is expected. Fluorescence decay curves can provide information concerning the size of the aggregates.¹⁶³ SDS micelles in aqueous solution have $N = 60$. Lissi et al.¹⁶⁴ have determined the aggregation numbers of SDS micelles formed on PEO and PVP. This has been done by fluorescence quenching experiments. In the presence of PEO, $N = 35 \pm 5$ and in the presence of PVP, $N = 28 \pm 6$ surfactant molecules. This means that there is reduction in the aggregation number of micelles in the presence of the polymer. This result supports Cabane's picture of polymer-induced micellization. The polymer chain helps the formation of micelles by reducing the repulsion of head-groups of the surfactant. Also by sitting at the hydrocarbon-water interface, the polymer reduces the interfacial tension. So a stable aggregate can be formed with fewer surfactant molecules per aggregate. Similar reduction in aggregation numbers has also been observed in other studies of PVA/SDS,¹⁶⁵ PPO/SDS¹⁶⁶ and PPO/CTAB.¹⁶⁷ It has been concluded that the aggregation number increases with surfactant concentration and with decreasing polymer concentration, independent of polymer molecular weight above a critical molecular weight.¹⁶⁸

¹⁶² Ramachandran, R.; Kennedy, G. *J. Colloids Surf.* **1991**, *54*, 261–266.

¹⁶³ Zana, R.; Yiv, S.; Strazielle, C.; Lianos, P. *J. Colloid Interface Sci.*, **1981**, *80*, 208–223.

¹⁶⁴ Lissi, E. A.; Abuin, A. *J. Colloid Interface Sci.*, **1985**, *105*, 1–6.

¹⁶⁵ Gilyani, T.; Wolfram, E. In *Microdomains in Polymer Solutions*, Dubin, P., Ed.; Plenum Press: New York, 1985; p. 383.

¹⁶⁶ Witte, F. M.; Engberts, J. B. F. N. *J. Org. Chem.* **1987**, *52*, 4767–4772.

¹⁶⁷ Brackman, J. C.; Engberts, J. B. F. N. *Chemical Society Reviews* **1993**, *22*, 85–92.

¹⁶⁸ Zano, R.; Lang, J.; Lianos, P. In *Microdomains in Polymer Solutions*, Dubin, P., Ed.; Plenum Press: New York, 1985; p. 357.

Use of Fluorescence to Determine the Microenvironment

As is the case in surfactant solutions, fluorescence probes can be used to obtain information about the microenvironment of the polymer-surfactant systems.¹⁶⁹ By comparing the intensity of the highest energy vibrational bond (I1) to the third highest energy vibrational bond (I3), the polarity of the medium can be determined.

For polymer-surfactant systems, Turro et al.¹⁷⁰ have used pyrene as the fluorescent probe to study PVP/SDS and PEO/SDS systems and found evidence for micellar structures below the cmc of the surfactant. However, these micelles had a more polar environment than the ordinary free micelles. This showed that the micelles had a more open structure due to the presence of water and, PEO or PVP.

Hu et al.¹⁷¹ have studied the same system by end-labeling the polyethylene chain (Mw = 8000) with pyrene. They have found that at low SDS concentrations, the polymers cyclize so that the two end groups of a polymer chain share a single mixed micelle. It is highly probable that the presence of pyrene groups at the ends of the polymer chain affects the outcome of this experiment and therefore this is not a good method for studying polymer-surfactant microenvironment.

Recently, a fluorescence quenching method¹⁷² has been used to study the interactions of non-ionic polymers (PEO) with non-ionic surfactants (C₁₂E₈). It has been found that neither the aggregation numbers nor the fluorescence lifetime of pyrene has changed in the presence of PEO at 20 °C. However, the dynamic light scattering data showed an increase in the hydrodynamic radius of micelles in the presence of PEO at high concentrations of the surfactant.

1.5.3. Polymer-Surfactant Mixtures on Solid Surfaces

When polymers and surfactants are present together in the vicinity of a solid, they can either affect each other's adsorption properties or form complexes on the surface. There has been interest in the investigation of the adsorption properties since late

¹⁶⁹ Bloor, D. M.; Wyn-Jones, E. *J. Chem. Soc. Faraday Trans. 2* **1982**, 78, 657–669.

¹⁷⁰ Turro, N. J.; Baretz, B. H.; Kuo, P. L. *Macromolecules* **1984**, 17, 1321–1324.

¹⁷¹ Hu, Y.; Zhao, C.; Winnik, M.A.; Sundararajan, P.R. *Langmuir* **1990**, 6, 880–883.

¹⁷² Feistosa, E.; Brown, W.; Swanson-Vethamuthu, M. *Langmuir* **1996**, 12, 5985–5991.

1960s.^{173,174,175} Both enhancement and inhibition of adsorption have been observed for both adsorbing components, depending on the addition sequence, the nature of the solid surface and the pH.^{176,177} The analysis in these studies was similar to the analysis of the determination of surfactant adsorption isotherms, i.e. centrifuging the slurry and analyzing the supernatant.

PEO/SDS:

Cosgrove et al.¹⁷⁸ have performed dynamic light scattering measurements to determine the adsorption of PEO and SDS on negatively charged silica. Below the cmc, the addition of surfactant caused a decrease in hydrodynamic thickness of the adsorbed layer as compared to a PEO-only layer. The decrease in hydrodynamic thickness was attributed to desorption of the polymer from the silica surface. Therefore, SDS did not adsorb on silica and furthermore induced desorption of PEO from the silica surface. Above the cmc, the hydrodynamic thickness gradually increased from the minimum observed at the cmc and, at 4 x cmc, passed its value in PEO-only solution. This was ascribed to the presence of an extended adsorbed layer of the polymer decorated with micelles.

The same system has also been investigated by Somasundaran et al.¹⁷⁹ using centrifugation and two-phase titration technique to determine the adsorbed SDS concentration. The SDS adsorption on silica increased with the preadsorption of PEO on silica, contrary to the results of Cosgrove et al. Somasundaran et al. did not provide data on PEO residual concentration after the SDS was put into the system. So, it is not possible to know whether PEO desorbed after the addition of SDS.

Mears et al.¹⁸⁰ have used ¹H NMR solvent relaxation to solve this problem. Their results indicated that the structure of bound water in the adsorbed PEO layer was significantly affected by the addition of SDS and this could be explained by the

¹⁷³ Somasundaran, P. *J. Colloid Interface Sci.* **1969**, *31*, 557–565.

¹⁷⁴ Saunders, F.L. *J. Colloid Interface Sci.* **1968**, *28*, 475–480.

¹⁷⁵ Tadros, T.F. *J. Colloid Interface Sci.* **1974**, *46*, 528–540.

¹⁷⁶ Chibowski, S. *J. Colloid Interface Sci.* **1980**, *76*, 371–374.

¹⁷⁷ Moudgil, B. M.; Somasundaran, P. *Colloids Surf.*, **1985**, *13*, 87–101.

¹⁷⁸ Cosgrove, T.; Mears, S. J.; Thompson, L.; Howell, I. In *Surfactant Adsorption and Surface Solubilization*, Sharma, R. Ed.; ACS: Washington DC, 1995; p. 138–152.

¹⁷⁹ Somasundaran, P.; Maltesh, C. *J. Colloid Interface Sci.*, **1992**, *153*, 298–301.

¹⁸⁰ Mears, S. J.; Cosgrove, T.; Thompson, L.; Howell, I. *Langmuir* **1998**, *14*, 997–1001.

desorption of PEO with increasing SDS concentration. However, their results did not explain why the hydrodynamic thickness increased above the cmc.

The same system has been investigated on polystyrene latex particles (PS) by dynamic light scattering and small-angle neutron scattering measurements.¹⁸¹ In this case, both the polymer and the surfactant can adsorb onto the substrate. However, the hydrodynamic thickness of PEO on PS showed the same behavior as on silica (e.g. going through a minimum at a surfactant concentration close to the cmc and then increasing toward its original value at high concentrations). The similarity of results between the experiments on silica and on PS shows that the adsorption behavior is governed by the complex formation of PEO/SDS in the bulk solution. This group's proposed scheme of the effect of SDS on an adsorbed PEO layer is shown in Figure 1.8.

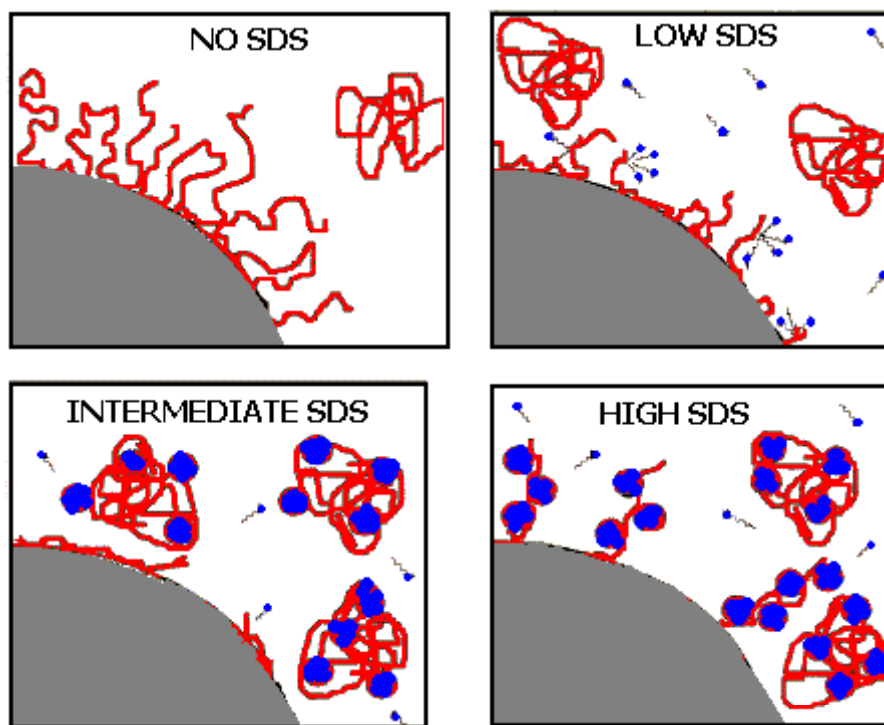


Figure 1.8 Effect of SDS on PEO adsorption. Reprinted with permission from *Langmuir* **1998**, *14*, 4997–5003. Copyright [1998] American Chemical Society.

¹⁸¹ Cosgrove, T.; Mears, S. J.; Obey, T.; Thompson, L.; Wesley, R. D. *Colloids Surf.* **1999**, *149*, 329–338.

PVP/LiDS, PVP/SDS:

Esumi et al. have studied the adsorption of PVP/LiDS system on alumina. The adsorption of PVP increased at low concentrations due to the formation of PVP/LiDS complex at the alumina-solution interface and the adsorption of both adsorbates decreased at high LiDS concentrations due to the formation of a PVP/LiDS complex in solution.¹⁸² The same polymer-surfactant system was investigated on hydrophilic and hydrophobic silica.¹⁸³ It was found that the adsorption of PVP on hydrophobic silica showed a sharp increase at low surfactant concentrations. A smaller effect was observed on hydrophilic silica. As the surfactant concentration was increased, a decrease in the adsorption of PVP was detected. PVP/LiDS system has also been studied on hydrophobic graphite¹⁸⁴ and on polystyrene latex particles.¹⁸⁵ PVP is found to adsorb more in the presence of the surfactant on graphite, due to the probable complex formation on graphite. On polystyrene, the same adsorption behavior is observed as that on alumina. Following these studies, the use of an AFM gave information about the organization of PVP/SDS system on graphite.¹⁸⁶ The non-equilibrium adsorbed layer was found to be heterogeneous on the micrometer scale, consisting of 2 types of coverage: surfactant rich and surfactant poor. The surfactant rich domains had hemicylindrical structures and covered the whole surface at equilibrium. These findings offer a new method to study the polymer-surfactant interactions at the solid-liquid interface.

1.6. Forces between Particles and Surfaces

Surfactants and macromolecules are widely used in colloidal processes. The addition of these molecules to colloidal suspensions can induce stabilization of the colloidal suspension by producing a repulsive force between particles, or coagulation of the particles by creating an attractive force. The forces between particles also control the density and viscosity of colloidal suspensions. In this section, I will describe the forces of

¹⁸² Esumi, K.; Otsuka, H. *Langmuir* **1994**, *10*, 45–50.

¹⁸³ Esumi, K.; Otsuka, H.; Ring, T. A.; Li, J.; Caldwell, K. D. *Colloids Surf.* **1996**, *116*, 161–171.

¹⁸⁴ Otsuka, H.; Esumi, K. *J. Colloid Interface Sci.* **1995**, *170*, 113–119.

¹⁸⁵ Otsuka, H.; Ring, T. A.; Li, J.; Caldwell, K. D.; Esumi, K. *J. Phys. Chem. B* **1999**, *103*, 7665–7670.

¹⁸⁶ Fleming, B. D.; Wanless, E. J.; Biggs, S. *Langmuir* **1999**, *15*, 8719–8725.

interaction between particles and/or surfaces in the absence of any surface active reagents, and in the presence of adsorbed macromolecules.

As a first approximation, the force, F , between macroscopic particles or surfaces can be viewed as the sum of forces between each pair of molecules in each body. So, the net interaction depends on the size of the particles.¹⁸⁷ Therefore, we introduce an intensive property, E_A , the energy per unit area of one infinite flat plate interacting with another parallel infinite flat plate of same material. E_A is usually defined for half spaces, but because surface forces are short-ranged, only the first micrometer or so contributes to the interaction. Therefore, it is common to refer to these forces as surface forces. The Derjaguin approximation¹⁸⁸ is used to interconvert the measured force in simple geometries to E_A . For two spheres of radius R_1 and R_2 :

$$F(S) = 2\pi \left(\frac{R_1 R_2}{R_1 + R_2} \right) E_A(S) \quad (1.5)$$

where S is the separation between the surfaces. If one of the spheres, R_2 , is very large, the equation reduces to a form of $2\pi R_1 E_A(S)$. This form of the equation is ideal for transforming force measurements between a sphere and a flat surface (AFM force measurements). It is important to remember that this is just an approximation. It only holds when the range of the force and the separation between particles are much smaller than both R_1 and R_2 .

The first direct measurement of forces was done by Derjaguin et al.^{189,190} between a convex lens and a flat glass surface in vacuum. They used an electrobalance to measure the forces and an optical technique to measure the distance between surfaces in the regime of 100–1000nm.

There are now three major techniques for measuring forces between surfaces: surface forces apparatus,^{191,192,193,194,195,196} total internal reflection microscopy^{197,198} and

¹⁸⁷ Israelachvili, J. *Intermolecular and Surface Forces*; Academic Press: San Diego, 1992; Chapter 10.

¹⁸⁸ Derjaguin, B. V. *Kolloid Zeits.* **1934**, 69, 155–164.

¹⁸⁹ Derjaguin, B. V.; Abrikossova, I. I. *Discuss. Faraday Soc.* **1954**, 18, 24–41.

¹⁹⁰ Derjaguin, B. V.; Abrikossova, I. I.; Lifshitz, E. M. *Quart. Rev. Chem. Soc.* **1956**, 10, 295–329.

¹⁹¹ Tabor, D.; Winterton, R. H. S. *Proc. R. Soc. Lond.* **1969**, 312, 435–450.

atomic force microscopy (AFM).^{199,200,201,202} The details of each technique are out of the scope of this review. However, since I have used AFM in my experiments, I am going to give a brief introduction on AFM only. There are three major components in an AFM: a piezoelectric crystal, which controls the movement of one of the solids relative to the other; a cantilever spring, which deflects in proportion to the force between the probe attached to it and the other surface; a laser beam, which hits the back of the cantilever and then reflects onto a detector to follow the extent of deflection of the cantilever. The details of the determination of a force-separation relation from an AFM measurement are given in Section 2.3.1. It is important to mention that it is not possible to directly measure the zero separation with an AFM, and therefore the absolute distance between the two surfaces. Recently by the combination of TIRM with AFM,²⁰³ the absolute distance between two surfaces can be determined.

There are three most important forces between particles or surfaces in liquids: van der Waals, electrostatic and steric-polymer forces, which are all long-range forces. At shorter distances (below 1 to 3nm) solvation and other types of steric forces may be significant. In the following sections, a general overview of the long-range forces will be given.

1.6.1. Van der Waals Forces

There are two theories on van der Waals forces: microscopic theory of London and macroscopic theory of Lifshitz.²⁰⁴ The microscopic theory of London is based on the assumption that the interactions between *pairs* of molecules are additive to give the total interaction. Therefore, the interaction between two molecules in separate bodies is

¹⁹² Israelachvili, J. N.; Tabor, D. *Proc. R. Soc. Lond. A* **1972**, *331*, 19–38.

¹⁹³ Israelachvili, J. N.; Tabor, D. *Prog. Surf. Membr. Sci.* **1973**, *7*, 1–55.

¹⁹⁴ Israelachvili, J. N.; Adams, G. E. *J. Chem. Soc. Faraday Trans. I* **1978**, *74*, 975–1001.

¹⁹⁵ Israelachvili, J. N. *Accounts Chem. Res.* **1987**, *20*, 415–421.

¹⁹⁶ Israelachvili, J. N. *Chemtracts-Analy. Phys. Chem.* **1989**, *1*, 1–12.

¹⁹⁷ Prieve, D. C.; Frej, N. A. *Langmuir* **1990**, *6*, 396–403.

¹⁹⁸ Prieve, D. C.; Bike, S. G.; Frej, N. A. *Faraday Discuss. Chem. Soc.* **1990**, *90*, 209–222.

¹⁹⁹ Hansma, P. K.; Elings, V. B.; Marti, O.; Bracker, C. E. *Science* **1988**, *242*, 209–216.

²⁰⁰ Rugar, D.; Hansma, P. K. *Physics Today* **1990**, *October*, 23–30.

²⁰¹ Ducker, W. A.; Senden, T. J.; Pashley, R. M. *Langmuir* **1992**, *8*, 1831–1836.

²⁰² Ducker, W. A.; Senden, T. J.; Pashley, R. M. *Nature* **1991**, *353*, 239–241.

²⁰³ Clark, S. C.; Waltz, J. Y.; Ducker, W. A. *Langmuir* **2004**, *20*, 7616–7622.

²⁰⁴ Hunter, R.J. *Foundations of Colloid Science*; Oxford University Press: New York, 1995; Vol. 1, Chapter 4.

assumed to be unaffected by the presence of all other molecules. The macroscopic theory of Lifshitz corrects this assumption. Macroscopic theory of Lifshitz^{205,206} is based on the idea that the interaction between macrobodies in a medium is propagated as an electromagnetic wave. Each macroscopic body is regarded as a collection of many oscillating dipoles that are continuously radiating and absorbing energy from *all of their neighbors*. The vdW interaction between two macrobodies originates from the electromagnetic waves that leak from the surface of the two neighboring bodies. There is maximum absorption of energy when dipoles in each body generate electromagnetic fields at the same frequencies. This is the reason why the vdW interaction energy is always attractive between macrobodies of the same type.

Both the London²⁰⁷ and the non-retarded Lifshitz theory give the same vdW interaction energy relations as a function of separation between two bodies of same type:

$$\text{Two spheres: } E(S) = -\frac{A}{6S} \left(\frac{R_1 R_2}{R_1 + R_2} \right) \quad (1.6)$$

$$\text{Two flat surface: } E(S) = -\frac{A}{12\pi S^2} \quad (1.7)$$

where R_1 and R_2 are the radii of the spheres, and A is the Hamaker constant. The two theories differ in the way they calculate the Hamaker constant. For London theory, calculation of A is simple; one simply adds up all the contributions. For Lifshitz theory, calculation of A is not trivial, involving the knowledge of the whole absorption spectrum of the body under investigation, therefore the details will not be given here. Hamaker constants for substances immersed in water are in the range $30\text{--}10 \times 10^{-20}$ J for metals, $6\text{--}1 \times 10^{-20}$ J for oxides, 0.3×10^{-20} J for hydrocarbons.

The equations above are valid only when the molecules are close to one another. However, as the bodies move away from another, there is a finite propagation travel time for the electromagnetic waves, which causes the polarizations in each surface to lose their

²⁰⁵ Lifshitz, E. M.; *Sov. Phys. JETP*. **1956**, *2*, 73–83.

²⁰⁶ Dzyaloshinski, I. E.; Lifshitz, E. M.; Pitaevski, L. P. *Adv. Phys.* **1961**, *10*, 165.

²⁰⁷ Hamaker, H. C. *Physics* **1937**, *4*, 1058–1072.

phase coupling and therefore results in a reduction in the magnitude of the interaction energy. This is called *retardation*.

1.6.2. Electrostatic Double Layer Forces

Most surfaces in *water* acquire a surface charge by the selective dissociation of ions from the surface into solution or by adsorption of ions from solution onto the surface, because the high dielectric constant of water reduces the coulombic interactions between charges/ions. The surface charge, σ_0 , is balanced by an equal but an oppositely charged layer of ions (counterions) in the solution. Some of these counterions are bound loosely onto the surface forming what is called a Stern or Helmholtz layer, and some of them form a diffuse atmosphere in the vicinity of the surface, known as the diffuse part of the double-layer (See Figure 1.9).²⁰⁸ The distance over which this double layer merges into the bulk solution is called the Debye length.

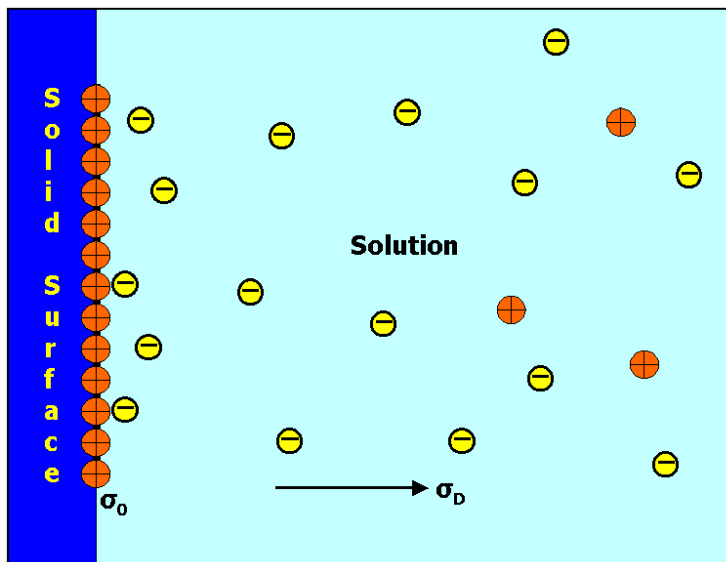


Figure 1.9 Surface charge and diffuse part of the double-layer. The σ_0 and σ_D represent the surface charge and the diffuse double-layer charge ($\sigma_0 = -\sigma_D$).

When two surfaces with double-layers of like sign approach one another, there is a repulsive interaction as the two double-layers begin to overlap with each other. This

²⁰⁸ Israelachvili, J. *Intermolecular and Surface Forces*; Academic Press: San Diego, 1992; Chapter 12.

repulsion can be understood through the free energy increase when the overlap occurs.²⁰⁹ There are two contributions: a positive enthalpic change and a negative entropic change. The enthalpic contribution comes from the repulsion of similarly charged species and the entropic contribution comes from the fact that the ions are constrained in a smaller volume when the two surfaces are brought together. At equilibrium, force is the same everywhere and it is usually calculated at the midplane, where the electrostatic contributions are zero so only the entropic effect has to be considered. This entropic effect is simply the osmotic pressure; when the two surfaces approach one another, the concentration of ions in the gap between the surfaces is higher than the concentration of ions in the bulk. This leads to repulsion as the water molecules in the bulk try to enter the gap. Thus,

$$\Pi = kT \sum_i (\rho_i^{mid} - \rho_i^{bulk}) \quad (1.8)$$

where Π is the repulsive pressure or the difference in the osmotic pressure between the mid plane and the bulk, k is the Boltzmann constant, T is the absolute temperature, ρ_i^{mid} and ρ_i^{bulk} are the concentration of the ion, i , at the mid plane and in the bulk, respectively.

The concentration of ions at the mid plane, where the potential is Ψ_m , can be determined by solving the Poisson-Boltzmann, PB, equation. For a $Z:Z$ electrolyte:

$$\frac{d^2 \psi}{dS^2} = -\frac{e}{D \epsilon_0} \sum_i \rho_i^{mid} = -\frac{e}{D \epsilon_0} Z \rho_{bulk} \left[\exp\left(-\frac{Z \psi_m e}{kT}\right) - \exp\left(\frac{Z \psi_m e}{kT}\right) \right] \quad (1.9)$$

where S is the distance between the two surfaces, D is the dielectric constant of the medium, ϵ_0 is the dielectric permittivity of vacuum, and e is minus the charge on an electron. In this thesis, the PB equation has been solved numerically, but some appreciation for the form of the solution can be gained from the analytical solution to the low potentials, $e \Psi/kT \ll 1$. The solution is,

²⁰⁹ Hunter, R.J. *Foundations of Colloid Science*; Oxford University Press: New York, 1995; Vol.1, Chapter 7.

$$\psi(S) = \psi_0 \exp(-\kappa S) = \psi_0 \exp\left(-\frac{S}{\kappa^{-1}}\right) \Rightarrow \psi_m = 2\psi_0 \exp\left(-\frac{S}{2\kappa^{-1}}\right) \quad (1.10)$$

where the κ^{-1} is the Debye length and Ψ_m is calculated assuming that the total potential at the mid plane is the sum of the potentials for each isolated surface.

$$\kappa^{-1} = \sqrt{\frac{D\varepsilon_0 kT}{2\rho_{bulk} Z^2 e^2}} \quad (1.11)$$

By inserting Ψ_m in the Boltzmann equation, the total concentration of each ion at the mid plane can be determined. The final form of the pressure between the two plates is given in eq 1.12.

$$\Pi = 2D\varepsilon_0 \kappa^2 \psi_0^2 \exp\left(-\frac{S}{\kappa^{-1}}\right) \quad (1.12)$$

Since the pressure has the units of energy per unit volume or force per unit area, the energy per unit area is found by integrating the pressure with respect to the distance between the two surfaces. For low potentials, the energy per unit area between flat sheets is given below.

$$E(S) = -\int_{\infty}^S \Pi d(S) = 2D\varepsilon_0 \kappa \psi_0^2 e^{-S/\kappa^{-1}} \quad (1.13)$$

1.6.3. DLVO Theory

As mentioned in the previous sections, the vdW interaction is always present among macrobodies and it is always attractive between similar bodies. If the surfaces are charged, there is also the contribution of the repulsive electrostatic double-layer forces. The sum or the combination of the van der Waals interaction and the electrostatic double layer interaction to produce the total interaction energy is known as the DLVO

theory.^{210,211} For flat surfaces, at low surface potentials, the total interaction energy per unit area can be written as:

$$E_{total}(S) = -\frac{A}{12\pi S^2} + 2D \varepsilon_0 \kappa \psi_0^2 e^{-\kappa S} \quad (1.14)$$

Figure 1.10 shows the vdW and electrostatic forces and the total interaction energy.

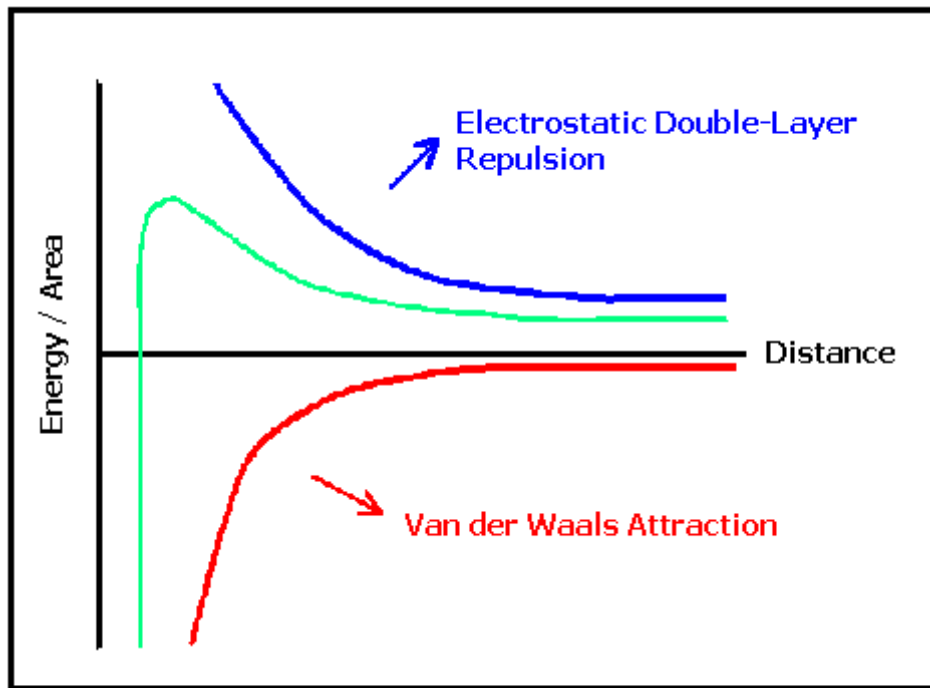


Figure 1.10 The green curve shows the total energy per unit area between two surfaces. According to the DLVO theory, the total interaction is the sum of the vdW and electrostatic double-layer energies.

It is important to realize that Ψ_0 is not necessarily independent of S . The Ψ_0 on an isolated surface arises because of the association or dissociation of ions. In the vicinity of a second surface, the degree of association/dissociation depends on the electric fields

²¹⁰ Derjagin, B. V.; Landau, L. *Acta Phys. Chim. URSS* **1941**, *14*, 633–662.

²¹¹ Verwey, E. J. W.; Overbeek, J. Th. G. *Theory of the Stability of Lyophobic Colloids*; Amsterdam: Elsevier, 1948.

emanating from the second surface. Generally, this effect is insignificant for $S > \kappa^{-1}$ and Ψ_0 can be measured. For $S < \kappa^{-1}$ one must know the charge regulation of the surfaces.

Using DLVO theory, the interaction energies between surfaces can be predicted and they were found to be in good agreement with experimental results.²¹² An important point to keep in mind while performing a DLVO analysis is that the interaction between charged surfaces can be either at constant surface potential, or at constant charge or charge regulated. So, one can use either of these assumptions to predict the energy profile between two surfaces. Usually these fits are not accurate below one decay length of the forces measured. The poor fit is probably a result of the presence of other short range forces in experimental measurements, like solvation and short-range steric forces, which are not taken into account in the DLVO theory.

1.6.4. Steric-Polymer Forces

The vdW and double-layer electrostatic forces are well-established and well studied in the literature. Therefore in the previous sections, a brief introduction of the theory behind these forces was given without a review of the experimental studies. This is not the case for steric-polymer forces. In fact, there is not a single theory^{89,84,213,214,215} like DLVO theory to predict the quantitative energy profiles of steric-polymer interactions. Hunter²¹⁶ attributes this to two reasons: first being the dependence of the theory to other semi-quantitative theories of polymer solution thermodynamics, and second being the dependence of the theory on the prediction of the conformation of polymers attached to a planar interface and at the same time confined between two surfaces. Therefore here, I give a review of the experimental force measurements carried out in the presence of polymers and between polymer brush covered surfaces prepared through the adsorption of diblock copolymers on surfaces.

²¹² Ducker, W. A.; Senden, T. J.; Pashley, R. M. *Langmuir* **1992**, *8*, 1831–1836.

²¹³ de Gennes, P. G. *Adv. Colloid Interface Sci.* **1987**, *27*, 189–209.

²¹⁴ Oshima, H. *Colloid Polym. Sci.* **1999**, *277*, 535–540.

²¹⁵ Huang, H.; Ruckenstein, E. *J. Colloid Interface Sci.* **2004**, *273*, 181–190.

²¹⁶ Hunter, R. J. *Foundations of Colloid Science*; Oxford University Press: New York, 1995; Vol. 1, Chapter 8.

The first well-defined direct force measurements on adsorbed polymer layers were made on PS adsorbed on mica from cyclohexane (a poor solvent) by Klein.^{217,218} They have reported an attraction between layers. Israelachvili et al.^{219,220} have published the first data on forces between polymer layers in a good solvent, water, for PEO layers. They have observed long-range repulsive forces between PEO covered surfaces on mica and a hysteresis in the force profiles. The results of these studies can be rationalized theoretically on the basis of the Flory^{221,222} theory through the expression given by Napper²²³ for the free energy of mixing ΔG_m ,

$$\Delta G_m \propto (0.5 - \chi)\Phi(z, d) \quad (1.15)$$

where $\Phi(z, d)$ is a geometric overlap term which depends on the plate separation and the detailed form of the volume fraction profile of the polymer, and χ is the Flory-Huggins parameter.²²⁴ In a poor solvent, $\chi > 0.5$ and the free energy term is negative, i.e. the layers are attractive; whereas in a good solvent, $\chi < 0.5$ and the free energy is positive and the layers repel one another. At low surface coverages,²²⁵ an attractive bridging force due to polymer chains simultaneously adsorbing on both surfaces can also be present in forces between adsorbed polymer layers, even at good solvent conditions.²²⁶

There have been numerous studies done on the forces between polymer layers.²²⁷ My main interest is in the effect of the diblock copolymer adsorption on the interaction forces between surfaces, so the rest of this review covers the forces in the presence of diblock copolymers and forces between polymer brushes.

²¹⁷ Klein, J. *Nature* **1980**, 288, 248–250.

²¹⁸ Klein, J. *J. Chem. Soc. Faraday Trans. 1* **1983**, 79, 99–118.

²¹⁹ Israelachvili, J. N.; Tandon, R. K.; White, L. R. *Nature*, **1979**, 277, 120–121.

²²⁰ Israelachvili, J. N.; Tandon, R. K.; White, L. R. *J. Colloid Interface Sci.* **1980**, 78, 430–443.

²²¹ Flory, P. J. *Principles of Polymer Chemistry*; Cornell University Press: Ithaca, 1953.

²²² Flory, P. J. *Statistical Mechanics of Chain Molecules*, Interscience: New York, 1969.

²²³ Napper, D.H. *Polymeric Stabilization of Colloidal Dispersions*; Academic Press: London, 1983.

²²⁴ Cosgrove, T.; Luckham, P. F.; Richardson, R. M.; Webster, J. R. P.; Zarbakhsh, A. *Colloids Surf., A* **1994**, 86, 103–110.

²²⁵ Almog, Y.; Klein, J. *J. Colloid Interface Sci.* **1985**, 106, 33–44.

²²⁶ Klein, J.; Luckham, P. F. *Nature* **1984**, 308, 836–837.

²²⁷ For reviews see:

Patel, S. S.; Tirrell, M. *Annu. Rev. Phys. Chem.* **1989**, 40, 597–635.

Ploehn, H. J.; Russell, W. B. *Adv. Chem. Eng.* **1990**, 15, 137–228.

1.6.4.1. Forces between Polymer Brushes

When two polymer brush layers on surfaces approach each other, they experience a force once the tails of the adsorbed polymers begin to overlap with each other. This leads to a repulsive force due to the unfavorable entropy associated with compressing the chains and due to the rise in the osmotic pressure in the gap between the surfaces.²²⁸ This is the origin of the steric forces observed between polymer brush covered surfaces. These forces have been measured with the aid of surface forces apparatus and atomic force microscopy.

1.6.4.1a. Measurements with Surface Forces Apparatus

Hadziioannou et al.^{229,230} were the first to study the forces between polymer brushes, through the adsorption of diblock copolymers on mica, using a conventional surface force apparatus. Their system was a PVP-PS block copolymer adsorbed onto mica from toluene and force measurements were made in toluene (a good solvent) and cyclohexane (a theta solvent). The forces were monotonically repulsive in both solvents, but shorter ranged in cyclohexane than in toluene. Under the same conditions in cyclohexane, the force between adsorbed (homopolymer) PS layers was found to be attractive.²³¹ Monotonic repulsive forces have also been measured between PVP-poly(tert-butylstyrene) adsorbed on mica by Ansarifar and Luckham.²³²

Taunton et al.^{233,234} have measured steric forces that arose when an end-functionalized PS adsorbed on mica in toluene and xylene. The PS chain had either a zwitterionic head group or a small PEO block that grafts the PS chain on mica surface. They have observed repulsion beginning at separations corresponding to 12–14 R_g over the molecular weights they have studied. They have found that their data could be well fit both by scaling and mean-field predictions, because they have seen a linear dependence of the adsorbed layer thickness on molecular weight. They have also observed a repulsion between surfaces only one of which was covered with the polymer brush. However, when

²²⁸Israelachvili, J. *Intermolecular and Surface Forces*; Academic Press: San Diego, 1992; Chapter 14.

²²⁹Hadziioannou, G.; Patel, S.; Granick, S.; Tirrell, M. *J. Am. Chem. Soc.* **1986**, *108*, 2869–2876.

²³⁰Tirrell, M.; Patel, S.; Hadziioannou, G. *Proc. Natl. Acad. Sci. USA* **1987**, *84*, 4725–4728.

²³¹Israelachvili, J. N.; Tirrell, M.; Klein, J.; Almog, Y. *Macromolecules* **1984**, *17*, 204–209.

²³²Ansarifar, A.; Luckham, P. F. *Polymer* **1988**, *29*, 329–335.

²³³Taunton, H. J.; Toprakcioglu, C.; Fetters, L. J.; Klein, J. *Macromolecules* **1990**, *23*, 571–580.

²³⁴Taunton, H. J.; Toprakcioglu, C.; Fetters, L. J.; Klein, J. *Nature* **1988**, *332*, 712–714.

a homopolymer was adsorbed to one of the surfaces, an attractive force has been previously reported.²³⁵ A similar study was done by Raviv et al.²³⁶ with a quaternary ammonium functionalized PEO.

Watanabe et al.²³⁷ have done measurements of the forces between PVP-PS and PVP-PI covered surfaces adsorbed on mica from toluene. In symmetric systems, PVP-PS vs. PVP-PS and PVP-PI vs. PVP-PS in toluene, they have observed monotonic repulsion. In asymmetric systems, PVP-PS vs. PVP-PI with same molecular weights of PVP, PS and PI blocks, (PS and PI are strongly immiscible in bulk and phase separate in toluene), there was no significant difference among the force curves of symmetric systems and asymmetric systems.

Cosgrove et al.²³⁸ have studied the effect of the solvent quality on the interaction forces between PVP-PS covered mica surfaces. The adsorption was done in toluene, a good solvent, and the forces were found to be purely repulsive. Cyclohexane at 24 °C is about 10 °C below the theta temperature of PS and the force curves were attractive.

Schillen et al.²³⁹ have also measured long-range steric forces between PEO-PBO covered hydrophobized mica in water. The range of these forces indicated the presence of extended chains as predicted qualitatively by the theoretical calculations they have performed based on the theory of Scheutjens and Fleer.⁸⁶

1.6.4.1b. Measurements with Atomic Force Microscopy

Kelley et al.²⁴⁰ have measured the interaction forces between a Si₃N₄ tip and a polymer brush surface. They have studied a neutral polymer brush and a polyelectrolyte brush formed from the adsorption of PVP-PS and poly(tert-butylstyrene)–sodium poly(styrenesulfonate), PtBS-NaPSS, on mica, respectively. They have observed steric forces in good solvent conditions, i.e. toluene for PS and water for NaPSS. The range of the forces decreased upon salt addition for the polyelectrolyte brushes. However, the

²³⁵ Granick, S.; Patel, S.; Tirrell, M. *J. Chem. Phys.* **1986**, *85*, 5370–5371.

²³⁶ Raviv, U.; Frey, J.; Sak, R.; Laurar, P.; Tadmor, R.; Klein, J. *Langmuir* **2002**, *18*, 7482–7495.

²³⁷ Watanabe, H.; Tirrell, M. *Macromolecules* **1993**, *26*, 6455–6466.

²³⁸ Cosgrove, T.; Phipps, J. S.; Richardson, R. M.; Hair, M. L.; Guzonas, D. A. *Colloids Surf., A* **1994**, *86*, 91–101.

²³⁹ Schillen, K.; Claesson, P. M.; Malmsten, M.; Linse, P.; Booth, C. *J. Phys. Chem B* **1997**, *101*, 4238–4252.

²⁴⁰ Kelley, T. M.; Schorr, P. A.; Johnson, K. D.; Tirrell, M.; Frisbie, C. D. *Macromolecules* **1998**, *31*, 4297–4300.

decay lengths were not comparable with the calculated debye lengths, for example in 0.1 M and 1 M salt where the debye lengths are ~ 1 nm and ~ 0.3 nm, respectively; the measured decay lengths were approximately 7 nm and 3nm, respectively. Therefore, the origin of these forces was not electrostatic but steric and the polyelectrolyte brush shrank with increase in salt concentration. Balastre et al.²⁴¹ have also studied the steric forces between PtBS-NaPSS brushes on hydrophobized mica (with SFA) and had similar conclusions.

Butt et al.²⁴² have measured steric forces between a Si_3N_4 tip and a PS brush covalently-anchored on silicon, and PMMA-PEO brush physisorbed on alumina at various temperatures. In the case of PS, the forces in cyclohexane were repulsive and their range and magnitude increased roughly linearly with temperature as the solvent changed from being a poor to a good solvent, indicating that the steric force was entropic in origin. The force curves changed from being attractive with bare alumina in water to being repulsive in the presence of PMMA-PEO. However, there was no temperature dependence in the range 19–52.5 °C due to the fact that the radius of gyration of PEO does not change in water in that temperature range.

There have also been studies with AFM force measurements on graft-polymerized surfaces,^{243,244} however the polymer brushes formed that way are more dense and beyond the scope of this review. As an example, Yamamoto et al.^{245,246} have used AFM to measure forces between a very high-density PMMA brush (2.5 nm^2 per chain) and a silica probe in toluene as a function of chain length and grafting density. These forces cannot be explained by the earlier scaling relations, which are true for moderately dense brushes formed mainly from diblock copolymers.

²⁴¹ Balastre, M.; Li, F.; Schorr, P.; Yang, J.; Mays, J. W.; Tirrell, M. V. *Macromolecules* **2002**, *35*, 9480–9486.

²⁴² Butt, H-J.; Kappl, M.; Mueller, H.; Raiteri, R. *Langmuir* **1999**, *15*, 2559–2565.

²⁴³ Kidoaki, S.; Ohya, S.; Nakayama, Y.; Matsuda, T. *Langmuir* **2001**, *17*, 2402–2407.

²⁴⁴ Vermette, P.; Meagher, L. *Langmuir* **2002**, *18*, 10137–10145.

²⁴⁵ Yamamoto, S.; Ejaz, M.; Tsiji, Y.; Fukuda, T. *Macromolecules* **2000**, *33*, 5602–5607.

²⁴⁶ Yamamoto, S.; Ejaz, M.; Tsiji, Y.; Fukuda, T. *Macromolecules* **2000**, *33*, 5608–5612.

CHAPTER 2: DECAY LENGTHS OF DOUBLE-LAYER FORCES IN SOLUTIONS OF PARTLY-ASSOCIATED IONS*

2.1. Introduction

Electrostatic double-layer forces are one of the principal determinants of colloid stability.¹ These forces can be calculated by solving the Poisson–Boltzmann equation and have been accurately measured using the surface forces apparatus² or an atomic force microscope.³ The range of the double-layer force between colloidal particles depends on the concentration of electrolyte in solution. For weak interactions between identical particles, the force is repulsive and decays exponentially with distance. This decay length is known as the Debye length, κ^{-1} . For a symmetrical electrolyte, the Debye length is given by the following equation,

$$\kappa^{-1} = \left\{ \frac{kT\varepsilon_0 D}{2Z^2 e^2 \rho(\text{bulk})} \right\}^{1/2} \quad (2.1)$$

where k is the Boltzmann constant, T is the absolute temperature, ε_0 is the vacuum permittivity, D is the dielectric constant of the solution, Z is the absolute value of the valency of the cation or the anion, e is the charge on a proton, and $\rho(\text{bulk})$ is the bulk concentration of the electrolyte. This equation accurately predicts the change in measured decay length for dilute electrolyte solutions, for example, 10^{-3} mol L⁻¹ NaCl.^{2,3}

In this study, I examine whether eq 2.1 provides satisfactory agreement with experimental measurements in solutions where the ions are partly associated, either with a counterion (the acids) or with counter- and co-ions (the surfactants). I use known

* This chapter has been reproduced in part with permission from Tulpar, A.; Subramanian, V.; Ducker, W. *Langmuir* **2001**, *17*, 8451–8454. Copyright 2001 American Chemical Society.

¹ Hunter, J. R. *Foundations of Colloid Science*; Oxford University Press: New York, 1986; Vol.1, Chapter 2.

² Israelachvili, J.N.; Adams, G. E. *J. Chem. Soc., Faraday Trans. 1* **1978**, *74*, 975–1001.

³ Ducker, W. A.; Pashley, R. M.; Senden, T. J. *Nature* **1991**, *353*, 239–241.

values of the equilibrium constant in bulk or measurements of activity to determine the ion density.

This study follows more complex issues raised in a recent paper by Kohonen et al.⁴ They also examined whether the activity of an ion should be used in eq 2.1. There is not a universally adopted system of assigning activities for weak electrolytes. Kohonen et al. have used the scheme of Davies,⁵ where the activity coefficient, γ_{\pm} , is used to encompass both the non-ideality of the dissociated ions and the incomplete dissociation of weak electrolytes. For example, for symmetric, Z:Z, electrolytes,⁵

$$\gamma_{\pm} = f_{\pm}\alpha \text{ and } a_{\pm} = \gamma_{\pm}c \quad (2.2)$$

where α is the fraction of free ions, f_{\pm} is the mean ionic activity coefficient of the dissociated ions (which can, for example, be estimated from Debye-Hückel theory), a_{\pm} is the activity, and c is the total concentration of neutral and charged species. The advantage of this approach is that sometimes it is difficult to distinguish incomplete dissociation from non-ideality of individual ions. This convention is also used here. (Other authors use the symbol γ_{\pm} for the activity co-efficient of the dissociated ion.⁶)

Here I set aside the issue of whether f_{\pm} should be included in the Debye length expressions. There are few circumstances where both f_{\pm} deviates from unity and the double-layer has a significant width. (In any case, the mean-field and point ion approximations of traditional double-layer theory begin to fail under these circumstances.) Instead, the focus here is on whether α can be used to calculate Debye lengths. In natural organic material, many organic acids and bases are incompletely dissociated. Surfactants, which are common in colloidal systems, are also often partially associated into micelles. Intuition suggests that only the dissociated ions should be included in Debye length calculations.

I have measured the force on a colloidal particle in a monoprotic weak-acid solution at a concentration where α is small, f_{\pm} is close to unity, and decay lengths are long enough to measure accurately. I compare decay lengths measured experimentally to

⁴ Kohonen, M. K.; Karaman, M.E.; Pashley, R. *Langmuir* **2000**, *16*, 5749–5753.

⁵ Davies, C.W. *Ion Association*; Butterworth: Washington, 1962; p. 36.

⁶ Atkins, P.W. *Physical Chemistry*; Oxford University Press: New York, 1995.

decay lengths calculated from eq 2.1 where $\rho(\text{bulk})$ is calculated in one of two ways: (1) from the total concentration (assuming $\alpha = 1$) and (2) from the concentration of dissociated ions using known equilibrium constants or measured activity coefficients. The second method is described by the following equation:

$$\kappa^{-1} = \left\{ \frac{kT\epsilon_0 D}{2Z^2 e^2 \alpha(\text{bulk}) \rho(\text{bulk})} \right\}^{1/2} \quad (2.3)$$

I show, as expected, that only the dissociated ions should be included in the Debye length calculations.

If α values are used to obtain Debye lengths, then a method is required for obtaining α . Pashley and Ninham⁷ have used estimates of α from conductivity measurements to correct Debye length calculations in ionic surfactant solutions for the partial association of surfactant molecules into micelles. For hexadecyltrimethylammonium bromide (C_{16}TABr) solutions, they find that the measured decay length is accurately predicted when the bulk concentration in eq 2.1 is replaced by an estimate of the concentration of unassociated ions. That is, above the cmc,

$$\kappa^{-1} = \left\{ \frac{kT\epsilon_0 D}{Z^2 e^2 (2\rho_{cmc} + (\rho_s - \rho_{cmc})\beta)} \right\}^{1/2} \quad (2.4)$$

where ρ_{cmc} is the concentration at the cmc, ρ_s is the concentration of the solution and β is the fraction of counterions not bound to micelles in the bulk solution. This analysis relies on experimentally determined values of β . Although α does not occur explicitly in eq 2.4, $(2\rho_{cmc} + (\rho_s - \rho_{cmc})\beta)$ is the concentration of unassociated ions in solution. The highly charged micelles are assumed to make no contribution because of the very small concentration near the similarly charged surfaces.

Results of activity measurements (from ion selective electrodes, osmotic pressure experiments, etc.) can also be used to determine α . As stated earlier, for most cases when

⁷ Pashley, R. M.; Ninham, B.W. *J. Phys. Chem.* **1987**, *91*, 2902–2904.

double-layer forces are measured, $f_{\pm} \sim 1$, so the degree of dissociation can be obtained directly from the activity coefficient. For Z:Z electrolytes, the degree of dissociation is equal to the mean activity coefficient when $f_{\pm} = 1$. This suggests that for many cases relevant to colloid science the activity coefficient can be used to calculate the Debye length:

$$\kappa^{-1} = \left\{ \frac{kT\epsilon_0 D}{2Z^2 e^2 a_{\pm}} \right\}^{1/2} \quad \text{for } f_{\pm} = 1 \quad (2.5)$$

In this study, I present results of force measurements in sodium dodecyl sulfate (SDS) and dodecyltrimethylammonium bromide ($C_{12}TABr$) solutions. Forces in SDS solutions have also been described previously. Hair et al.⁸ have measured forces between mica sheets in SDS solutions above the cmc. Analysis using eq 3 yields $\beta = 0.25$. Bard et al.⁹ have also measured decay lengths of SDS solutions. They observe an increase in decay length at the cmc and attribute it to binding of Na^+ ions to the surface of the micelles. The extra binding would mean a decrease in free Na^+ ion concentration on addition of Na^+ , which contradicts results from ion activity measurements.

2.2. Experimental Section

2.2.1. Materials

SDS (Sigma, St. Louis, MO) was recrystallized twice from ethanol and dodecyltrimethylammonium bromide ($C_{12}TABr$) (Aldrich, Milwaukee, WI) was recrystallized three times from acetone. Glacial acetic acid (Fischer Scientific, Pittsburgh, PA) and formic acid (Aldrich, Milwaukee, WI) were used without further purification. Solutions were prepared with 18.3M Ω deionized, charcoal-filtered water (EASYpure UV, Barnstead Thermolyne Corp., Dubuque, IA). SDS solutions were used within 1 h of preparation from the solid to prevent formation of dodecanol.

⁸ Hair, M. L.; Marra, J. J. *Colloid Interface Sci.* **1989**, *128*, 511–522.

⁹ Hu, K.; Bard, A. J. *Langmuir* **1997**, *13*, 5418–5425.

2.2.2. Surface Tension Measurements

Surface tension measurements were carried out to check the purity of SDS and C₁₂TABr. The apparatus was a simple rod hanging from a balance onto the free surface of a liquid in a glass crystallizing-dish. The surface tension of the solutions was calculated from the maximum pull on that rod.¹⁰ The surfactant solutions were freshly prepared before each measurement. The room temperature was 22 ± 2 °C. The concentration of surface-active contaminants in SDS and C₁₂TABr was low because surface tension data revealed no minimum in the surface tension versus concentration curves.

2.2.3. Force–Distance Measurements

Force–Distance measurements between a glass sphere (radius~3.5 μm) and a quartz plate were obtained with an AFM (Molecular Imaging, Phoenix, AZ). Quartz plates (Alfa Aesar, Ward Hill, MA) were cut into 2 × 2 × 0.1 cm pieces and were left in 300°C H₂SO₄ for 3 h. They were allowed to cool and then rinsed with purified water. Before being put into the liquid cell, they were dried with N₂. Glass spheres were obtained from Polysciences (Warrington, PA). Silica probe preparation is described elsewhere.¹¹ Immediately before injecting electrolyte solutions, the plate and sphere were cleaned by immersion in ~2 mol L⁻¹ NaOH solution for 1 min then rinsed thoroughly with water. The NaOH was baked overnight at 400°C.

The z-axis of the piezo was calibrated by a silicon calibration reference of 22.0 nm step height (Silicon-MDT, Moscow, Russia). The calibration was cross-checked by measurement of decay length of double-layer forces in 10⁻⁴, 10⁻³ and 10⁻² mol L⁻¹ NaCl solutions before injection of electrolyte solutions. In every case, the measured decay length of the solution was given by eq 1 within 1–3 %. Therefore, force measurements in NaCl solutions can be used to calibrate a piezo-electric crystal during each experiment. The electrolyte solutions were left inside the liquid cell for 15–30 min before data acquisition. The experiments were repeated twice on different days and the decay lengths have been found to be reproducible.

¹⁰ Padday, J.F.; Pitt, A.R.; Pashley, R.M. *Faraday Transactions*, **1974**, 71, 1919–1931.

¹¹ Ducker, W. A.; Senden, T. J.; Pashley, M. *Langmuir* **1992**, 8, 1831–1836.

2.2.4. pH Measurements

Hydrogen ion activities were determined by a pH meter (Orion, Beverly, MA). Measurements were made relative to standard buffers of potassium hydrogen phthalate, pH 4.01 (Orion, Beverly, MA), and potassium tetraoxalate, pH 1.68 (VWR, Bridgeport, NJ).

2.3. Analysis of Raw Data

2.3.1. Force–Separation

Force measurements are done by moving the AFM-piezo in the vertical direction to the surface (there is a separate z-piezo in an AFM) and recording the deflection of the cantilever as a function of this movement. Therefore force measurements from AFM give two columns of data. One of them is the distance that the z-piezo moves, x . The other one is the deflection of the cantilever as it is read from the detector in terms of voltage, V . The former needs to be converted into the separation between the two surfaces and the latter needs to be converted into the force between the two surfaces.

One drawback of AFM force measurements is that it is not possible to measure the zero separation between two surfaces directly. However, there is a region in the force-distance curve where the slope of V versus x stays constant (but not zero). This region is called the constant compliance region, where the two surfaces are assumed to be in contact. The onset of this region is defined as the zero separation, x_0 . There is also a region where the slope of V versus x is zero and this region is defined as zero-force, V_0 . Here, the surfaces are too far apart from each other to exert any force to each other.¹¹ When there is a force acting between the two surfaces, the real separation between them is not equal to $x-x_0$. The additional separation between the surfaces, Δy , can be calculated from the division of $V-V_0$ by the slope of the constant compliance region. The sum of $(x-x_0)$ with Δy gives the true separation between surfaces.

The force that is exerted on the sphere, which is glued to the tip of the cantilever, is the product of the distance that the cantilever deflects upward/downward (Δy) and the spring constant of the cantilever, k . This is the y-axis of a force versus separation graph.

In this study, the decay lengths are determined by fitting a line to the linear region of $\ln(\text{force})$ versus separation plots, at separations greater than one decay length.

2.4. Results

Figure 2.1 shows the forces between a glass sphere and a flat silica sheet in acetic acid solutions. The calculated and measured decay lengths for acetic acid and formic acid solutions are given in Table 2.1 and Table 2.2, respectively. Values for eq 2.1 assume $\alpha = 1$, whereas values for eq 2.3 utilized α calculated from literature values⁶ of the acid dissociation constants, K_a , of acids. Values for eq 2.5 were obtained from pH measurements (to obtain a_{H^+}) and the assumption that $a_{\pm} = a_{H^+}$. According to these results, the decay lengths of the weak acid solutions are predicted by eq 2.3 with an average of 2% error and by eq 2.5 within an average of 4% error. This validates the use of eq 2.3 with bulk values of dissociation.

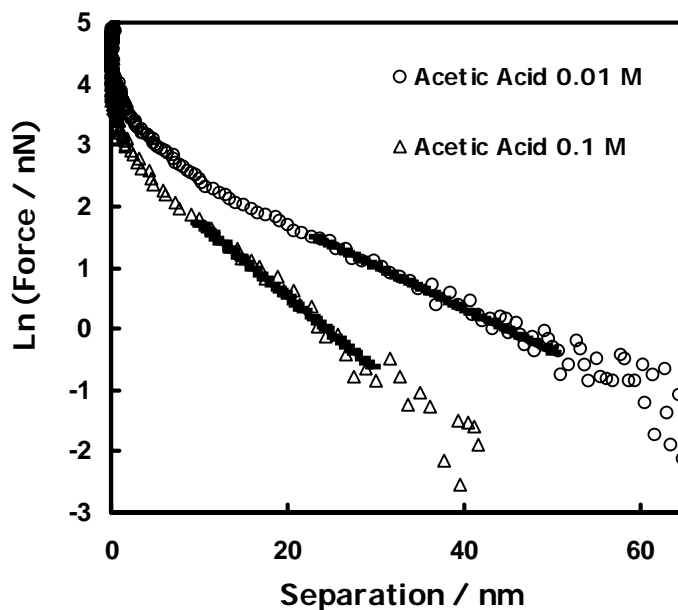


Figure 2.1 Forces between a glass sphere and a silica sheet in acetic acid solutions. The solid lines show the linear fit used to determine the decay lengths.

Table 2.1 Decay lengths in acetic acid solution calculated from equations 2.1,2.3 and 2.5, and measured by experiment.

| Concentration (mol/L) | Eq 2.1 (nm) | Eq 2.3 (nm) | Measured (nm) | Measured pH | Eq 2.5 (nm) |
|-----------------------|-------------|-------------|---------------|-------------|-------------|
| 0.01 | 3.03 | 14.8 | 14.6 | 3.42 | 15.5 |
| 0.1 | 0.958 | 8.22 | 8.35 | 2.90 | 8.54 |

Table 2.2 Decay lengths in formic acid solution calculated from equations 2.1,2.3 and 2.5, and measured by experiment.

| Concentration (mol/L) | Eq 2.1 (nm) | Eq 2.3 (nm) | Measured (nm) | Measured pH | Eq 2.5 (nm) |
|-----------------------|-------------|-------------|---------------|-------------|-------------|
| 0.001 | 9.58 | 16.3 | 14.8 | 3.47 | 16.5 |
| 0.01 | 3.03 | 8.48 | 8.24 | 2.89 | 8.44 |

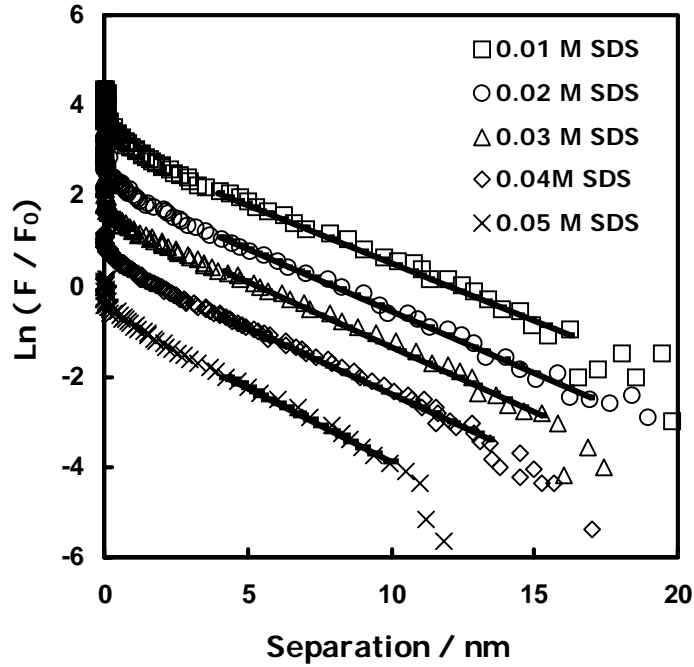


Figure 2.2 Forces between a glass sphere and a silica sheet in 0.01 M, 0.02 M, 0.03 M, 0.04 M, and 0.05 M SDS solutions. The forces vary little between concentrations so I have displaced each curve by dividing the forces by a constant, F_0 . F_0 is e^0 , e^1 , e^2 , e^3 , e^4 and e^5 , respectively for the SDS concentrations. The solid lines show the linear fit used to determine the decay lengths.

Figure 2.2 shows the forces between a glass sphere and a flat silica sheet in SDS solutions. The measured decay lengths for SDS and C₁₂TABr solutions are shown in Figure 2.3. In both SDS and C₁₂TABr solutions, the decay length decreases according to eq 2.1 ($\alpha = 1$) below the cmc and more slowly with concentration above the cmc. Only the data above the cmc will be discussed.

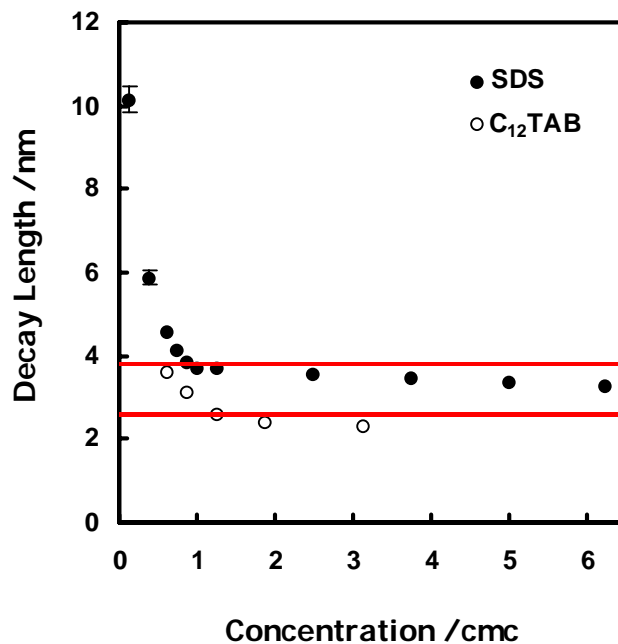


Figure 2.3 Decay lengths of SDS and C₁₂TABr solutions. The red lines show the decay length at the cmc. Where error bars are not shown, the error lies within the symbol.

Figure 2.4 and Figure 2.5 show the experimental decay lengths for SDS and C₁₂TABr solutions from Figure 2.2 divided by the calculated decay lengths as a function of the concentration normalized to the cmc.

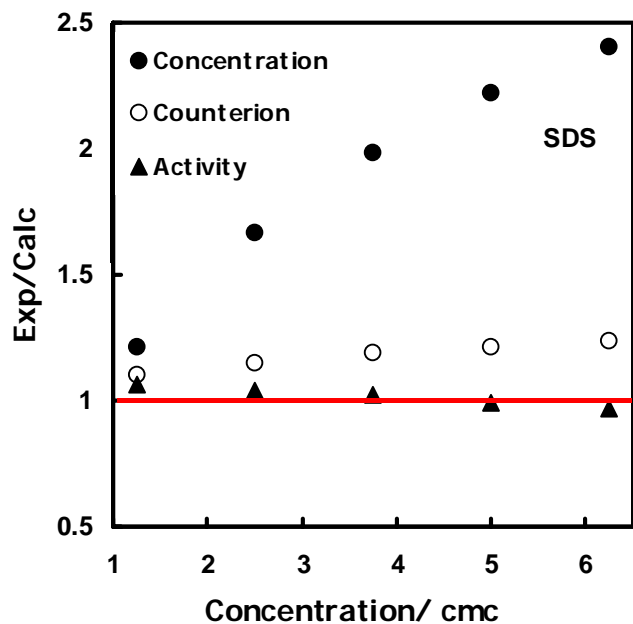


Figure 2.4 Ratio of Experimental:Calculated values of decay lengths for SDS.

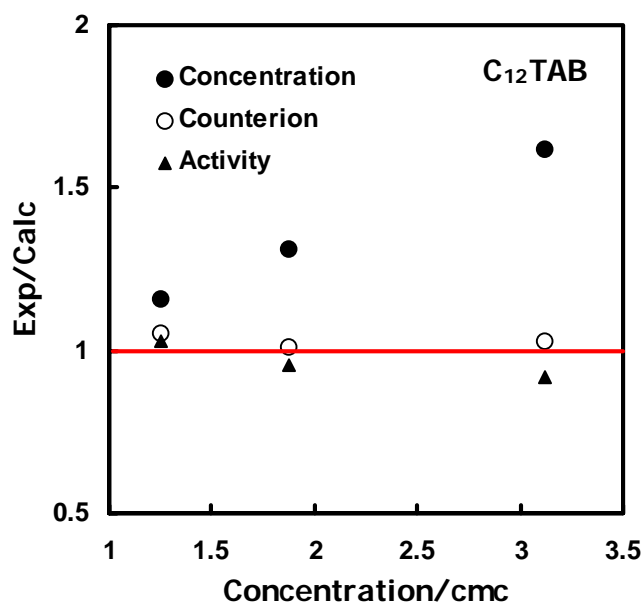


Figure 2.5 Ratio of Experimental:Calculated values of decay lengths for C₁₂TABr.

The calculated decay lengths have been obtained in three ways:

- (1) Ignoring association (eq 2.1),
- (2) by replacing the concentration in eq 2.1 with an estimated concentration of ions that are not bound to the micelle based using $\beta = 0.25$ (eq 2.4),

(3) by replacing the concentration in eq 1 with the measured activity^{12,13} (eq 2.5)

Clearly, eq 2.1 is not a good predictor of the experimental decay length, whereas eqs 2.4 and 2.5 do provide good predictions of decay lengths. The close agreement between eq 2.4 and eq 2.5 is not surprising because they both attempt to convert the nominal concentration into the concentration of unassociated ions.

2.5. Discussion

The degree of dissociation, α , can deviate significantly from 1 and is easy to calculate (from the equilibrium constant or the activity), and its incorporation into expressions for the Debye length leads to good agreement with experiment. This suggests that eq 2.3 should be used when the equilibrium constant is available. We have also shown, phenomenologically, that the activity can be used to predict the Debye length in surfactant solutions (eq 2.5). Calculation of the decay lengths in surfactant solutions is complicated by the existence of multiple equilibria involving multivalent ions, but apparently the activity is a measure of the degree of the dissociation of the surfactant in solution.

Given the good agreement between eq 2.3 and my experimental data, it is worthwhile to briefly consider the conditions under which solutions to the Poisson–Boltzmann equation (See eq 1.9) yield a force that decays according to eq 2.3. Only dissociated ions contribute to the ion density in the Poisson equation, so the ion density (ρ_{bulk}) is reduced by a factor α . Incorporation of α is simple and obvious at low surface potentials: the potential (See eq 1.10) also decays according to eq 2.3. The pressure is calculated from the concentration at the midplane, which is in turn calculated from the potential. (See Section 1.4.2.) Thus the change in decay of the potential causes the same change in decay of the pressure and the interaction energy per unit area (See eqs 1.12 and 1.13).

¹² Cutler, S. G.; Meares, P.; Hall, D.G. *J. Chem. Soc., Faraday Trans. 1* **1978**, 74, 1758–1767.

¹³ De Lisi, R.; Fisticaro, E.; Milioto, S. *J. Solution Chem.* **1988**, 17, 1015–1041.

2.6. Conclusion

Using a weak acid, I have shown that incomplete dissociation of ions should be accounted for in Debye length calculations and therefore that part of the Davies' activity co-efficient (α) should be included in the Debye-length calculation. Clearly, the Debye length should be calculated from some estimate of the actual concentration of ions present and should not include neutralized species. When $f_{\pm} = 1$, activity data provide a means to estimate the actual concentration. In fact, f_{\pm} is very close to 1 for most cases when the surface potential can be measured. Corrections to the nominal concentration using the degree of association in bulk solution from conductivity measurements or the activity are similar, and both provide good estimates of Debye lengths in surfactant solutions.

The good agreement between experimental results and simple equations for decay lengths suggests that decay lengths can be used for estimating bulk solution properties. The equilibrium constant of weak symmetrical electrolytes can be obtained from measurement of the decay of double-layer forces. Apparently, the mean activity of surfactant solutions above the cmc can also be estimated from the decay of colloidal forces.

CHAPTER 3: SURFACTANT ADSORPTION AT SOLID-AQUEOUS INTERFACES CONTAINING FIXED CHARGES*

3.1. Introduction

Surfactant adsorption is widely used to achieve changes in wetting, colloidal properties, and lubrication. Many surfactants are charged, and it is well-known that the charge on the solid–liquid interface affects the amount of adsorption, the shape of the adsorption isotherm,^{1,2,3} and the organization of the adsorbed surfactant molecules.⁴ The adsorption of cationic surfactants to solid-aqueous interfaces has recently been reviewed.⁵ However, to date there has not been a study of the adsorption of surfactants in which the magnitude and or the distribution of surface charges has been controlled independently of the surfactant adsorption. The reason is that, for most solid–liquid interfaces, the interfacial charge is not fixed but is regulated by adsorption and desorption of ions, including the surfactant ions. For example, the surface charge of silica is regulated by adsorption of H⁺ ions⁶ and by adsorption of quaternary ammonium surfactants.⁷ In this chapter I describe the fabrication of solid–aqueous interfaces with a controlled and fixed density of surface charges that are covalently bound to the solid, and I describe the adsorption of the surfactant, sodium dodecyl sulfate (SDS), to these interfaces.

Unfortunately, there is no universally accepted definition of surface charge. This is a consequence of the finite width of the interface and our difficulty in directly probing the structure of the interface. On some occasions the term ‘surface charge’ is used to

* This chapter has been reproduced in part with permission from Tulpar, A.; Ducker, W.A. *J. Phys. Chem. B* **2004**, *108*, 1667–1676. Copyright 2004 American Chemical Society.

¹ Somasundaran, P.; Fuerstenau, D. W. *J. Phys. Chem.* **1966**, *70*, 90–96.

² Bohmer, M. R.; Koopal, L. K. *Langmuir* **1992**, *3*, 2649–2659.

³ Fleming, B. D.; Biggs, S.; Wanless, E. J. *J. Phys. Chem. B* **2001**, *105*, 9537–9540.

⁴ Lamont, R. E.; Ducker, W. A. *J. Am. Chem. Soc.* **1998**, *120*, 7602–7607.

⁵ Atkin, R.; Craig, V. S. J.; Wanless, E. J.; Biggs, S. *Adv. Colloid Interface Sci.* **2003**, *103*, 219–304.

⁶ Yates, D. E.; Levine, S.; Healy, T. W. *J. Chem. Soc., Faraday Trans 1* **1974**, *70*, 1807–1818.

⁷ Goloub, T. P.; Koopal, L. K.; Bjsterbosch, B. H.; Sidorova, M. P. *Langmuir* **1996**, *12*, 3188–3194.

describe the charge developed either by dissociation of groups covalently bound to the solid² or dissolution of lattice ions, and on other occasions it is obtained from fits to surface force or from electrophoretic measurements. The latter evaluate electrostatic properties at a plane further from the bulk solid, and so ions that are not directly bound to the solid are included in the surface charge. Examples of the former are hydrogen ions adsorbed to silica, and examples of the latter are hydrated sodium ions adsorbed to silica. It is not always possible to categorize adsorption into one or other of these categories. In this chapter I describe adsorption to surfaces with a controlled and fixed amount of charge that is covalently bound to the solid, so I sidestep the difficulties in describing the position of the surface charge and simply use the symbol σ_c to represent the covalently bound charge per unit area. For brevity, I refer to this as the surface charge density. I will use the term “outer surface charge” to describe the charge in the plane separating the diffuse double-layer from more strongly held adsorbates. The outer surface charge is equal to minus the diffuse layer charge, $-\sigma_D$, (See Figure 3.1) and is necessarily a vague term because not all details of the interfacial structure are known.

Charge regulation is of fundamental importance to the adsorption of ionic surfactants because it allows surfactant adsorption to increase without a stoichiometric change in the outer surface charge.⁷ A stoichiometric change in the outer surface charge inhibits the adsorption of like-charged surfactant by raising an electrostatic barrier to adsorption. Charge regulation can occur both at the solid surface directly (for example, on silica, by dissociation of a silanol group) and in the thin film adjacent to the surface (outer-charge regulation) through the adsorption of surfactant, surfactant counterions, and other salts.

Charge regulation is very important in the adsorption of charged surfactants. For example, at low surfactant concentrations the adsorption of sodium dodecyl sulfate to alumina increases while the zeta potential is approximately constant.⁸ This suggests that the (positive) surface charge of the alumina increases to compensate for the increase in the negative charge caused by the surfactant adsorption. Work by Koopal and coworkers on silica has revealed charge regulation by the measurement of H^+ ions that are released

⁸ Chandar, P; Somasundaran, P.; Turro, N. J. *J. Colloid Interface Sci.* **1987**, *117*, 31–46.

from silica during the adsorption of quaternary alkylammonium and pyridinium surfactants.⁷ On silica, the maximum surface charge regulation occurs at low salt and low surfactant concentrations. At low salt and surfactant concentrations, approximately one proton desorbs for every two surfactant molecules that adsorb, and when the outer surface charge is zero, approximately one proton desorbs for every additional surfactant molecule that adsorbs. Koopal and co-workers have also studied the effect of salt concentration on adsorption. They find a “common intersection point” (cip) where adsorption isotherms at different salt concentrations approximately intersect and the outer charge on the surface is approximately zero. Goloub and Koopal⁹ explain this phenomenon by suggesting that salt hinders adsorption below the cip when electrostatic interactions between the silica and the surfactant promote adsorption and salt promotes adsorption above the cip when electrostatic interactions among surfactant molecules hinder adsorption. At higher surfactant concentrations the outer surface charge is strongly regulated by the adsorption of surfactant counterions.¹⁰

Surfactant adsorption is also controlled by forces acting on the hydrophobic tail. There is often a concentration range where the surface excess of surfactant increases rapidly with concentration. This concentration range is known as the hemimicelle concentration,¹¹ and there is evidence to support the idea that the acceleration in adsorption is due to a decrease in the amount of water in contact with the alkyl chains. The energy decrease through partial or full removal of the alkyl chain from the aqueous environment (~ 1 kT per methylene group¹²) is often enough to overcome the energy penalty of charging the surface.

One critical role of charge regulation is therefore to suppress the electrostatic penalty for adsorption until the surfactant density is high enough to allow many lateral interactions between the surfactant tails. So, charge regulation enables hemimicelle formation at low concentrations. Implicit in most ideas of charge regulation is the idea that charges are free to migrate across the surface. Thus, a charge-regulating surface facilitates adsorption of a cluster of surfactant molecules through the creation of a cluster

⁹ Goloub, T. P.; Koopal, L. K. *Langmuir* **1997**, *13*, 673–681.

¹⁰ Bijsterbosch, B. H. *J. Colloid Interface Sci.* **1974**, *47*, 186–98.

¹¹ Gaudin, A. M.; Fuerstenau, D. W. *Trans. AIME* **1955**, *202*, 958–962.

¹² Somasundaran, P.; Healy, W. T.; Fuerstenau, D. W. *J. Phys. Chem.* **1964**, *68*, 3562–3566.

of surface charges on *neighboring* surface sites. In a recent review, Atkin et al.⁵ suggest that the adsorption of charged surfactant to silica should enhance adsorption of surfactant to neighboring sites by increasing the acidity of neighboring silanol groups.

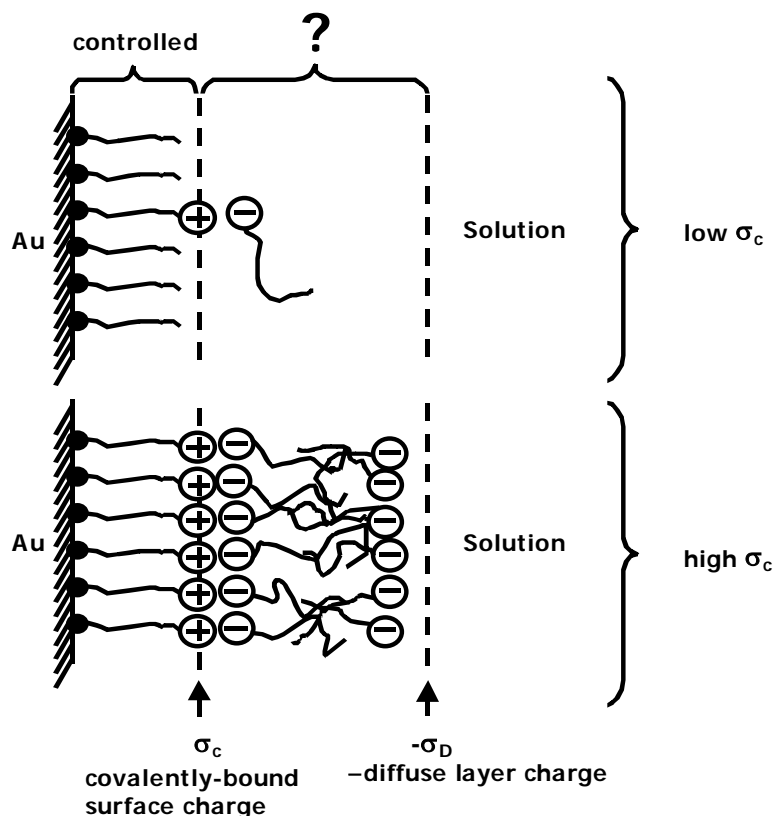


Figure 3.1 Model for surface charge density and surfactant adsorption. The black spheres, the positively charged head groups and the negatively charged head groups represent $-S$, $-N^+(CH_3)_3$, and $-OSO_3^-$, respectively.

In this study, I further the understanding of the role of charge regulation in the adsorption of ionic surfactants by controlling one component of the surface charge: the density of charged groups that are covalently bound to the solid. I create these fixed-charge surfaces by adsorption to gold of mixed self-assembled monolayers (SAMs)¹³ of

¹³ Nuzzo, R. G.; Allara, D. L. *J. Am. Chem. Soc.* **1983**, *105*, 4481–4483. Porter, M. D.; Bright, T. B.; Allara, D. L.; Chidsey, C. E. D. *J. Am. Chem. Soc.* **1987**, *109*, 3559–3568. Bain, C. D.; Troughton, E. B.; Tao, Y. -T.; Ewall, J.; Whitesides, G. M.; Nuzzo, R. G. *J. Am. Chem. Soc.* **1989**, *111*, 321–335.

ω -functionalized thiols from solution. The monolayer components are $S(CH_2)_{11}OH$, which I abbreviate as ω -OH, and $S(CH_2)_{11}N^+(CH_3)_3$, which I abbreviate as ω -TMA. (See Figure 3.1.) The surface density of ω -TMA can be changed during the deposition of the thiol monolayer by altering the concentration of $HS(CH_2)_{11}N^+(CH_3)_3Cl^-$ in the deposition solution. I am not able to control or measure the distribution of ω -TMA on the surface, but I assume that Coulombic repulsion during film formation prevents the formation of clusters of charge. I also assume that ω -TMA and ω -OH do not reorganize in the SAM during surfactant adsorption because of the strong sulfur–gold bonds between the thiolate and the gold.¹⁴ The water wettability is approximately constant over the composition range from 0% to 100% ω -TMA (see the results section), so I am able to change the surface charge density while maintaining wettability almost constant.

Each ω -TMA contains one fixed positive charge, so σ_c is dictated by the density of ω -TMA on the surface:

$$\sigma_c = e \alpha \Gamma_{SAM} \quad (3.1)$$

where e is the magnitude of the charge on an electron, α is the surface mole fraction of ω -TMA in the SAM, and Γ_{SAM} is the number of molecules per unit area in the SAM.

The outer surface charge can be regulated by adsorption of ions from solution. I have not used any buffers or extraneous ions, so free ions only arise from the surfactant (Na^+ and DS^-), the initial counterions to the TMA (Cl^-), the dissociation of water, and the hydration of CO_2 . SDS is a strong electrolyte, so the DS^- concentration is stoichiometric to the added SDS up to the critical micelle concentration (cmc). The OH^- , CO_3^{2-} , and HCO_3^- concentrations can be calculated from the pH and the carbonate dissociation constants. These concentrations are approximately 10^{-8} M, 10^{-11} M, and 10^{-6} M, respectively; all are much smaller than the DS^- concentration. The very few Cl^- ions will be washed out in the initial rinse with water. Earlier work from the Ducker lab¹⁵ has indirect evidence that suggests that the OH^- , CO_3^{2-} , and HCO_3^- ions have no particular affinity for the $-N^+(CH_3)_3$ group, so we will assume that DS^- is the only significant

¹⁴ Nuzzo, R. G.; Dubois, L. H.; Allara, D. L. *J. Am. Chem. Soc.* **1990**, *112*, 558–569.

¹⁵ Subramanian, V.; Ducker, W. A. *Langmuir* **2000**, *16*, 4447–4454.

counterion. Likewise, the most abundant co-ion is the Na^+ produced by dissociation of SDS. So, to a good approximation the only outer charge regulation occurs through adsorption of the surfactant (Na^+ and DS^-). I also report on the results of an experiment in which additional outer charge regulation is introduced by adding NaCl into solution. Studies of ion binding to quaternary ammonium surfactants show that there is a nonionic contribution to the binding of halides to the $-\text{N}^+(\text{CH}_3)_3$ group.¹⁶

In summary, I am able to produce interfaces in which the average covalently bound surface charge density is controlled, known, and fixed in magnitude and the position of each surface charge is fixed to the end of an alkyl chain. Thus, I can study surfactant adsorption to highly controlled surfaces where outer charge regulation is limited to adsorption of the surfactant, and I can introduce further charge regulation by the addition of salt.

3.2. Experimental Section

3.2.1. Materials

SDS (Sigma, St. Louis, MO) was recrystallized twice from 200-proof ethanol (Aaper Alcohol Chemical Co., USA). The concentration of surface-active contaminants was low as shown by the fact that surface tension measurements revealed no minimum in the surface tension versus $\ln(\text{concentration})$ curves. (See Section 2.2.2) Solutions were prepared with 18.3 MW deionized, charcoal-filtered water (EASYpure UV, Barnstead Thermolyne Corp., Dubuque, IA). SDS solutions were used within 1 h of preparation from the solid to prevent formation of dodecanol. KOH (Aldrich, Milwaukee, WI) was semiconductor grade and was used as received. NaCl (Sigma, St. Louis, MO) was roasted in air at 400 °C for 16 h. 11-Mercapto-1-undecanol (Aldrich, Milwaukee, WI), 97%, was used as received.

N,N,N-Trimethyl(11-mercaptoundecyl)ammonium chloride was synthesized according to the procedure in ref. 17. It was recrystallized from *tert*-butyl methyl ether and ethanol (90:10). NMR ($\text{D}_2\text{O}, \delta$): 1.24–1.49 (m, 14 H, CH_2), 1.53–1.66 (m, 2 H,

¹⁶ Ninham, B. W.; Yaminsky, V. *Langmuir*, **1997**, *13*, 2097–2108.

¹⁷ Tien, J.; Terfort, A.; Whitesides, G. M. *Langmuir* **1997**, *13*, 5349–5355.

$\text{CH}_2\text{CH}_2\text{SH}$), 1.67–1.84 (m, 2 H, $\text{CH}_2\text{CH}_2\text{NMe}_3^+$), 2.52 (t, 8 Hz, 2 H, CH_2SH), 3.12 (s, 9 H, NMe_3^+), 3.30–3.41 (m, 2 H, $\text{CH}_2\text{NMe}_3^+$). MS (FAB): 246 (100%). MS(high-resolution): 246.2259.

3.2.2. Atomic Force Microscopy (AFM)

Images were captured in situ using a Nanoscope III AFM (Digital Instruments, CA) using silicon cantilevers (Park Scientific, CA) with nominal spring constants of 0.26 N/m. Before each experiment, the cantilevers were irradiated for at least 30 min in a laminar flow cabinet with ultraviolet light ($\sim 9 \text{ mW/cm}^2$ at 253.7 nm) generated from a PENRAY Lamp (UVP, Inc., Upland, CA). The solution was held in a fluid cell and sealed by a silicone O-ring. Prior to use, the fluid cell and the O-ring were soaked in SDS solution, rinsed with water, and dried with high-purity N_2 . The z-axis of the piezo was calibrated by a silicon calibration reference of 22.0 nm step height (Silicon-MDT, Moscow, Russia). The x- and y- axes of the piezo were calibrated by imaging a diffraction grating replica of 2160 lines/mm waffle pattern (Ted Pella, Redding, CA).

Measurements were performed in the temperature range $22 \pm 2 \text{ }^\circ\text{C}$, at pH 6, and at 16 mM SDS. The integral and proportional gains were in the range 0.1–0.6, and scan rates were in the range 3–6 Hz. All images reported here are unfiltered deflection images. Images were captured at the maximum force that would allow stable imaging before the characteristic instability that is associated with displacement of the surfactant film.

The gold samples for AFM measurements were fabricated from a 1 cm long, 1 mm diameter 99.99% gold wire (Alfa Aesar, Ward Hill, MA). The Au wire was cleaned in piranha solution (7:3 concentrated H_2SO_4 / 30% H_2O_2), rinsed with water, and left in ethanol. After removing the Au wire from ethanol, one end of the Au wire was heated in a H_2/O_2 flame until it was red hot and molten. The end of the wire was approximately spherical (~ 2 – 3 mm diameter) and contained about two small flat facets.^{18,19,20} When the Au ball was annealed in a cooler region of the H_2/O_2 flame, the size of each Au (111) facet was increased, and it was readily observed with an optical microscope.²¹

¹⁸ Schmidt, L. D. *CRC Crit. Rev. Solid State Mater. Sci.* **1978**, 7, 129–141.

¹⁹ Hsu, T.; Cowley, J. M. *Ultramicroscopy* **1983**, 11, 239–250.

²⁰ Honbo, H.; Sugawara, S.; Itaya, K. *Anal. Chem.* **1990**, 62, 2424–2429.

²¹ Synder, S. R. *J. Electrochem. Soc.* **1992**, 139, 5C–8C.

Immediately after the removal of the Au wire from the H₂/O₂ flame, the gold ball was immersed in a 2 mM solution of the thiol (mixture) in chloroform (HPLC grade) and was left immersed for 24–48 h. Before the AFM experiment, the Au wire was sonicated for 5 min in chloroform to remove the physisorbed molecules and leave only molecules that are bound by strong gold–sulfur bonds. The Au ball was oriented in a home-built specimen holder to expose a facet for AFM measurements.

3.2.3. Surface Plasmon Resonance (SPR)

SPR data were obtained from a Reichardt Bio-SPR 9000 (Reichardt Inc., Depew, NY). This system uses a 10-Watt tungsten halogen lamp with filters for p-polarized 760 nm light. The substrates for SAMs were 1 cm² glass slides coated with 1 nm of chromium and 40 nm of gold (Reichardt Inc.). The gold-plated glass slides were optically coupled to the prism using a high refractive index liquid, 1.5150 (Cargille, Cedar Grove, NJ). The flow cell surface area was 11 mm x 4 mm. Flow cell volume was 5 µl. Prior to each experiment, the fluidics of SPR instrument was rinsed with purified water for 2 h. SDS solutions were analyzed after the SAM substrate was put into the cell and a steady baseline was established in water. The concentration range for SDS solutions was 0.02 mM–33 mM. Each solution was run for 5 min. Between measurements of different SDS solutions, the cell was rinsed with water for 5 min.

All gold on glass substrates for the SPR experiments were cleaned in freshly prepared piranha solution for 1 min and then rinsed with water, ethanol and chloroform. SAMs were prepared by 24–48 h exposure of the gold substrates to 2 mM solutions of the thiols in chloroform (HPLC grade) in single-use scintillation vials (20 ml). The slides were removed from the solutions, washed with chloroform and ethanol, and dried with N₂ prior to experiments. Measurements were recorded at 22 ± 2 °C.

3.2.4. X-ray Photoelectron Spectroscopy (XPS)

Spectra were obtained using a Perkin-Elmer PHI 5400 model X-Ray photoelectron spectrometer with an Mg K_α achromatic X-ray source (1253.6 eV), operating at 14 keV and 400 W. The chamber pressure was ~ 1x10⁻⁸ Pa, and the takeoff angle (measured as the angle between the sample normal and the photoelectron analyzer) was 15 °. Each sample was examined with both a survey scan, encompassing the region

0–1100 eV, and a Multiplex scanning of carbon, oxygen, sulfur, gold and nitrogen. Binding energies of all photopeaks were referenced to the C1s photopeak position for C-C and C-H species at 285 eV. The X-Ray anode was adjusted to 1246.6 eV to bring the C1s peak to 285 eV.

Slides of 4 cm² glass–gold substrates (Evaporated Metals Inc., Ithaca, NY) were used for the XPS experiments. One slide was cut into four squares so as to keep the Au layer the same. This was necessary because the photopeak area ratios of S and Au depended on the thickness of Au on glass. SAMs of ω -OH, ω -TMA and mixed SAMs (0.25 and 0.5 mole fractions of HS(CH₂)₁₁N(CH₃)₃Cl in solution) were prepared from these 4 slides.

3.2.5. Cyclic Voltammetry

Experiments were performed in a three-electrode cell with an electrochemical analyzer (CH Instruments, TN). The working electrode was a Au (111) single crystal (Evaporated Metals Inc., Ithaca, NY), and the exposed area was defined by an elastomer O-ring^{22,23} (geometric area 0.66 cm²). A Pt coil and a Ag/AgCl/KCl_{sat} electrode were used as the auxiliary and reference electrodes, respectively. All measurements were made in 0.1 M KOH solutions at a scan rate of 0.1 V/s. The solutions were degassed with N₂ for 10 min prior to cycling.

3.2.6. Contact Angles

Sessile contact angles were measured by using a FTA125 contact angle/surface tension instrument (First Ten Angstroms, Portsmouth, VA) on both sides of static drops. Before the characterization of surfactant solutions, the contact angle of water was determined on each slide, five times on different areas. The slide was then dried and surfactant solution drops were applied. Measurements were recorded at 22 ± 2 °C.

²² Rowe, G. K.; Creager, S. E. *Analytica Chimica Acta*. **1991**, 246, 233–239.

²³ Widrig, C. A.; Chung, C.; Porter, M. D. *J. Electroanal. Chem.* **1991**, 310, 335–359.

3.3. Analysis of Raw Data

3.3.1. Analysis of XPS Data

The photopeaks were analyzed by subtracting the X-Ray source line width and by determining the number of counts for each peak on an Apollo 3500 computer, by using PHI software version 4.0. For each photopeak, this analysis was carried out 10 times. The average value, with appropriate sensitivity factors, was used to calculate the peak areas. The error in peak areas was determined from the standard deviation.

Although the SAM–Au samples were rinsed with chloroform, ethanol and water before they were analyzed with XPS, there were still some physisorbed thiol molecules on the samples. This was deduced from the presence of two kinds of sulfur peaks in sulfur scans. The S photopeaks were therefore analyzed as described in the previous paragraph, but by fitting a Gaussian fit to the two different types of sulfurs.

3.3.2. Calculation of Adsorbed Amount from SPR Experiments

I have employed SPR to measure the adsorption of SDS on SAMs. This procedure was pioneered by Sigal et al.²⁴ SPR is used to probe refractive index changes that occur within the immediate vicinity (~200 nm) of a sensor (gold) surface. Therefore, any physical phenomenon that alters the refractive index will elicit a response. In SPR, a monochromatic, p-polarized light excites the surface plasmons (SP) as well as being partially reflected off the gold film to an optical photodetector. The reflected light intensity is the analytical signal. A lower intensity of light reflected from the gold film indicates a higher degree of SP excitation. The maximum excitation of SP occurs at a specific angle, Θ , where the reflected light intensity has a minimum. The value of Θ depends on the refractive index of the adjacent medium.²⁵

SPR is sensitive both to the adsorbed surfactants and to the presence of molecules dissolved in the medium.²⁶ Here, I wish to obtain the surface excess of SDS, so I must subtract the contribution due to the bulk solution. In surfactant solutions the existence of a constant chemical potential, μ , region above the critical micelle concentration provides

²⁴ Sigal, G. B.; Mrksich, M.; Whitesides, G. M. *Langmuir* **1997**, *13*, 2749–2755.

²⁵ For a review, see: Earp, R. L.; Dessy, R. E. *Chemical Analysis* **1998**, *148*, 99–164.

²⁶ Sigal, G. B.; Mrksich, M.; Whitesides, G. M. *J. Am. Chem. Soc.* **1998**, *120*, 3464–3473.

a convenient regime for calibrating the contribution from the bulk solution. When μ is constant, I assume that the adsorption is constant, and in support of this assumption I observe a linear relationship between $\Delta\theta$ and c . (See Figure 3.2)

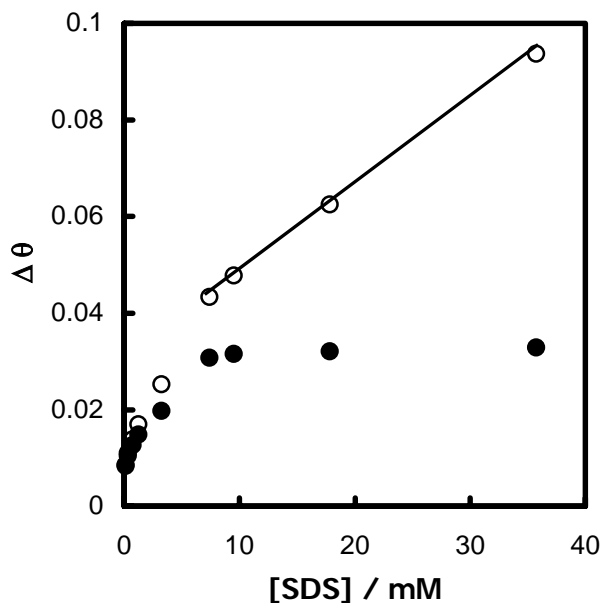


Figure 3.2 Change in angle of minimum reflected light intensity as a function of SDS concentration for a surface with $\sigma_c = 0.6 \text{ e/nm}^2$. Open circles show the change in angle with respect to water. The straight line is fitted to the points above the cmc, where I assume that the surface excess is approximately constant. The filled circles are determined by subtracting the bulk contribution, which is obtained from the best-fit line.

The value of $\delta\theta/\delta c$ is determined to be $0.0017 \pm 0.0001 \text{ }^\circ/\text{mM}$ from the slope of the line. Subtracting this bulk effect leaves only the angle change due to the surfactant adsorption on the surface, $\Delta\theta_a$.²⁴

$$\Delta\theta_a = \Delta\theta - c \frac{\partial\theta}{\partial c} \quad (3.2)$$

To obtain the amount of SDS adsorbed on self-assembled monolayers, the following equation is used:^{27,28}

$$\Gamma = d\Delta n \frac{1}{\partial n / \partial c} \quad (3.3)$$

²⁷ de Feijter, J. A.; Benjamins, J.; Veer, F. A. *Biopolymers* **1978**, *17*, 1759–1772.

²⁸ Schaaf, P.; Déjardin, P.; Schmitt, A. *Langmuir* **1987**, *3*, 1131–1135.

where d is the thickness of the adsorbed layer, $\delta n/\delta c$ is the refractive index increment of the surfactant, and Δn is the difference between the refractive index of the adsorbed SDS layer (1.45)^{24, 26, 29, 30} and water (1.33).

The refractive index increment of the surfactant can be determined as follows:

$$\frac{\partial n}{\partial c} = \frac{\partial n}{\partial \Theta} \frac{\partial \Theta}{\partial c} \quad (3.4)$$

Here, $\delta \Theta/\delta n$ is an instrument constant (53 °) and is supplied by the manufacturer of the SPR instrument. I have also carried out Fresnel calculations for a glass slide with a 40 nm gold layer on a sapphire prism. From these I find $\delta \Theta/\delta n = 53.6$ °.³¹ Using eq 3.4, I find the refractive index increment of SDS to be $(3.2 \pm 0.2) \times 10^{-5} \text{ mM}^{-1}$, which is within 3% of previously reported values.^{24,32}

The thickness of the layer is determined using eq 3.5:

$$d = \Delta \Theta_a \frac{\partial d}{\partial \Theta} \quad (3.5)$$

The value of $\delta \Theta/\delta d = 0.04$ °/nm is obtained from a Fresnel calculation.³¹

In summary, the surface excess is experimentally obtained as follows:

$$\Gamma = \Delta \Theta_a \frac{\partial d}{\partial \Theta} \Delta n \frac{\partial \Theta}{\partial n} \frac{\partial c}{\partial \Theta} \quad (3.6)$$

3.4. Results and Analysis

3.4.1. Determination of Covalently-Bound Surface Charge Density

Each ω -TMA molecule has exactly one positive charge. Hence, σ_c can be determined from eq 3.1. The surface fraction of ω -TMA molecules in the SAM, α , and the SAM density, Γ_{SAM} , are determined experimentally. Γ_{SAM} is measured by cyclic voltammetry. Figure 3.3 shows the cyclic voltammetric curve for a ω -OH monolayer on a

²⁹ Kavanagh, R. J.; Iu, K. K.; Thomas, J. K. *Langmuir* **1992**, *8*, 3008–3013.

³⁰ Tiberg, F.; Ederth, T. *J. Phys. Chem. B* **2000**, *104*, 9689–9695.

³¹ The simulation program is provided by Prof. Raymond Dessy, Chemistry Department, Virginia Tech, Blacksburg, VA.

³² Nakagaki, M.; Shimabayashi, S. *Nippon Kagaku Kaishi* **1976**, *9*, 1353–1357.

Au (111) surface. The potential is scanned at a rate of 0.1 V/s from 0.0 V to -1.3 V. A sharp peak is observed at -1.06 V, which I assign to the reductive desorption of ω -OH on the basis of the similarity of this peak to results obtained for alkane thiols.^{23,33,34,35} The area under the peak, after compensating for the charging current, gives the charge associated with the reduction of ω -OH. If we assume that a single electron is required for the reduction of one ω -OH molecule, Γ_{SAM} ³⁶ is 3.4 ± 0.3 molecules/nm². I am unable to accurately determine the SAM densities of ω -TMA and mixed SAMs, because the voltammograms are more complex. This complexity probably arises from the presence of highly-charged N⁺(CH₃)₃ groups.

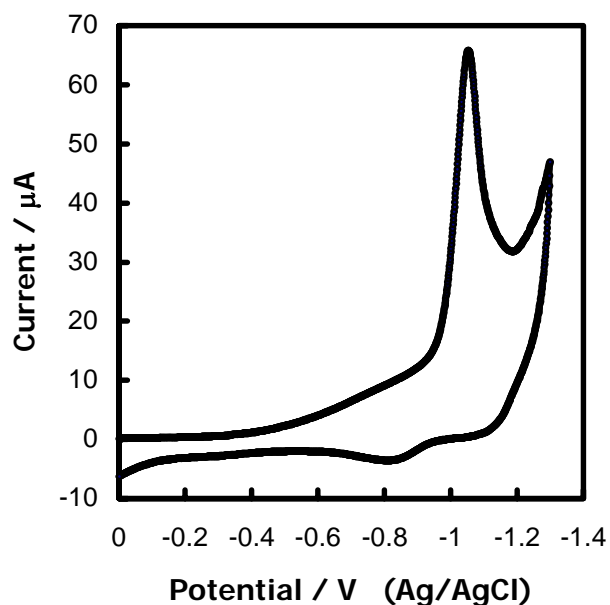


Figure 3.3 Cyclic voltammogram for S(CH₂)₁₁OH. The voltammetric scan rate is 0.1V/s.

For SAMs containing ω -TMA, I use XPS measurements to calculate the SAM density. These measurements are calibrated using the value of Γ_{SAM} obtained from cyclic

³³ Zhong, C.; Porter, M. D.; *J. Electroanal. Chem.* **1997**, *425*, 147–153.

³⁴ Yang, D. F.; Wilde, C. P.; Morin, M. *Langmuir* **1996**, *12*, 6570–6577.

³⁵ Hobara, D.; Ota, M.; Imabayashi, S.; Niki K.; Kakiuchi, T. *J. Electroanal. Chem.* **1998**, *444*, 113–119.

³⁶ Walczak, M. M.; Popenoe, D. D.; Deinhammer, R. S.; Lamp, D. B.; Chung, C.; Porter, M. D. *Langmuir* **1991**, *7*, 2687–2693.

voltammograms for the SAM containing only ω -OH. I assume that, on substrates with the same Au layer thicknesses, the ratio of the sulfur peak area S to the Au peak area Au (i.e., S/Au) is be directly proportional to the density of thiolate molecules chemisorbed on Au. Therefore,

$$\Gamma_{SAM} = \frac{\Gamma_{SOH-only}}{(S/Au)_{SOH-only}} (S/Au) \quad (3.7)$$

The peak area ratios of S/Au for SAMs prepared from H ω -TMA and H ω -OH are given in Table 3.1.

The only parameter left to determine the surface charge density is the surface mole fraction of ω -TMA on SAMs, α . The value for α can be directly obtained from XPS measurements from the ratio of the areas of the nitrogen, N , and sulfur, S , peaks (N/S) and is shown in Table 3.1. Given Γ_{SAM} and α , the calculation of σ_c is trivial by using eq 3.1.

Table 3.1 Normalized XPS photopeak area ratios for SAM films prepared from chloroform solutions of $HS(CH_2)_{11}N^+(CH_3)_3Cl^-$ and $HS(CH_2)_{11}OH$. X_N is the mole fraction of $HS(CH_2)_{11}N^+(CH_3)_3Cl^-$ in 2 mM chloroform solutions.

| X_N | N/S | S/Au |
|-------|-----------------|-------------------|
| 1 | 1.00 ± 0.06 | 0.053 ± 0.007 |
| 0.5 | 0.4 ± 0.1 | 0.06 ± 0.01 |
| 0.25 | 0.21 ± 0.06 | 0.065 ± 0.005 |
| 0 | 0 | 0.076 ± 0.009 |

The surface charge densities of SAMs prepared from H ω -TMA, H ω -OH, and their mixtures are plotted in Figure 3.4 as a function of the mole fraction of H ω -TMA in solution. As expected, when the mole fraction of H ω -TMA is increased in solution, σ_c increases. The linear relationship between the film density and solution composition supports our assumption that there are no clusters of ω -TMA and facilitates the interpolation to other solution compositions. For a mole fraction of 0.75 H ω -TMA, I interpolate the surface charge density to be 1.7 e/nm^2 . As expected, the presence of charged and bulky ω -groups on the surface reduces the SAM density. (See Figure 3.5.)

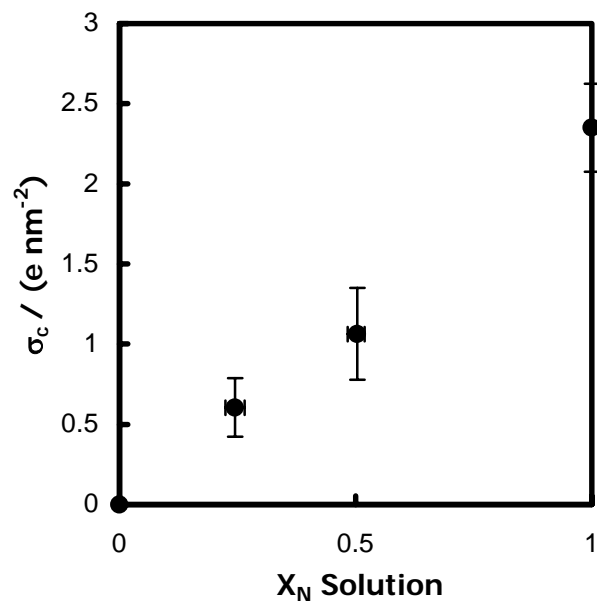


Figure 3.4 Surface charge density vs. mole fraction of $\text{HS}(\text{CH}_2)_{11}\text{N}^+(\text{CH}_3)_3\text{Cl}^-$ in solution. X_N is the mole fraction of $\text{HS}(\text{CH}_2)_{11}\text{N}^+(\text{CH}_3)_3\text{Cl}^-$ in 2 mM chloroform solution.

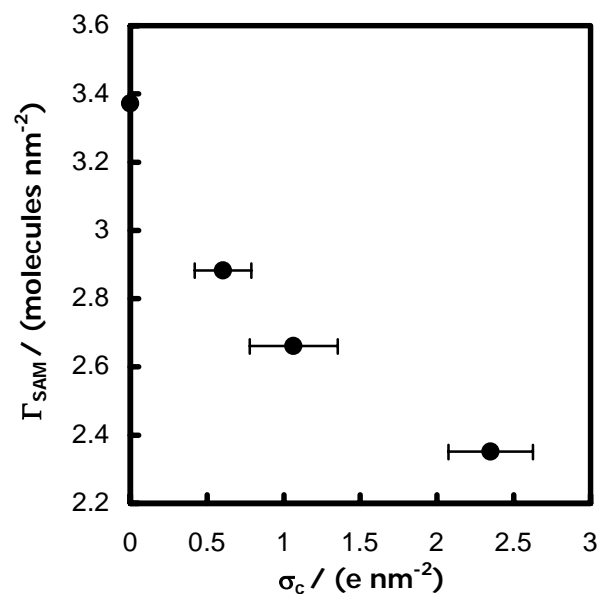


Figure 3.5 SAM density vs. surface charge density. There is a systematic error of 0.3 molecules / nm^2 in SAM density in all data points. The presence of ω -TMA decreases the density of the SAM.

3.4.2. Adsorption Isotherms of SDS

Figure 3.6 shows the adsorption of SDS from aqueous solution to SAMs of various surface charge densities. Note that the raw data do not allow us to distinguish DS^-

from SDS. There is little adsorption onto the uncharged ω -OH SAM up to about 2 mM SDS. The shape of the adsorption isotherms for charged surfaces is independent of the surface charge density: all show two plateau regions. The first-plateau region ends at about 0.3 mM (cmc/25). For all surfaces, there is a plateau above 8 mM (the cmc). Above this concentration, the chemical potential is only a weak function of concentration.

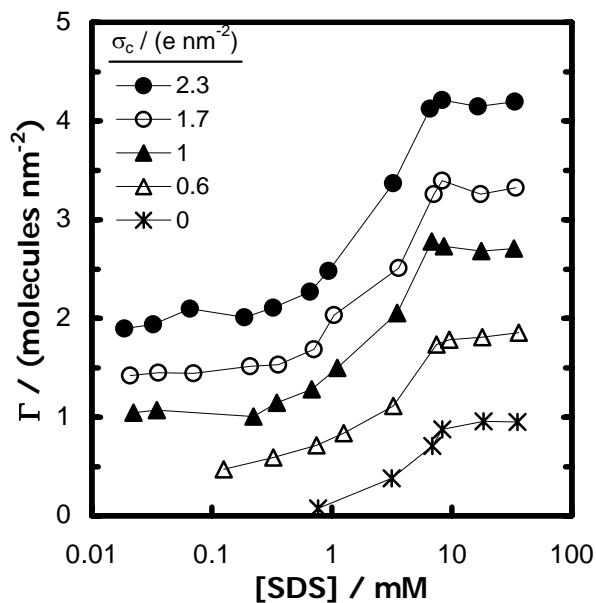


Figure 3.6 Adsorption of SDS to a series of SAMs of fixed surface charge, σ_c . Note that the error in σ_c is large (see Figure 3.4). The lines are guides to the eye.

Figure 3.7 shows the adsorbed amount of SDS (from Figure 3.6) as a function of surface charge density. All data points are the average values for the adsorbed amount of SDS in the respective region. The filled circles represent the SDS adsorption in the first-plateau regions. The data points fall on a line with a slope of one, showing that the amount of adsorbed SDS per unit area in the first plateau corresponds to the surface charge density. DS^- is the most common counterion and every positive surface site has an attached DS^- counterion. But, there appears to be no additional SDS adsorption, even when the density of surface charge is high, that is, the high density of alkyl chains does not promote adsorption of a superequivalent amount of DS^- or SDS. The unfilled circles represent the surface excess of SDS in the second-plateau regions. Adsorption in the

second plateau increases linearly with surface charge density. This indicates that there is no abrupt change in SDS adsorption as a function of surface charge density. Again, there is no critical charge density that produces a superequivalent adsorption of DS^- or SDS.

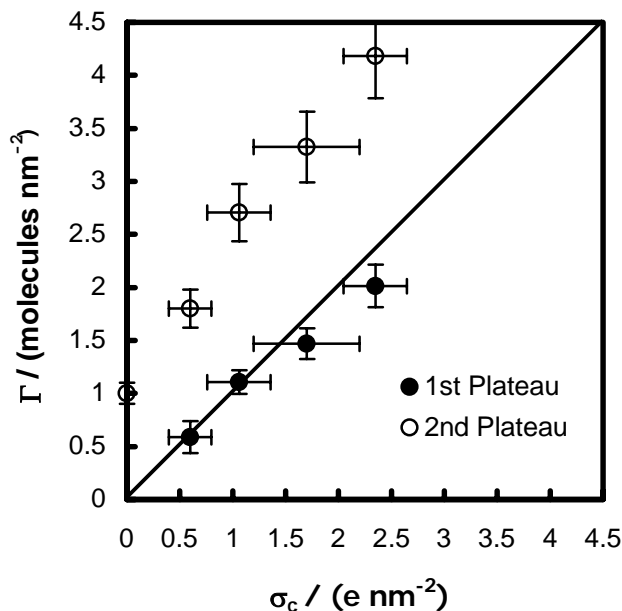


Figure 3.7 Adsorbed density of SDS vs. surface charge density. In the first plateau region, approximately one surfactant molecule adsorbs for each covalently-bound surface charge.

There is some adsorption on surfaces with $\sigma_c = 0 \text{ e/nm}^2$ ($\omega\text{-OH}$ -only SAMs) at concentrations greater than 0.8 mM. This adsorption was also observed in ref 26. To examine the effect of the change in charge on SDS adsorption, I have plotted the same data in Figure 3.8 as in Figure 3.6 after subtraction of an estimate of the contribution due to adsorption from the $\omega\text{-OH}$ groups. The adsorption of SDS to $\omega\text{-OH}$ groups is approximated as the product of the amount of SDS adsorbed per OH group to the $\omega\text{-OH}$ -only film and the density of OH groups. This is only a rough estimate, as it is reasonable to expect interaction of the surfactant with more than one surface group. The same procedure has been repeated for all surfaces except for $\sigma_c=2.3 \text{ e/nm}^2$, which does not have any $\omega\text{-OH}$. This adjustment has no effect on the first-plateau regions of the adsorption isotherms of surfaces with $\sigma_c=1.7$ and 1.0 e/nm^2 .

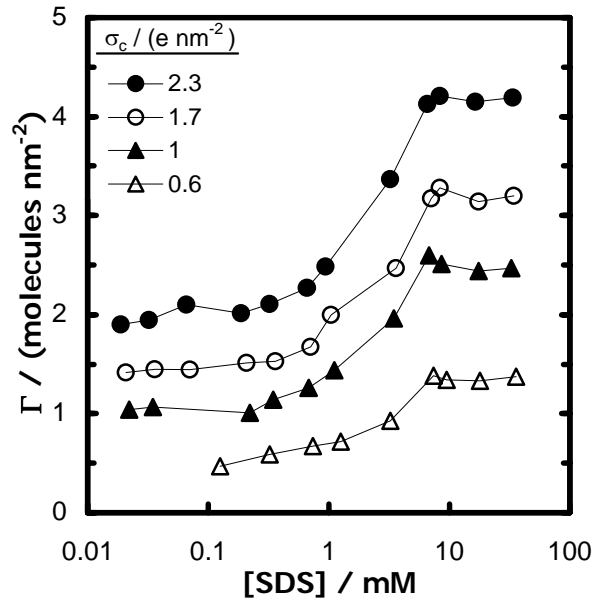


Figure 3.8 Adsorption isotherms of SDS. The amount of SDS adsorbed per OH group at $\sigma_c=0 \text{ e/nm}^2$ surfaces has been subtracted from each adsorption isotherm.

Figure 3.9 shows the ratio between the adsorbed amount in the first- and second-plateau regions. The filled and unfilled circles represent the data used from Figure 3.8 and Figure 3.6, respectively. This graph shows that SDS adsorption in the second plateaus is approximately 2–2.8 times the adsorption in the first plateaus. If the second-plateau data are adjusted to account for adsorption to the ω -OH groups, the adsorption in the second plateaus is about twice the adsorption in the first plateaus, independent of surface charge.

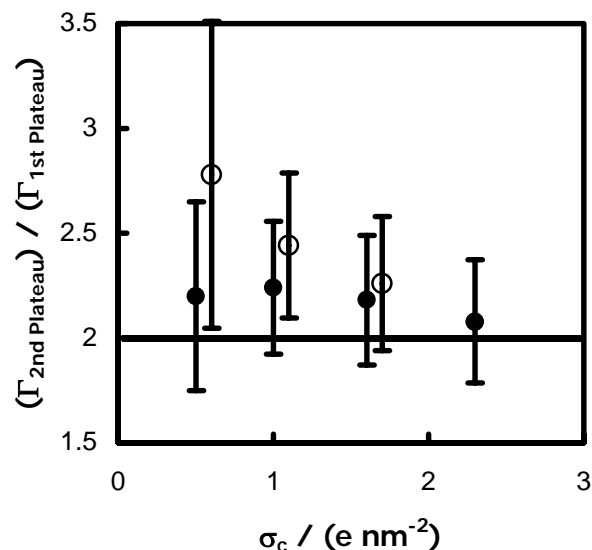


Figure 3.9 Comparison of SDS adsorption in the first and second plateaus regions. The filled and unfilled circles represent the ratio of the adsorbed amount of SDS in the second and first plateaus regions calculated from Figure 3.8 and Figure 3.6, respectively.

Table 3.2 Contact angles, θ , of aqueous SDS solutions on SAMs with different surface charge densities. The contact angle of water on the ω -OH surface is $36 \pm 4^\circ$.

| Concentration (mM) | θ ($\sigma_c = 0.6 \text{ e nm}^{-2}$) | θ ($\sigma_c = 1.0 \text{ e nm}^{-2}$) | θ ($\sigma_c = 1.7 \text{ e nm}^{-2}$) | θ ($\sigma_c = 2.3 \text{ e nm}^{-2}$) |
|--------------------|---|---|---|---|
| 0 | 44 ± 9 | 48 ± 7 | 36 ± 4 | 38 ± 10 |
| 0.16 | 65 ± 5 | 65 ± 8 | 51 ± 2 | 66 ± 3 |
| 0.32 | 65 ± 4 | 64 ± 3 | 57 ± 3 | 70 ± 1 |
| 4 | 50 ± 3 | 43 ± 5 | | 61 ± 1 |
| 16 | 32 ± 6 | 49 ± 7 | 43 ± 5 | 45 ± 3 |
| 16 advancing | 44 ± 6 | 70 ± 7 | 61 ± 6 | 49 ± 4 |
| 16 receding | 26 ± 4 | 37 ± 6 | 20 ± 5 | 15 ± 3 |

Table 3.2 gives contact angles of water and SDS solutions on SAMs. The data show that I am able to vary the surface charge density from 0 to 2.3 e/nm^2 with only a small variability in the wettability by water ($36\text{--}48^\circ$). The surfactant concentrations shown in bold are 0.32 mM and 16 mM. The 0.32 mM concentration is the end of the first plateau and the 16 mM concentration is in the second plateau. The contact angle has a maximum at 0.32 mM and from there it decreases for all surfaces. This increase in wettability at concentrations above the first plateau is consistent with the adsorption of

additional surfactant with their heads toward the solution. Above the cmc, the contact angle has a large hysteresis, which is consistent with facile adsorption and desorption of at least part of the adsorbed surfactant. Therefore, the contact angle data is consistent with a first layer of surfactant with tails oriented toward the solution in the first plateau and a second layer of surfactant with heads oriented toward the solution in the second plateau.

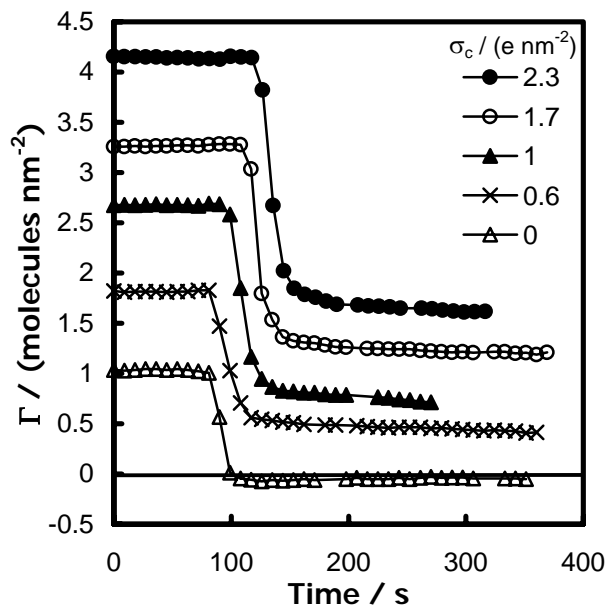


Figure 3.10 Desorption isotherms of SDS from SAMs with different surface charge densities. The SDS concentration is 16mM (2cmc) at time zero. The time at which the solution was switched from 2cmc to water was shifted arbitrarily to allow a clear view of all the curves.

Figure 3.10 shows the *desorption* of SDS from SAMs with different surface charge densities into pure water. The variation in bulk concentration during this experiment affects the analysis of these data. When 16 mM SDS is present in the cell (approximately the first 100 s), the adsorbed amount of SDS is calculated as described previously. When there is only water flowing through the cell (approximately after 150 s), there is no need to make a correction for SDS in the bulk solution. Therefore, eq 3.6 is used by replacing $\Delta\theta_a$ with $\Delta\theta$. During the switch from 16 mM SDS to water, I should subtract a contribution due to the changing of the SDS concentration *near* the interface (the bulk effect in eq 3.2), but the time dependence of the change in concentration near

the surface is not known. However, this error in surface excess does not have a significant effect on our current analysis because the initial desorption is almost vertical (instantaneous) on the timescale of our results.

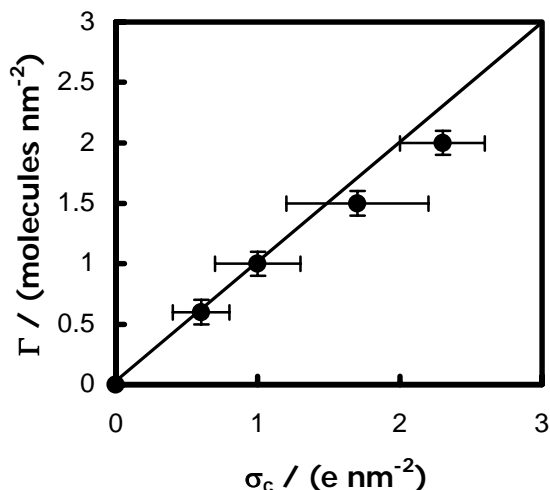


Figure 3.11 The surface excess remaining ~30 seconds after bathing solution was switched from 2cmc to pure water.

The desorption isotherms show two regions for charged surfaces: a fast rate of desorption followed by a slow rate of desorption. Similar fast desorption rates were obtained by Sigal et al.²⁴ for the desorption of SDS from hexadecanethiol SAMs. In their study, there is only a single layer of SDS bound to the hydrophobic SAM. The onset of the slow desorption region corresponds approximately to the surface charge density of the surfaces. (See Figure 3.11.) For example, in the films with no surface charges (ω -OH SAMs) the surface excess drops to zero within a few seconds. This data is consistent with two adsorption sites. There is a rapid loss of nonelectrostatically bound surfactant (as for ref. 24) followed by a slow loss of electrostatically bound surfactant. Recent work from the Ducker lab³⁷ shows that desorption of the electrostatically bound surfactant is accelerated by the presence of additional electrolyte. This suggests that desorption of charged species in water is hindered by the production of an opposite potential on the surface. This potential is reduced through adsorption of counterions from the electrolyte.

³⁷ Clark, S. C.; Ducker, W. A. *J. Phys. Chem. B.* **2003**, *107*, 9011–9021.

3.4.3. Structure of Adsorbed SDS Aggregates

I have employed AFM to investigate the surface homogeneity of SAMs³⁸ and the structure of adsorbed surfactant aggregates³⁹ on SAMs.⁴⁰

In water, the force between the negatively charged AFM tip and the positively charged SAMs are attractive, as expected. The images are featureless in water: there are no holes or aggregates and the root mean square roughness is 0.12 ± 0.05 nm for an area of 200 nm x 200 nm. These observations support the homogeneity of SAMs formed from ω -TMA, ω -OH, and mixtures of the two on gold.

Figure 3.12a shows the AFM image of the interface between the SAM with $\sigma_c = 2.3$ e/nm² and the 16 mM (2 x cmc) SDS solution. No features on the surface are resolved by my imaging. This is consistent with the formation of a bilayer on the surface, although it is possible that imaging with the tip does disrupt surface aggregates that are there in the absence of the tip. That my imaging technique does have the ability to resolve features is demonstrated through the addition of salt. In Figure 3.12b micelles are clearly observed (16 mM SDS and 0.1 M NaCl). The images are consistent with cylindrical micelles because the structures in Figure 3.12b have one long axis and one short axis, and their thickness (~3nm) corresponds to approximately twice the length of the SDS alkyl chain. The determination of the thickness is explained on page 92. The sum of the cylinder diameter and the intermicellar separation is 7.0 ± 0.3 nm. The cylinders are mainly parallel to each other. I observe a similar behavior for surfaces with $\sigma_c = 1.7$ e/nm². In contrast, in bulk the addition of salt usually causes aggregates to adopt a smaller curvature.⁴¹ The formation of discrete structures on the surface in the presence of the salt suggests that charge regulation is important for the formation of discrete structures on surfaces.

³⁸ a) Appelhans, D.; Ferse, D.; Adler, H. -J. P.; Plieth, W.; Fikus, A.; Grundke, K.; Schmitt, F. -J.; Bayer, T.; Adolph, B. *Colloids Surf., A* **2000**, *161*, 203–212.

b) Shon, Y. -S.; Lee, S.; Perry, S. S.; Lee, T. R. *J. Am. Chem. Soc.* **2000**, *122*, 1278–1281.

c) Abdelghani, A. *Materials Letters* **2001**, *50*, 73–77.

³⁹ For reviews see:

a) Manne, S. *Prog. Colloid. Polym. Sci.* **1997**, *103*, 226–233.

b) Ducker, W. A. In *Adsorption and Aggregation of Surfactants in Solution*; Mittal, K. L., Shah, D., Eds.; Marcel Dekker: New York, 2003; p 219.

⁴⁰ Grant, L. M.; Ederth, T.; Tiberg, F. *Langmuir* **2000**, *16*, 2285–2291.

⁴¹ Israelachvili, J. N. *Intermolecular and Surface Forces*, 2nd ed.; Academic Press: San Diego, CA, 1991, Chapter 17.

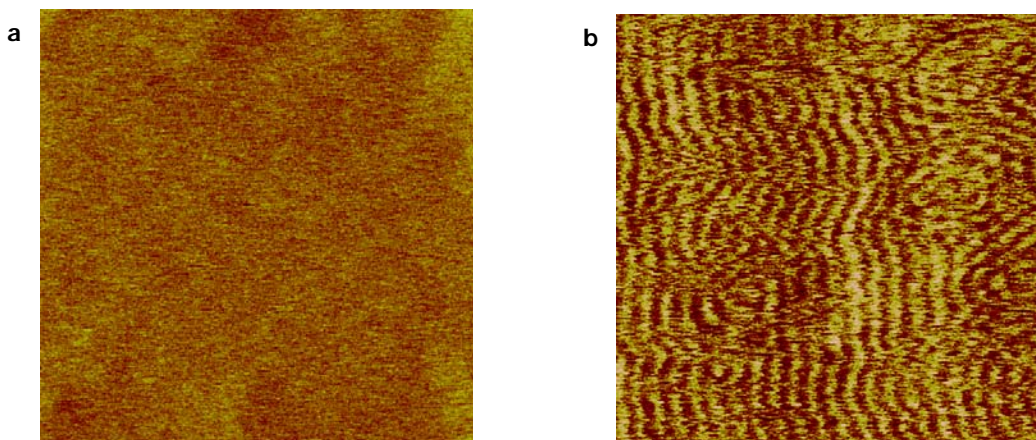


Figure 3.12 (a) 150-nm AFM deflection image of the interface between a SAM with $\sigma_c = 2.3 \text{ e/nm}^2$ and 16mM SDS solution. (b) 150-nm AFM deflection image of the interface between SAM with $\sigma_c = 2.3 \text{ e/nm}^2$ and 16 mM SDS solution with 0.1M NaCl. The period of the cylindrical micelles is $\sim 7 \text{ nm}$.

The images are featureless on pure ω -OH surfaces in the presence of 16 mM SDS. The force curves change from being slightly attractive in water to being repulsive in SDS solution, with no jump-in. The repulsive force is expected for the interaction between a charged and a neutral surface. AFM images of surfaces with $\sigma_c = 0.6 \text{ e/nm}^2$ and $\sigma_c = 1.0 \text{ e/nm}^2$ do not have any distinct features in 16 mM SDS solutions nor in 0.1 M NaCl and 16 mM SDS solutions. On some occasions, I have observed some structures that are 7 nm in size (not shown), but the structure is not force-sensitive. Resolution of surfactant aggregates is always force-sensitive,^{39b} so I do not attribute these structures to adsorbed material.

The position of a mechanical instability of the AFM tip on approach to an adsorbed surfactant film is sometimes used to indicate the thickness of the film.⁴² The instability (jump-in) occurs when the spring constant is smaller in magnitude than the gradient of the surface force. This jump-in is not simply related to the thickness of the film; however, I will use it as an indicator of a trend in thickness.⁴³ Table 3.3 shows that

⁴² Wanless, E. J.; Ducker, W. J. *Phys. Chem.* **1996**, *100*, 3207–3214.

⁴³ Recent theoretical work in the Ducker lab shows that this instability in the force curves are caused by a phase transition in the adsorbed surfactant aggregates on surfaces. Please see the PhD thesis of William Lokar Jr. for a detailed description.

at 2 x cmc there is a systematic increase in jump-in distance with an increase in surface charge density. This is consistent with an increase in surfactant film thickness with an increase in surface charge density.

Table 3.3 Tip–SAM separation for the mechanical instability in AFM force measurements in 2cmc SDS solution.

| σ_c ($e \text{ nm}^{-2}$) | Separation (nm) |
|---------------------------------------|--------------------|
| 0 | no instability |
| 0.6 | 0.8 |
| 1.0 | 2.7 |
| 2.3 | 3.4 |

3.5. Discussion

3.5.1. Mechanism of SDS Adsorption on Fixed-Charge Surfaces

Interpretation of adsorption isotherms gives useful information about the mechanism of SDS adsorption on fixed charged surfaces in the absence of salt. In the first plateau region in Figure 3.6, the 1:1 relationship between the surfactant adsorption and surface charge density shows that surface charge governs the surfactant adsorption. These experimental results agree well with the theoretical calculations of Böhmer and Koopal⁴⁴ for adsorption of ionic surfactants on constant charge surfaces. Their calculations have also shown that there is a plateau region at low concentrations where the surfactant adsorption per area equals the surface charge density. Experiments on (charge-regulating) silica surfaces show that there is an adsorption plateau in which the surface excess of the cationic surfactant is approximately equal to the surface charge density.⁷

At higher SDS concentrations, there is an increase in the adsorbed amount and contact angle measurements suggest that the headgroups are directed towards the solution. There is approximately twice the level of adsorption at the second-plateau

⁴⁴ Böhmer, M. R.; Koopal, L. K. *Langmuir* **1992**, *8*, 1594–1602.

region compared to the first-plateau region (Figure 3.9) for all σ_c . All these data are consistent with the formation of a bilayer of surfactant molecules for all surface charge densities but with a thickness that increases with the surface charge density.

It is interesting that the adsorbed amount in the first plateau is always about the same as the surface charge. There does not appear to be a critical surface density of surfactant that leads to adsorption of surfactant in excess of one molecule per charged site. Therefore, the phenomenon of a hemimicelle concentration does not appear to exist for the conditions of our experiment, where there is no charge regulation. This is contrary to a recent review by Atkin et al.⁵ where they suggest that a certain density of surfactant is required to cause aggregation: I can vary the average density of surfactant over a large range without initiating hemimicelle formation.

In addition, the second plateau is always about twice the level of the first plateau. The first layer does not appear to be a nucleation site for a much larger structure. A reasonable model for adsorption after the first plateau is a repeat of the structure in the first plateau but with the opposite orientation of the molecules.

There is no a priori reason that the effects of compositional changes in the SAM should produce additive changes in adsorption. However, noting that the adsorption in the first plateau scaled directly with the density of charged groups, I sought a simple relationship for adsorption in the second layer. If I subtract an estimate for adsorption due to the ω -OH groups, I find that adsorption due to the ω -TMA groups at and above the cmc is about double the adsorption due to the ω -TMA groups in the first plateau. If this subtraction is performed, the curves for all charge densities follow a simple form: a plateau with a one-to-one relationship between adsorption and surface charge followed by a plateau with a two-to-one relationship between adsorption and surface charge at and above the cmc.

3.5.2. Morphology of Surfactants on Fixed-Charge Surfaces

I did not observe any discrete surfactant aggregates on the SAMs in 2 x cmc SDS. It is very interesting that no micelles are detected at the lower surface charge densities, where the magnitude of the surface charge density is comparable to that of silica. In

contrast, surface micelles of tetradecyltrimethylammonium bromide⁴⁵ and hexadecyltrimethylammonium bromide have been imaged on silica. There is enough SDS adsorption to form micelles at 2 x cmc on the SAMs (Figure 3.6) but the surfactant forms a homogeneous film (as observed by AFM) rather than discrete micelles. I hypothesize that the inability to form discrete surface aggregates of SDS surfactants is due to the lack of clusters of counter charges on the solid. The clustering of charges is normally made possible by charge regulation.

On natural surfaces like silica and alumina the surface charges are not fixed because the surfaces contain dissociable groups that respond to the surface electrical potential (charge regulation).^{1,5,7} Charge regulation on these surfaces has two effects: it can change the average surface charge density and it can change the distribution of charges on the surface. Considering now an anionic surfactant, when one molecule of surfactant adsorbs with its charge near the solid, a new positive surface charge can be created by association or dissociation of a surface ion. The net effect is an increase in the surface charge density but not an equimolar increase in the outer surface charge. The important point is that on a chemically homogenous surface, the most favorable site for the creation of the new surface charge is in the immediate vicinity of the adsorbed surfactant, because the anionic surfactant has decreased the *local* electrical potential. This concept has also been discussed by Atkin et al. in a recent review.⁵ For cationic surfactant adsorbed to silica, they describe how surfactant adsorption will increase the acidity of nearby silanol groups thereby creating new negatively charged sites near the site of the originally adsorbed surfactant. In contrast, Goloub and Koopal⁹ suggest that new charges are *not* created in the vicinity of adsorption sited on *silica* but that new charges are created in the vicinity of adsorption sited on *rutile*.

Surface micellization is facilitated by the lateral mobility of surface ions because continued surfactant adsorption can occur without locally building up a charge that is unfavorable to the surfactant adsorption and without the entropic cost of pulling counterions from the solution. Surface charge regulation that leads to the formation of counterions for the surfactant that are remote from the initial adsorbed surfactant molecule or the creation of more charges (through SAM techniques) that are remote from

⁴⁵ Manne, S.; Gaub, H. E. *Science* **1995**, 270, 1480–1482.

each other does not aid surface micellation by as much, even though both processes lead to greater average surface charge. Thus, average surface charge density (or potential) is not a sufficient parameter to predict surface micellization.

On a homogenous SAM surface, prepared from fixed charged groups, I expect random or evenly distributed surface charges and therefore no inducement to form a surface micelle. The very different adsorption behavior on charge-regulating surfaces and on nonregulating surfaces supports the hypothesis that clusters of counter charges are important to promote surface micellization. Clusters of surface charges can be achieved through lateral mobility of surface sites or through surface charge regulation on a surface with a high density of dissociable sites. This is shown schematically in Figure 3.13.

By experiment, I find that when the density of fixed charges is made very high the surfactant adsorbs to form a continuous layer on the surface, despite the fact that SDS forms spherical micelles in solution. Again, there are no discrete surface micelles in the absence of surface charge regulation.

Although the covalently bound surface charge cannot regulate, micelles are formed in the presence of NaCl, presumably because Cl^- competes with DS^- for quaternary ammonium sites and reduces the number of available positive sites. The mobility of the Cl^- ions allows the clustering of *available* cationic surface sites, and therefore, allows the formation of micelles. The extra Na^+ can also bind to the DS^- headgroups, reducing the interaction between the DS^- and the surface charges. This relaxes the templating effect of the fixed, planar arrangement of surface charges on the adsorbed micelle shape. A similar phenomenon was observed for C_{16}TABr on mica: a flat layer of C_{16}TABr formed on mica in the absence of salt and discrete micelles were formed in the presence of salt.^{4, 46}

⁴⁶ Ducker, W. A.; Wanless, E. J. *Langmuir* **1999**, *15*, 160–168.

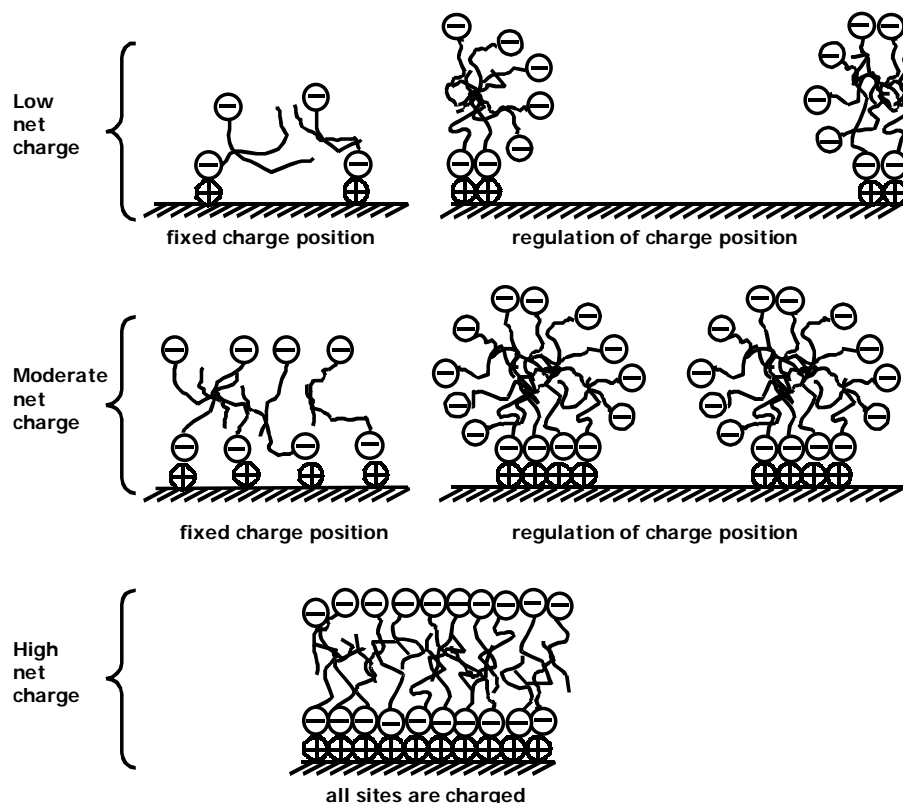


Figure 3.13 Effect of surface charge distribution on surfactant adsorption above the cmc. The situation in the top right would only occur in the unusual case where there is a fixed number of mobile surface charges (e.g. on a short chained or high temperature SAM). More commonly, the surface groups will have a finite pK and effective mobility is attained by association at one point and dissociation at another point. One would always expect the net charge of this type of surface to increase in magnitude due to adsorption of oppositely charged surfactant.

The absence of adsorbed micelles of SDS on fixed-charge surfaces leads me to conclude that *lateral mobility* at the interface of ions other than the surfactant is very important for forming surface micelles of charged surfactants. In this paragraph I consider exceptions to this idea. First, I predict that surface micellization of charged surfactants will be found for a surface that contains preexisting micellar-size clusters of counter charges. Second, the molecular shape of certain surfactants might prevent those surfactants from forming flat sheets of adsorbate even on fixed-charge surfaces. A prediction of this effect could be based either on the packing parameter model⁴¹ or on the experimental absence of lamellar structures anywhere in the phase diagram. For example,

ionic surfactants that have a very large van der Waals cross section through the headgroup or fixed spacing between headgroups (e.g., Gemini surfactants) may not be able to form lamellar structures on surfaces. Perhaps the closest examples of a fixed charge surface is mica, which however does undergo charge regulation due to adsorption of protons.^{47,48} Experiments show that surfactants with bulky headgroups (e.g., triethylammonium and tripropylammonium)⁴⁹ and Gemini surfactants^{50,51} form discrete micelles on mica. The arrangement of charge on the solid surface should cause the largest differences between solution and surface micelle shapes when there is a large difference between the headgroup area in a bulk micelle (the effective headgroup area)⁴¹ and the headgroup area calculated from van der Waals radii.

3.6. Conclusions

I have prepared surfaces with known and controlled surface charge densities, σ_c , in the range 0–2 e/nm² from SAMs prepared from HS(CH₂)₁₁OH and HS(CH₂)₁₁N⁺(CH₃)₃Cl⁻ on gold. The adsorption isotherm of SDS on the charged SAM surfaces in the absence of additional salt shows two plateau regions. The first plateau ends at about cmc/25. For each surface charge density, the density of surfactant adsorbed in the first plateau is approximately equal to the surface charge density, so clearly σ_c governs the surfactant adsorption. There is a second plateau above the cmc (where the chemical potential rises very slowly). Above the cmc, the adsorption is about two times the adsorption in the first plateau, for a range of surface charge densities. The change in wettability suggests that the headgroups of the additional surfactant face toward the aqueous phase. Surprisingly, there is no critical value of σ_c that leads to a disproportionate rise in surfactant adsorption, and the *shape* of the isotherm is almost independent of σ_c .

Micelles are not observed using AFM on any of the surfaces in the absence of salt. My results show that when the surface charge is homogeneously distributed and

⁴⁷ Pashley, R. M. *J. Colloid Interface Sci.* **1981**, *83*, 531–546.

⁴⁸ Pashley, R. M. *J. Colloid Interface Sci.* **1981**, *80*, 153–162.

⁴⁹ Patrick, H. N.; Warr, G. G.; Manne, S.; Aksay, I. A. *Langmuir* **1999**, *15*, 1685–1692.

⁵⁰ Manne, S.; Schaffer, T. E.; Huo, Q.; Hansma, P. K.; Morse, D. E.; Stucky, G. D.; Aksay, I. A. *Langmuir* **1997**, *13*, 6382–6387.

⁵¹ Fielden, M. L.; Claesson, P. M.; Verrall, R. E. *Langmuir* **1999**, *15*, 3924–3934.

fixed and the surfactant is almost the only counterion available, a homogeneous distribution of the surfactant across the surface is at a lower energy than an inhomogeneous distribution. The addition of mobile counterions to the surface charge (other than the surfactant) allows the introduction of lateral inhomogeneity in the surfactant adsorption. This leads me to hypothesize that, for ionic surfactants, a lateral redistribution of surface charge to produce a heterogeneous surface charge (a form of charge regulation) is important for forming the heterogeneous surfactant layers known as surface micelles. This effect should be particularly important for surfactants in which the optimal area occupied by the surfactant headgroup in solution is a function of solution conditions. Because lateral charge regulation is an important factor in allowing the formation of surface micelles, it is also an important factor in determining the shape of the adsorption isotherm for ionic surfactants.

CHAPTER 4: UNNATURAL PROTEINS FOR THE CONTROL OF SURFACE FORCES*

4.1. Introduction

Many items are fabricated from a dense suspension of colloidal particles. The suspension is formed into the desired shape and then fixed, usually by heating to increase the area of contact between the particles. This colloidal processing technique relies on the ability to form a suspension of controlled density and viscosity. For example, in ceramic processing, it is desirable to form a high-density and low-viscosity suspension. A high density of particles is required for strength of the fired ceramic, and a low viscosity is required for ease of molding (workability). Many clay minerals exhibit these properties naturally in water. Water is the preferred solvent because it has the minimum environmental impact, and it is inexpensive. However, to achieve the workability of clay with a different type of particle requires knowledge of the origin of workability, and a means to implement this knowledge.

It is now well known that workability arises from repulsive forces between particles.¹ If the forces are monotonically attractive and strong, then each particle collision results in the particles becoming trapped in an adhesive minimum with a structure that relates to the geometry of the collision, and the structure is not controlled.² The colloidal suspension then has a low density and high viscosity. If the particles exhibit a short-ranged repulsion, then they won't be trapped in the primary van der Waals minimum, because the particles will be pushed away due to the repulsive force as they approach one another during a collision.^{3,4} This repulsive force will allow the particles to

* This chapter has been reproduced in part with permission from *Langmuir*, submitted for publication. Unpublished work copyright 2004 American Chemical Society.

¹ Norrish, K. *Dis. Faraday Soc.* **1954**, *18*, 120–134.

² Ottewill, R. H. In *Concentrated Dispersions*; Goodwin, J. W., Ed.; Dorset Press: Dorset, 1982.

³ Velamakanni, B. H.; Chang, J. C.; Lang, F. F.; Pearson, D. S. *Langmuir* **1990**, *6*, 1323–1325.

freely slide past each other. In fact, a low friction between surfaces has been found to correlate with a low-viscosity slurry.⁵

In more advanced applications, it is desirable to go beyond merely imitating the properties of clay and, for example, gain control over the architecture of mixtures of particles or manipulate the orientation of particles. This increased level of control will be achieved through the control of surface forces between the particles.

A van der Waals force will always be present, and is always attractive between like particles. The van der Waals force, F , has a power-law dependence

$$F = \frac{AR}{12 S^2} \quad (4.1)$$

where the objects are spheres of radius, R , S is the separation between the surfaces, and A is the Hamaker constant.⁶ Therefore, the force becomes very large and attractive at small separations. The ability to gain control over interparticle forces is largely a problem of either reducing the van der Waals force by immersing the particles in a medium or coating the surface, or overcoming the van der Waals force with another force such as the electrostatic double-layer force, a hydration force or a polymer steric force.

Unfortunately particle processing is sometimes hindered by the fact that some ceramic particles have a large Hamaker constant in water (e.g. $\sim 5 \times 10^{-20}$ for alumina–water–alumina)⁷. The high dielectric constant of water suggests that the remedy is a repulsive double-layer force. This solution is undesirable because of the need to add a large amount of salt, that brings the particles closer by shrinking the debye length of the electrostatic double layer force thereby increasing the density of the slurry. The salt added may remain in the clay after firing and may lead to changes in the property of the product.

An alternative means of stabilizing particles is to adsorb organic molecules to the surface of the particle. This has two advantages: the adsorbed molecules can generate additional repulsive steric forces, and the adsorption will often reduce the van der Waals

⁴ Ducker, W. A.; Clarke, D. R. *Colloids Surfaces A* **1994**, *93*, 275–292.

⁵ Ducker, W. A.; Luther, E. P.; Clarke, D. R.; Lange, F. E. *J. Am. Ceram. Soc.* **1997**, *80*, 575–583.

⁶ Israelachvili, J. N. *Intermolecular and Surface Forces*; Academic Press: San Diego, 1991.

⁷ Hough, D. B.; White, L. R. *Advances in Colloid and Interface Science* **1980**, *14*, 3–41.

force. A very thick dense hydrocarbon layer will cause a reduction of the Hamaker constant to $\sim 0.4 \times 10^{-20}$,⁷ a thick layer of polymer with a very high water content will effectively reduce the van der Waals force to zero.

There is already considerable prior work on the measurement of forces between polymer coated surfaces.⁸ The literature most relevant to my work is the measurement of forces between surfaces coated with polymer brushes. A polymer brush forms when the polymer is end-anchored to the solid with such a high density that the extent of the polymer chain normal to the interface, L , is greater than the size of the molecule free in solution. de Gennes has used a scaling argument to determine the energy of interaction between surfaces covered with polymer brushes.⁹ The interaction energy per unit area between two flat solids, E_A , as a function of the separation, S , is *approximately*:

$$E_A = \frac{100L}{\pi S^3} k_B T \exp\left(-\frac{\pi S}{L}\right) \quad (4.2)$$

for $0.2 < S/L < 0.9$. T is the temperature and k_B is the Boltzmann constant.

One method for anchoring the polymer to the interface is to use a diblock copolymer in which one block, the anchor block, has a strong affinity for the solid surface and the other block, the tail block, has a relatively high affinity for the solvent. Initial measurements of forces between diblock copolymer adsorbed surfaces have been done in organic solvents (See also Section 1.4.3).¹⁰ Here, I am interested in studies done in water only. Claesson et al.¹¹ have measured forces between poly(butyleneoxide)–poly(ethyleneoxide)-coated hydrophobic mica in water. The range of these steric forces was in approximate agreement with the theory of Scheutjens and Fleer.¹² Kelley et al.¹³

⁸ For reviews see:

Patel, S. S.; Tirrell, M. *Annu. Rev. Phys. Chem.* **1989**, *40*, 597–635.

Ploehn, H. J.; Russell, W. B. *Adv. Chem. Eng.* **1990**, *15*, 137–228.

⁹ de Gennes, P. G. *Adv. Colloid Interface Sci.* **1987**, *27*, 189–209.

¹⁰ Hadziioannou, G.; Patel, S.; Granick, S.; Tirrell, M. *J. Am. Chem. Soc.* **1986**, *108*, 2869–2876.

Tirrell, M.; Patel, S.; Hadziioannou, G. *Proc. Natl. Acad. Sci. USA* **1987**, *84*, 4725–4728.

Taunton, H. J.; Toprakcioglu, C.; Fetters, L. J.; Klein, J. *Macromolecules* **1990**, *23*, 571–580.

Watanabe, H.; Tirrell, M. *Macromolecules* **1993**, *26*, 6455–6466.

¹¹ Schillen, K.; Claesson, P. M.; Malmsten, M.; Linse, P.; Booth, C. *J. Phys. Chem. B* **1997**, *101*, 4238–4252.

¹² Scheutjens, J. M. H. M.; Fleer, G. J. *J. Phys. Chem.* **1979**, *83*, 1619–1635.

Scheutjens, J. M. H. M.; Fleer, G. J. *J. Phys. Chem.* **1980**, *84*, 178–190.

have measured steric forces between a silicon nitride tip and a polyelectrolyte brush formed by the adsorption of poly(tert-butylstyrene)–sodium poly(styrene-4-sulfonate), PtBS–NaPSS, on mica. They have observed a decrease in the range of the forces upon salt addition. They attribute this to the shrinking of the brush height with increase in salt concentration. Similar conclusions were also drawn by Balastre et al.¹⁴, who have used surface forces apparatus to measure the steric forces between two hydrophobized mica surfaces covered with PtBSS–NaPSS.

Butt et al.¹⁵ measured forces between a silicon nitride AFM tip and an alumina-coated glass slide in poly(methacrylic acid)–poly(ethylene oxide). Before adsorption, the force was attractive, after adsorption the force was repulsive and was fitted to a double-exponential with two decay-lengths: 3.4 and 11.2 nm. A very similar system was studied by Palmqvist et al.¹⁶ They studied the *consolidation* of alumina particles in the presence of poly(methacrylic acid)–poly(ethylene oxide) copolymer and measured the forces between polymer-coated BaTiO₃ surfaces. They found that the adsorption of polymer produced a repulsive force on separation of the surfaces.

All of the above systems utilized synthetic polymers for the steric stabilization of colloidal particles. The development of recombinant DNA technology and recent successes in producing unnatural proteins suggest a new route for obtaining polymers for the control of particle suspensions. Here, I am using a new strategy in which the colloidal scientist specifies the exact sequence of a polymer that is required (the target polymer) and that polymer is synthesized by microorganisms. Briefly, the desired protein sequence is coded into DNA, transferred into a microorganism (e.g. via a plasmid into *E. Coli*), the transformed microorganism is then allowed to reproduce into large numbers to express the target polymer, and finally the target polymer is extracted and used in colloidal processing.

¹³ Kelley, T. M.; Schorr, P. A.; Johnson, K. D.; Tirrell, M.; Frisbie, C. D. *Macromolecules* **1998**, *31*, 4297–4300.

¹⁴ Balastre, M.; Li, F.; Schorr, P.; Yang, J.; Mays, J. W.; Tirrell, M. V. *Macromolecules* **2002**, *35*, 9480–9486.

¹⁵ Butt, H.-J.; Kappl, M.; Mueller, H.; Raitereri, R.; Meyer, W.; Ruhe, J. *Langmuir* **1999**, *15*, 2559–2565.

¹⁶ Palmqvist, L. M.; Lange, F. F.; Sigmund, W.; Sindel, J. J. *Am. Ceram. Soc.* **2000**, *83*, 1585–1591.

There are numerous advantages to this biological synthesis of polymers. In contrast to conventional polymer synthesis, it is possible in principle to exactly specify in advance the type and position of every monomer in the sequence; one can form sequences with much greater complexity than the usual diblock or triblock synthetic polymers. Monodisperse polymers are produced. The entire process is environmentally friendly, in particular, the process creates no elemental pollution and water is the only solvent used in the synthesis. In practice, as shown below, there have been some difficulties in purification and in production of the desired sequence.

The generic unnatural protein design is shown schematically in Figure 4.1. Note that the blocks do not need to be homopolymers, and in fact this is preferred for the ease of protein expression for microorganisms.



Figure 4.1 The generic unnatural protein design.

In this design, there is a tether block, which should bind to the surface in preference to the solvent. It should also be able to displace the other blocks off the surface, so that the spacer and active blocks are pushed into solution. The chemical nature of the tether block can be found either by rational design, in the light of the surface chemical properties of the solid particle or by combinatorial search¹⁷. There is an active block at the opposite end of the sequence so that it is easily presented to solution. For some systems, a spacer segment may be required to move the active block away from the solid and to allow extra conformational freedom for the active block. This spacer segment would normally be hydrophilic to maintain its partitioning into the solvent (water). Additional segments may be required to promote the correct orientation of the active block (Joint, J, segments) and to allow identification (I) of the polymer during either

¹⁷ Whaley, S. R.; English, D. S.; Hu, E. L.; Barbara, P. F.; Belcher, A. M. *Nature* **2000**, *405*, 665–668.

purification or characterization process (e.g. aromatic groups for identification by UV spectrophotometry if such groups are not present in the other blocks). This type of architecture could, for example, be used to float an enzyme, or any other receptor above a surface in solution (active block= enzyme or receptor).

In this study, this generic unnatural protein design has been applied to devise proteins for the control of surface forces between alumina particles. The active block is hydrophilic and is designed such that restriction of it to a smaller volume requires an input of energy, and therefore produces a repulsive, stabilizing force in aqueous solutions. Thus, the same block can perform the task of both the spacer and the active segments. In addition, there are no specific joint or information segments incorporated into the unnatural protein structure in this study. The protein has been synthesized by Doug Henderson (via E.Coli) in the van Cott lab at the Chemical Engineering Department, Virginia Tech.

The active block of the unnatural protein consists of two segments, a homopolymer of proline, Pro₃₉, and a mutant of the natural protein thioredoxin. The original objective was to only incorporate the Pro₃₉ segment. Proline was chosen as the amino acid, because it forms the only water-soluble neutral homopolymer. The use of thioredoxin as a stabilizing block was originally unintentional; the code for a thioredoxin mutant, His-patch thioredoxin was incorporated into the gene to aid in the expression, detection and purification of the unnatural protein. His-patch thioredoxin (Trx) is a mutant in which the glutamic acid (Glu) residue at position 32 and the glutamine (Gln) residue at position 64 have been replaced with histidine residues.¹⁸ When the protein folds into its native 3-dimensional structure, these histidines along with a native histidine at position 8 form a 'histidine patch' on the protein surface (See Figure 4.2). Histidine patches have been shown to have high affinity for divalent cations and, therefore, can be used to easily purify the fusion protein on metal chelating resins.¹⁹ Trx also improves the solubility of the recombinant protein products,¹⁹ as well as in their detection by offering a moiety that is recognized by commercially available antibodies.

¹⁸ Lu, Z.; DiBlasio-Smith, E. A.; Grant, K. L.; Warne, N. W.; LaVallie, E. R.; Collins-Racie, L. A.; Follettie, M. T.; Williamson, M. J.; McCoy, J. M. *J. Biol. Chem.* **1996**, *271*, 5059–5065.

¹⁹ Lavallie, E. R.; DiBlasio, E. A.; Kovacic, S.; Grant, K. L.; Schendel, P. F.; McCoy, J. M. *Bio-Technology* **1993**, *11*, 198–193.

The aim was to cleave off and discard the Trx before using the remainder of the unnatural protein to stabilize particles. However, after expression, the cleavage of the linkage between Trx and the remainder of the protein was unsuccessful. Fortunately, Trx actually has desirable properties for particle stabilization. The key feature is that of the 113 amino acids in the protein, 13 are acidic and 14 are basic (including 3 partially charged histidine residues), so at neutral pH Trx is zwitterionic (the isoelectric point is pH = 6.2). Because the protein is approximately neutral at pH 5–7, the force contribution from adsorbed Trx layers should be relatively insensitive to salt and pH in the neutral range. The acidic and basic monomers are spread roughly evenly through the primary sequence and in the folded structure.²⁰ The approximate size of the thioredoxin is 2.5 nm × 3.4 nm × 3.5 nm.²¹

Polyproline is an unusual protein because proline is the only cyclic amino acid of the twenty common amino acids. The five-membered ring that spans the α -carbon and the nitrogen leads to a restriction of rotation about the α -carbon–carbonyl bond and therefore to the existence of *cis* and *trans* forms of the monomer at room temperature. The existence of a significant fraction of *trans* conformations leads to a larger persistence length than for other neutral homopeptides. The unnatural protein that is described in this study includes a block of 39 proline monomers. The root-mean-squared end-to-end distance of this polymer in water is approximately 5 nm, $R_{\text{RMS}} = [nl^2C_\infty]^{0.5} \sim 5$ nm. ($C_\infty = 13.7$ in water,²² effective bond length, $l = 0.127$ nm; the number of segments, $n = 39 \times 3$ bonds per monomer). So a free chain of Pro₃₉ is expected to have a distance of about 5 nm between its N and C termini in water and a radius of gyration of 2 nm, $R_g \sim 2$ nm. The secondary structure of polyproline chains is known to depend on the solvent conditions, and in particular, is known to adopt a shorter conformation (more *cis* forms) in concentrated salt solutions.²² Earlier work by Krsmanovic and Davis shows that polyproline adsorbs only very weakly to the surface of alumina, so the polyproline block should not lie flat on the surface.²³

²⁰ Protein Data Base www.rcsb.org/pdb/.

²¹ Holmgren, A.; Soderberg, B.; Eklund, H.; Branden, C. *Proc. Natl. Acad. Sci.* **1975**, *72*, 2305–2309.

²² Mattice, W. L.; Mandelkern, L. *J. Am. Chem. Soc.* **1971**, *93*, 1769–1777.

²³ Please see the PhD thesis of J. Krsmanovic.

The tether block is found by rational design, by use of the knowledge of the surface chemistry of alumina. Alumina is positively charged at neutral pH and has a large Hamaker constant in water. This large Hamaker constant makes it unstable in concentrated salt solutions. It can be dispersed in water through the adsorption of anionic polymers^{24,25} or through the adsorption of diblock copolymers.^{16, 26} Therefore for the tether block, a polyacid, a decamer of glutamic acid (Glu₁₀) is used. In retrospect, it would have been better to also incorporate some aspartic acid units as bacteria (E. Coli) tend to reject long sequences of repetitive DNA codes. Earlier work by Krsmanovic and Davis shows that polyglutamic acid adsorbs to alumina from dilute solutions, and that polyglutamic acid adsorbs almost exclusively from mixtures of polyglutamic acid and polyproline.²³ Earlier in the Ducker and Davis lab, a combinatorial search has also been performed in search for a tether block, but it was not successful.²⁷

To summarize, Figure 4.2 shows a schematic of the target unnatural protein and the target adsorbed polymer layer. The Glu₁₀ block is expected to adsorb strongly to the alumina surface and also to approximately neutralize the surface charge. The polyproline should not adsorb to alumina, and the Trx should be situated well away from the surface owing to the solubility of the Pro₃₉ block. The Trx is approximately neutral, so the net electrostatic forces between the unnatural protein coated surfaces should be small. The existence of a water-rich region between the Trx and the alumina surface should greatly reduce the van der Waals force between the adsorbed layers in water.

²⁴ Pan, Z.; Somasundaran, P.; Senak, L. *ACS Symposium Series* **2004**, *878*, 185-204.

Baklouti, S.; Ben Romdhane, M. R.; Boufi, S.; Pagnoux, C.; Chartier, T.; Baumard, J. F. *J. European Ceram. Soc.* **2003**, *23*, 905-911.

Fukuda, Y.; Togahi, T.; Suzuki, Y.; Naito, M.; Kamiya, H. *Chemical Engineering Science* 2001, *56*, 3005-3010.

Orth, J.; Meyer, W. H.; Bellmann, C.; Wegner, G. *Acta Polymerica* **1997**, *48*, 490-501.

Ishiduki, K.; Esumi, K. *Langmuir* **1997**, *13*, 1587-1591.

Tada, H.; Saito, Y.; Hyodo, M. *Shikizai Kyokaiishi* **1992**, *65*, 671-675.

²⁵ Kamiya, H.; Fukuda, Y.; Suzuki, Y.; Tsukada, M. *J. Am. Ceram. Soc.* 1999, *82*, 3407-3412.

²⁶ Zaman, A. A.; Tsuchiya, R.; Moudgil, B. M. *J. Colloid Interface Sci.* **2002**, *256*, 73-78.

²⁷ A combinatorial search using a (bacterial) FliTrxTM Library in PBS buffer was conducted by Nurxat Nieraji and Beth Caba. The buffer was included to aid the survival of the bacteria. The sequences that were found were all cationic, which was at first surprising. However, zeta potential measurements showed that the potential on alumina particles changed from positive to negative in the presence of the phosphate buffer, presumably through adsorption of divalent phosphate. This highlighted the necessity of performing the combinatorial search under the same conditions as for the application of the polymer. In future work, it would be better to use a microorganism library, (e.g. a viral library¹⁷) which could survive with fewer (or no) additional molecules in solution.

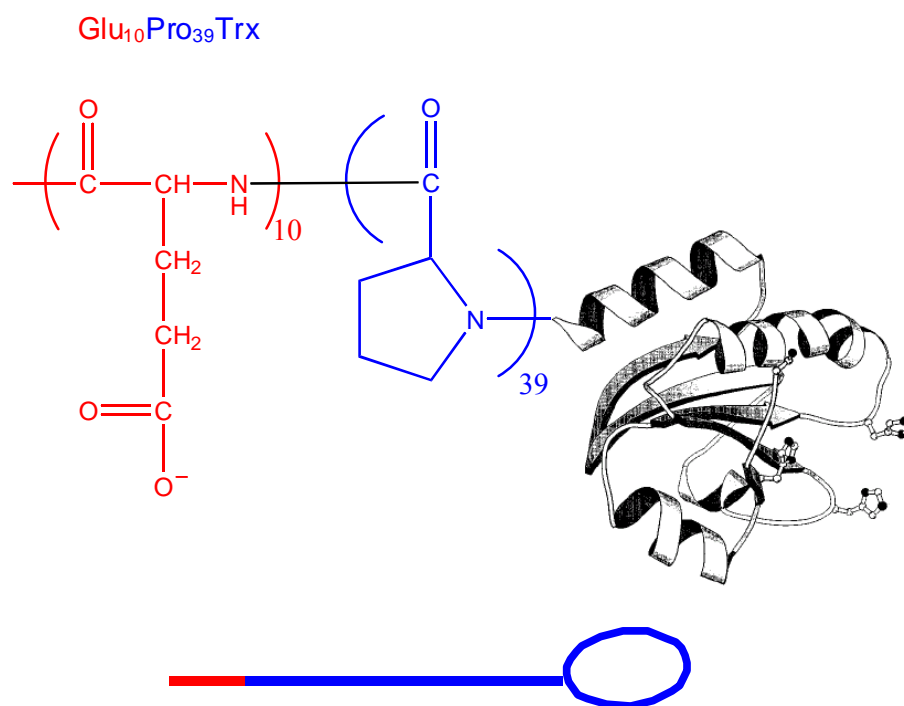


Figure 4.2a Target unnatural protein structure.

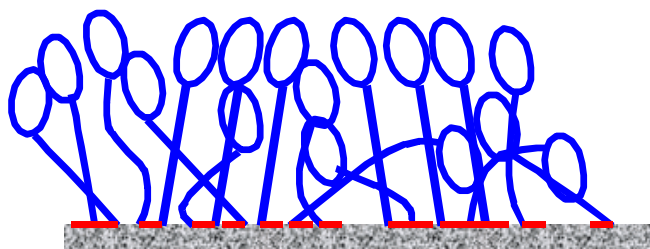


Figure 4.2b Target adsorbed layer structure.

In practice my results show that the interaction forces between alumina surfaces bearing adsorbed layers of the unnatural protein do exhibit a long-range repulsion that is independent of salt concentration, as expected and as required for colloidal stability. For a control experiment, surface forces between Trx covered alumina surfaces have also been measured. However, the synthesized Trx has extra amino acids on the C-terminus

which confers a slightly negative charge at pH~7 due to the excess of acidic monomers (7) over basic monomers (5). Thus, one might expect slightly greater adsorption of the Trx control than for a control that exactly matched the Trx domain of the unnatural polymer.

4.2. Experimental Section

4.2.1. Biosynthesis.

The synthesis of the unnatural protein has been performed by Doug Henderson in the van Cott lab at the Chemical Engineering Department, Virginia Tech.

4.2.2. Materials for Adsorption Experiments.

Water was purified with an EASYpure UV (Barnstead Thermolyne Corp., Dubuque, IA) that consisted of ion-exchange, charcoal, UV, and filtration stages. KNO₃ (Aldrich, Milwaukee, WI) was recrystallized twice from 200 proof ethanol (Aaper Alcohol Chemical Co., USA) and purified water (90:10). KOH (Aldrich, Milwaukee, WI) was roasted in air at 400°C for 16 h. HNO₃ (Fischer Scientific, Fairlawn, NJ) was used as received. Single crystal alumina (sapphire) plates (Commercial Crystal Laboratories, Naples, FL) with a 12 mm × 12 mm (0001) surface (c-axis) had an rms roughness of <0.5 nm over 1 μm² and polycrystalline alumina spheres of radius ~ 15 μm (R.S.A. Le Rubis S.A., Jarrie, France) had an rms roughness of 3 nm over 1 μm². Prior to each experiment the sapphire plates were soaked in warm HNO₃ overnight and boiled in HNO₃ for one hour then allowed to cool and then rinsed with purified water. Both solids were treated with oxygen plasma (March Instruments, Concord, CA) for 3 min at 40 Watts at ~250mTorr to render the surfaces hydrophilic and to remove organic material.

4.2.3. Solutions.

Protein solutions were prepared in 1.5 ml Eppendorph tubes and electrolyte solutions were prepared in 30 ml. polycarbonate bottles (Nalge Company, Rochester, NY) to prevent contamination of the alumina surfaces by dissolved or colloidal silica. Polycarbonate bottles were soaked in 10 % Liqui-Nox solution (Alconox, White Plains, NY) overnight and rinsed with copious amounts of water, left in water overnight, rinsed

with ethanol and again with water and left in water with caps on until use. They were rinsed with water prior to solution preparation. KOH and HNO₃ were used to adjust the pH of the solutions. Hydrogen ion activities were determined by a pH meter (Orion, Beverly, MA) and by a micro combination pH electrode (Lazar Research Laboratories, Los Angeles, CA) for protein solutions. Measurements were made relative to standard buffers of potassium hydrogen phthalate, pH 4.01 (Orion, Beverly, MA), pH 7.01 (Orion, Beverly, MA), and pH 10.01 (Orion, Beverly, MA).

4.2.4. Ellipsometry.

A phase modulation ellipsometer²⁸ (Beaglehole Instruments, Wellington, New Zealand) with a HeNe laser ($\lambda = 632.8$ nm) was used to measure adsorption to a sapphire plate that was effectively a transparent dielectric, having only a small value of the imaginary component of the reflectivity, $\text{Im}(r) \sim 0.005$ at Brewster angle, θ_B . Because the refractive index of the alumina plate is around 1.76,²⁹ the optical contrast between the alumina plate and water is too small for an accurate ellipsometric measurement. All measurements were performed in air, after adsorbing the protein in aqueous solution. After adsorption of the protein, the alumina plate was rinsed in exactly the same manner as for the AFM experiments, and then dried with nitrogen. The experiment was repeated four times and the results were consistent.

4.2.5. Atomic Force Microscopy (AFM).

Force–Separation measurements were obtained with an AFM (Molecular Imaging, Phoenix, AZ). The alumina spheres were attached to AFM cantilevers as described previously³⁰ using 5-minute epoxy (Devcon, Riviera Beach, FL). The spring constants (~ 0.5 Nm⁻¹) of the tipless cantilevers (Ultrasharp noncontact silicon cantilevers NSC12, Silicon-MDT, Moscow, Russia) were determined by the Cleveland method.³¹

The z-axis of the piezo was calibrated by a silicon calibration reference of 22.0 nm step height (Silicon-MDT, Moscow, Russia). The calibration was cross-checked by

²⁸ Beaglehole, D. *Physica A* **1980**, *100B*, 163.

²⁹ Palik, E. D. *Handbook of Optical Constants of Solids*; Academic Press: New York, 1985.

³⁰ Ducker, W.; Senden, T. J.; Pashley, R. M. *Langmuir* **1992**, *8*, 1831–1836.

³¹ Cleveland, J. P.; Manne, S.; Bocek, D.; Hansma, P. K. *Rev. Sci. Instrum.* **1993**, *64*, 403–406.

measurement of the decay length of double-layer forces in 10^{-3} , 10^{-2} and 10^{-1} molL⁻¹ KNO₃ solutions. Before the injection of the protein solutions, the point of zero charge of sapphire was determined by obtaining force curves at different pH solutions at 10^{-3} M KNO₃. The electrolyte solutions were left inside the liquid cell for 15–30 min before data acquisition. The protein solution was left inside the liquid cell for 12 hours during which time the surfaces were separated by 10µm and no force measurements were taken in order not to disturb the equilibrium adsorption of the protein. Multiple approach and separation runs were performed in each experiment and the entire experiment was performed three times (on different days). Measurements were performed in the temperature range 22 ± 2 °C.

4.3. Analysis of Raw Data

4.3.1. Calculation of Adsorbed Amount from Ellipsometry.

In ellipsometry, an elliptically polarized light is reflected off a surface and the ratio of the reflectivity of the p-polarized light to s-polarized light (r_p/r_s), r , is measured as a function of incident angle. The r has a real, Re , and an imaginary component, Im . At the Brewster angle, θ_B , $\text{Re}(r)$ is zero and a thin adsorbed film on the surface can be characterized by the change in $\text{Im}(r, \theta_B)$. The change in $\text{Im}(r, \theta_B)$ depends on the wavelength of the incident light, λ , which is 632.8 nm for our instrument, the dielectric constant of air, ϵ_1 , the sapphire, ϵ_2 , the thin protein film, ϵ , and the thickness of the film, z , according to the following equation:³²

$$\text{Im}(r, \theta_B) = \frac{\pi (\epsilon_1 + \epsilon_2)^{1/2} (\epsilon - \epsilon_1)(\epsilon - \epsilon_2)}{\lambda (\epsilon_1 - \epsilon_2) \epsilon} z \quad (4.3)$$

There are many combinations of the film dielectric constant, ϵ , and the film thickness, z , that satisfy eq 4.3, so it is impossible to obtain the refractive index n and thickness z from one measurement. To reduce the uncertainty in the adsorbed amount, we have made some assumptions about the refractive index and the thickness of the

³² Beaglehole, D.; Christenson, H. K. *J. Phys. Chem.* **1992**, *96*, 3395–3403.

monolayer. We have assumed that the thickness of the adsorbed protein layer in the *dried* state is less than 6 nm. Moreover, the refractive index of adsorbed protein layers usually is larger than 1.45.³³ On the basis of these restrictions, we can get a range of the possible thicknesses and refractive indices of the adsorbed protein layer from one measurement. For this reason, the surface density reported in the Section 4.4 has a large uncertainty. The surface density, Γ , was calculated according to the following equations,

$$n = n_0 + c \frac{dn}{dc} \quad \Gamma = cz \quad (4.4)$$

where n and n_0 are the refractive indices of the adsorbed protein layer and water, respectively. The common values of the dn/dc of protein, 0.16–0.2 ml/g,³⁴ were employed in this study and it was assumed that dn/dc is the same in solution and in the (hydrated) film after removing the bulk water with nitrogen gas.

4.3.2. Force Analysis.

The analysis of force curves has been explained in Section 2.3.1. The forces were converted to interaction energy per unit area for two flat surfaces using Derjaguin's approximation (See Section 1.4.). For the forces between alumina surfaces in the presence of 10^{-3} M KNO_3 as a function of pH, DLVO analysis was performed assuming constant potential surfaces.

4.4. Results and Discussion

4.4.1. Characterization of the Alumina Surfaces

Figure 4.3 shows the forces between an oxygen plasma treated polycrystalline alumina particle of radius, R , and a single crystal sapphire plate as a function of pH in 1 mM KNO_3 solution. The forces, F , are normalized by R . According to Derjaguin's approximation, $F/2\pi R$ is equal to the energy per unit area (See Section 1.6).

³³ Arwin, H. *Applied Spectroscopy* **1986**, *40*, 313–318.

Ball, V.; Ramsden, J. J. *Biopolymers* **1998**, *46*, 489–492.

³⁴ Jönsson, U.; Malmqvist, M.; Rönnberg, I. *J. Colloid Interface Sci.* **1985**, *103*, 360–372.

Peters, T. *Adv. Protein Chem.* **1985**, *37*, 161–245.

Ivarsson, B. A., Hegg, P. -O.; Lundström, K. I.; Jönsson, U. *Colloids Surfaces* **1985**, *13*, 169–192.

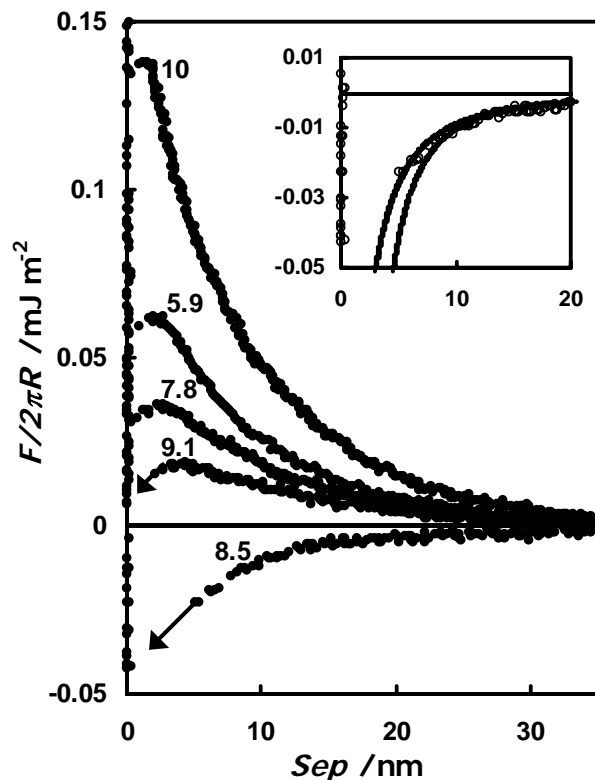


Figure 4.3 Forces between an alumina particle and a sapphire plate in the presence of 10^{-3} M KNO_3 as a function of pH. The insert shows the vdW fit for the curve at pH = 8.5.

There is a minimum in the force at about pH 8.5, indicating the loss of double-layer forces and a point of zero charge (pzc) at about 8.5. If I fit this force to a van der Waals force, using the onset of constant compliance as zero separation, then I obtain a non-retarded Hamaker constant of 4×10^{-20} J. This Hamaker constant is smaller than predicted theoretically by Hough and White (5.3×10^{-20} J)⁷ and measured previously by Horn et al. (6.7×10^{-20} J),³⁵ which is consistent with the observation that the particle is rough (~ 3 nm asperities). At zero separation in the figures, the particle is probably resting on asperities, not in smooth contact. If I shift the zero of the theoretical van der Waals force to -2.1 nm, then the fitted Hamaker constant is about 5×10^{-20} J.

Horn et al. found a pzc of about 6.7 through their force measurements.³⁵ In separate experiments, when I measured the forces without an oxygen-plasma treatment of

³⁵ Horn, R. G.; Clarke, D. R.; Clarkeson, M. T. *J. Mater. Res.* **1988**, 3, 413–416.

the surface, I found that the pzc was about 5–6. Therefore for all other experiments, I plasma-treated the surfaces to obtain a pzc of 8~9.³⁶ By this way my results can be applied to particulate alumina of the same pzc.³⁷ Clearly the pzc of alumina depends on the surface treatment.

The force increases when the pH deviates to higher or lower pH than the pzc of 8.5. The surface potentials are similar to those measured previously by Horn et al.³⁵, (22, 27, 28, 39 mV at pH = 9, 8, 6, 10, respectively.). After making measurements in pH 10 solution, the forces at pH 6 were altered: the pzc was lower. So, all measurements in protein solutions were performed on surfaces that were never exposed to solutions of pH > 8.5.

4.4.2. Adsorption and Forces in the Presence of Trx-Pro₃₉Glu₁₀

The density of Trx-Pro₃₉Glu₁₀ adsorbed to the sapphire plate from a 0.1 mg mL⁻¹ solution in 1mM KNO₃ was determined by ellipsometry. The density of adsorption was 4–10 nm²/molecule (2.8–7.2 mg/m²). When the density of adsorbed protein is compared with the approximate cross-sectional area of Glu₁₀ (2–2.5 nm²), it is seen that the short anchor block does not control the density of adsorption. Therefore, either the Trx or the Pro₃₉ block (or both) limits the adsorbed amount of the unnatural protein. An estimate for the hydrodynamic radius R_H for the Trx in water is ~ 3 nm²⁰ while the approximate cross-section of the thioredoxin crystal structure is 8–12 nm².²¹ As the range of measured adsorption areas has a maximum that is roughly equal to the cross-sectional area of a thioredoxin molecule in the crystalline state, it appears that the physical dimensions of Trx may limit adsorption. The R_g for a free Pro₃₉ chain in aqueous solution is approximately 2 nm, so the Pro₃₉ block has been confined to a smaller cross-sectional area on the surface than in free solution. This lateral confinement should also lead the adsorbed Pro₃₉ to have a greater extension normal to the surface than when free in solution, as in an adsorbed brush.

³⁶ In some cases, even though I plasma-treated the surfaces, I still got a pzc of 5~6. This is probably because of the heterogeneity of the sapphire spheres used: with a different sphere, and with the same sapphire plate and procedure, I have observed pzc at pH 8~9.

³⁷ Modi, H. J.; Fuerstenau, D. W. *J. Phys. Chem.* **1957**, *61*, 640–643.
Wiese, G.R.; Healy, T.W. *J. Colloid Interface Sci.* **1974**, *51*, 427–433.
Franks, G.V.; Meagher, L. *Colloids Surf., A* **2003**, *214*, 99–110.

Surface forces with adsorbed protein layers were measured by the following procedure. First, I measured the force in KNO_3 solution as a function of pH. I only continued if the pzc was ~ 8.5 . The surfaces were then exposed to a 0.1 mg mL^{-1} aqueous solution of Trx-Pro₃₉Glu₁₀ solution in 1 mM KNO_3 for about 12 hours. The forces were measured in the presence of protein, and were measured again after the protein was rinsed with 1 mM KNO_3 . The forces were usually slightly longer-ranged and more hysteretic in the presence of protein solution, suggesting that there was some weakly and reversibly adsorbed polymer that was easily removed by rinsing. All forces shown here were measured after rinsing.

Figure 4.4 shows the forces between alumina surfaces bearing the unnatural protein (Trx-Pro₃₉Glu₁₀) at pH ~ 6 (unbuffered). After adsorption of a thick Protein layer, it is not possible to determine the absolute separation between the alumina surfaces with an AFM. In the future, experiments using TIRM-AFM can be performed to determine the absolute separation between the alumina surfaces and to estimate the thickness of the adsorbed Protein layer. Surface forces apparatus may be used as well, but the requirement to use large volumes of solutions with this technique may limit us, unless we have enough of the unnatural Protein. For my results with AFM, the zero of the distance scale (zero on the x-axis in Figure 4.4a) represents the separation at which the sphere encounters a steep repulsive wall: at this separation, the Protein film is now less compliant than the cantilever spring. However, the Protein film still has a finite thickness at this position, so I have indicated an estimate of my uncertainty in the “real” distance between two alumina surfaces with the shaded area between 0 and -10 nm . Another observation that shows me the uncertainty in the determination of the absolute zero separation is the distribution of force-distance curves from multiple runs (sometimes upto 50% standard deviation of force at a specific distance below 5 nm). The distribution of force-distance curves may be a result of the choice of the constant compliance region and the effect of the compression of the Protein layer from a previous force run. The force-distance curves are usually superimposable beyond 5 nm.

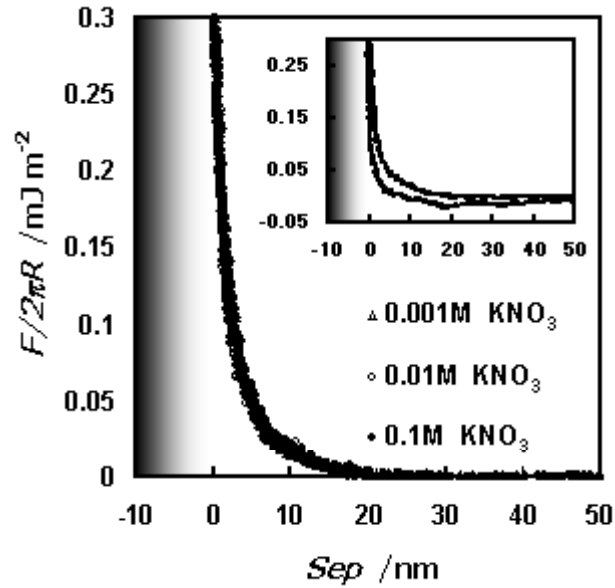


Figure 4.4a Forces between unnatural Protein covered alumina surfaces as a function of KNO_3 concentration. The insert shows the hysteresis in force measurements.

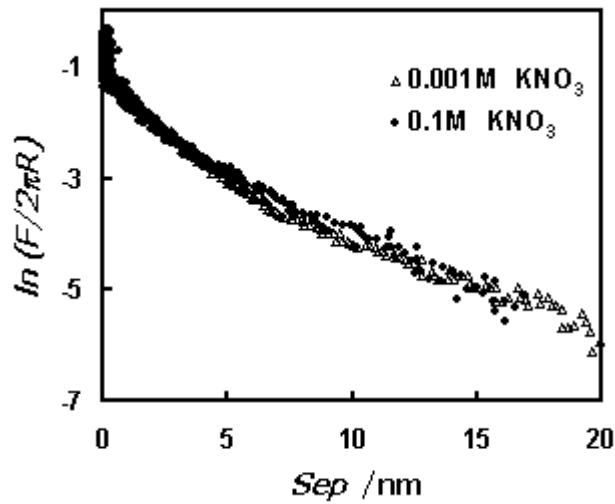


Figure 4. 4b Semi-logarithmic plot of forces between unnatural Protein covered alumina surfaces. The linearity shows an exponential Profile for the steric force.

Figure 4.4a shows that the force is now approximately independent of the salt concentration at all separations and thus double-layer forces are absent. I have created the desired repulsive force for colloidal Processing that is repulsive and is independent of salt

concentration. The Proposed mechanism is that the Glu₁₀ block has neutralized the alumina charge and the remaining Trx-Pro₃₉ blocks are providing steric stabilization by forming a brush-like layer at the surface.

In Figure 4.4b the forces plotted on a semi-log scale to show that the force is exponential with a decay length of 5.2 ± 0.5 nm. If I model the adsorbed layer as a brush, this is consistent with a brush length of 15–18 nm, suggesting that the Pro₃₉ block (and possibly the Trx block) may be more extended in the adsorbed film than free in bulk solution. However, I don't have any experimental proof for the conformation of the adsorbed protein. In the future, neutron reflectivity studies may be carried out for this purpose.

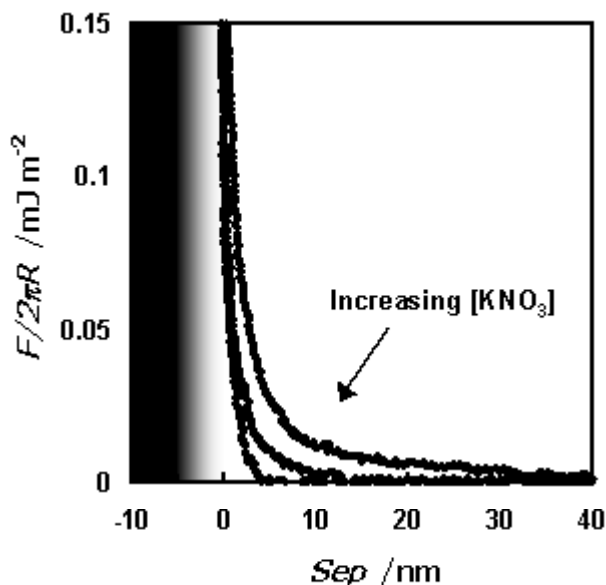


Figure 4.5 Forces between Trx covered alumina surfaces as a function of KNO₃ concentration. The KNO₃ concentration dependence of the forces shows that there is an electrostatic component in the measured forces.

Figure 4.5 shows the force in the presence of adsorbed thioredoxin that does not have the Pro₃₉Glu₁₀ tether. The force is repulsive, but the force also decreases with salt concentration. The reduction in the range with increased salt concentration shows that there is a double-layer or electrosteric force between the surfaces. Since the Trx is approximately neutral, this result suggests that the adsorption has not neutralized the alumina charge. So the role of the anchor block in Trx-Pro₃₉Glu₁₀ fusion protein is not

only to anchor the protein to enable steric forces, but also to neutralize the alumina charge. Support for the hypothesis of electrostatic forces comes from the correlation between the decay length of the force and the theoretical Debye-length, as shown in Table 4.1.

Table 4.1 Comparison between experimental decay length of measured forces between Trx-coated alumina and the theoretical Debye-length. The close agreement between theoretical and experimental decay lengths shows that the Trx does not neutralize the surface charge of alumina.

| [KNO₃] (mol/L) | Decay Length (nm) | κ^{-1} (nm) |
|--------------------------------------|------------------------------|--|
| 0.001 | 9.9 ± 2.6 | 9.5 |
| 0.01 | 3.4 ± 0.7 | 3.0 |
| 0.1 | 1.5 ± 0.5 | 0.95 |

The thioredoxin control is not identical to the thioredoxin block in Trx-Pro₃₉Glu₁₀: the control protein has an additional 30 amino acids, 5 positive and 7 negative, which make the protein slightly negative at neutral pH. If this addition has an effect, it is likely to enhance adsorption and neutralization of the positively-charged alumina, but clearly the effect is not enough to produce the desired forces.

4.5. Conclusions

A new method is introduced for the stabilization of colloidal particles via the synthesis and adsorption of unnatural proteins. An unnatural protein with the sequence: thioredoxin-Pro₃₉Glu₁₀, is used for the modification of the forces between alumina particles. The Glu₁₀ sequence is anionic (pH > 4) and is designed to anchor the protein to positively charged solids, e.g. alumina in water (pH <9). The Pro₃₉ is neutral and the thioredoxin (a natural globular protein) is zwitterionic. These two blocks are designed to remain in solution and provide a steric barrier to the approach of two particles in a range of salt and pH conditions. Ellipsometry experiments show that this unnatural protein does adsorb to alumina. Force measurements with the Atomic Force Microscopy (AFM) colloid probe technique show that adsorption of the unnatural protein leads to repulsive

forces that decay exponentially with separation between the surfaces, and are independent of salt concentration in the range 0.001–0.1 M KNO₃. The independence from salt concentration demonstrates that the repulsive forces are not electrostatic. The repulsion is due to the confinement of the adsorbed protein between two surfaces and loss of water from the confined adsorbed protein layer. The absence of a salt-dependent force also shows that adsorption of the protein has effectively neutralized the charge on the alumina. The forces are similar to those expected for a polymer brush, but the presence of the globular thioredoxin block probably produces a more complex structure than in a conventional brush. Force measurements on thioredoxin (only)-coated alumina surfaces also show a repulsive force, but the force has a decay length that is consistent with electrostatic double-layer forces: the thioredoxin has not neutralized the surface charge of the underlying alumina.

CHAPTER 5: POLYMER-SURFACTANT INTERACTIONS AT THE SILICA-WATER INTERFACE

5.1. Introduction

Polymer-surfactant mixtures are widely utilized in both biological and industrial processes. The colloidal science behind these processes involves the investigation of how these molecules interact at the solid-liquid interface. This interaction can be studied in terms of adsorption isotherms,¹ adsorbed layer thickness measurements and direct visualization of polymer-surfactant complexes on surfaces.²

The presence of a polymer/surfactant in the vicinity of a solid surface can either inhibit or promote the adsorption of surfactant/polymer. In some cases, the polymer forms a complex with the surfactant on the surface. The aim of this work is to study the adsorption behavior of a polymer-surfactant mixture at the solid-aqueous interface using atomic force microscopy (AFM). The system of choice is poly(ethyleneoxide)-sodium dodecyl sulfate, PEO/SDS, at the silica-water interface. The bulk properties of PEO/SDS mixtures have been thoroughly studied,³ but there is some discrepancy in the literature for the adsorption behavior of this system. Somasundaran et al.⁴ have observed an increase in the adsorption of SDS with a preadsorbed layer of PEO on silica, while Cosgrove et al.⁵ have observed desorption of PEO off the surface with the introduction of SDS to the medium. I have imaged the silica surface and performed force measurements in the presence of PEO and PEO/SDS mixtures as a function of SDS concentration in an effort to shed light onto the behavior of this system. My hypothesis is that above a critical surfactant concentration, there will be SDS aggregates adsorbed on the PEO covered

¹ Tadros, T. F. *J. Colloid Interface Sci.* **1974**, *46*, 528–540.

Esumi, K.; Otsuka, H. *Langmuir* **1994**, *10*, 45–50.

Otsuka, H.; Ring, T. A.; Li, J.; Caldwell, K. D.; Esumi, K. *J. Phys. Chem. B* **1999**, *103*, 7655–7670.

² Fleming, B. D.; Wanless, E. J.; Biggs, S. *Langmuir* **1999**, *15*, 8719–8725.

³ Francois, J.; Dayantis, J.; Sabbadin, J. *Eur. Polym. J* **1985**, *21*, 165–174.

Karlstrom, G.; Carlsson, A.; Lindman, B. *J. Phys. Chem.* **1990**, *94*, 5005–5015.

Ramachandran R.; Kennedy, G. *J. Colloids Surf.* **1991**, *54*, 261–266.

⁴ Somasundaran, P.; Maltesh, C. *J. Colloid Interface Sci.* **1992**, *153*, 298–301.

⁵ Cosgrove, T.; Mears, S. J.; Thompson, L.; Howell, I. *In Surfactant Adsorption and Surface Solubilization*, Sharma, R., Ed.; ACS: Washington DC, 1995; p. 138-152.

silica surface (maybe in the form of PEO/SDS complexes), if the presence of PEO induces the adsorption of SDS on silica.

5.2. Experimental Section

5.2.1. Materials and Solutions

PEO with a molecular weight of 200, 000 g/mol and a molecular weight distribution of 1.06 was supplied from Polymer Laboratories (Amherst, MA). NaCl (Sigma, St. Louis, MO) was roasted in oven at 400°C overnight. HCl was used without further purification. SDS (Sigma, St. Louis, MO) was purified according to the procedure described in Section 2.2.1. Quartz plates (Alfa Aesar, Ward Hill, MA) were prepared according to the procedure described in Section 2.2.3. The cantilevers were the same as those used for imaging in Section 3.2. The silica probe preparation was described in Section 2.2. Solutions were prepared with nanopure water (EASYpure UV, Barnstead Thermolyne Corp., Dubuque, IA) and PEO solutions were used after the polymer fully dissolved in water at room temperature.

5.2.2. AFM Measurements

Imaging and force measurements were performed with an AFM (Molecular Imaging, Phoenix, AZ). For imaging experiments, the cell was immersed in water initially, and the force between the silicon or silicon nitride tip and the quartz surface was measured. If the force curve is repulsive and there is no adhesion, the system was assumed to be free of contamination and the PEO solution (~ 200 ppm) was introduced into the cell. The PEO was left to equilibrate in the cell overnight. The quartz surface was then imaged in the presence of the PEO solution. The PEO solution was then replaced with PEO/SDS solutions in the range of 3mM–40mM SDS concentrations keeping the concentration of PEO constant and the surface was imaged. Force measurements were performed with a colloidal probe technique as described previously in Section 2.2. The PEO and PEO/SDS solutions were put into the liquid cell in the same order as described above.

5.3. Analysis of Raw Data

The analysis of force curves has been described previously in Section 2.3.1.

5.4. Results and Discussion

5.4.1. AFM Images

The silica-water interface in the absence of any SDS or PEO is smooth with an rms roughness of $\sim 1\text{nm}$ over 1μ . SDS is not expected to adsorb on silica, however for a control experiment, the silica surface was also imaged in SDS solutions. The image is not different from the one in pure water, therefore it is not shown here. In the PEO/SDS experiments, there were no features on the surface neither after the adsorption of PEO nor after the injection of mixtures of PEO/SDS solutions. This result suggests that either the AFM is not an appropriate technique to resolve the PEO/SDS complex on the surface or that the complex is not present on the surface. That my imaging technique does have the ability to resolve features on surfaces is demonstrated through the imaging of surface micelles of CTACl on the same quartz surface.

5.4.2. Force Measurements

Forces measured between two silica surfaces immersed in water and PEO solutions are shown in Figure 5.1a. There is apparently no significant change in the force profile in the presence of PEO. This is expected due to the presence of a large electrostatic force. The PEO is a neutral polymer and is not expected to cause a large change in the surface charge characteristics of silica. Silica has a point of zero charge at around pH 2 and therefore is negatively charged at neutral pH.⁶ Therefore, I have also done measurements at low pH conditions (pH \sim 2) close to the point of zero charge of silica. The forces are shown in Figure 5.1b. This time the forces become attractive on the injection of PEO solution at pH \sim 2, showing the bridging of PEO chains when the two surfaces come together. This result suggests that PEO does adsorb on silica. Although I could have continued the experiments at low pH solutions, this was not preferred as the

⁶ Rinsing of the cell with NaOH prior to force curve measurements may cause the creation of more negative charges on the silica surface.

contradictory literature conclusions were drawn from experiments carried out at neutral pH.

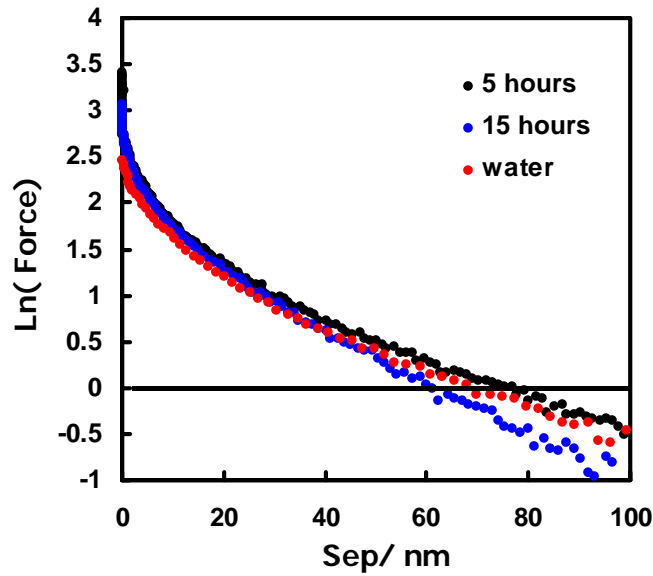


Figure 5.1a Forces between silica surfaces in water and in the presence of ~ 200 ppm PEO solutions.

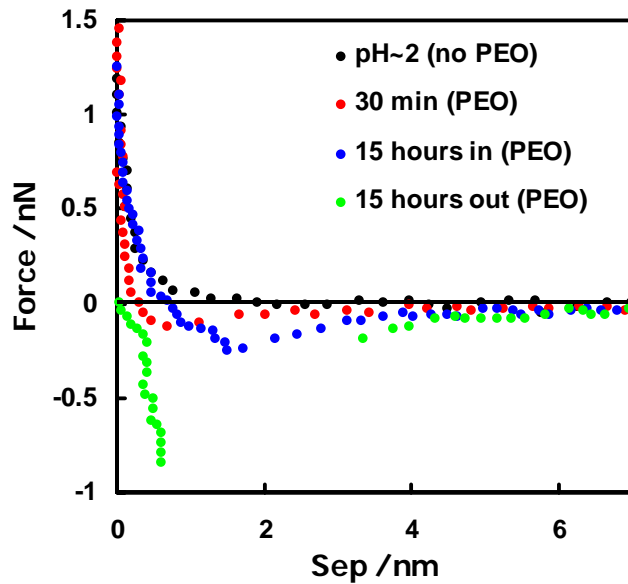


Figure 5.1b Forces between a silicon nitride tip and a quartz surface in pH ~ 2 and PEO solutions at pH ~ 2 . The adhesion in the out curve suggests the bridging of PEO between two surfaces.

The introduction of PEO/SDS solutions to the PEO-preadsorbed silica, does not change the repulsive behavior of the force curves. However, the presence of SDS introduces free ions to the solution, thereby decreasing the decay lengths of the force curves (Figure 5.2). At high SDS concentration, i.e. 40 mM, an oscillatory type force is observed (See Figure 5.3). The attractive part may be as a result of the depletion of the PEO/SDS complex in solution from the gap between adsorbed layers on two silica surfaces. We can speculate that this may happen because the complex in solution and the adsorbed complex layer are both negatively charged.

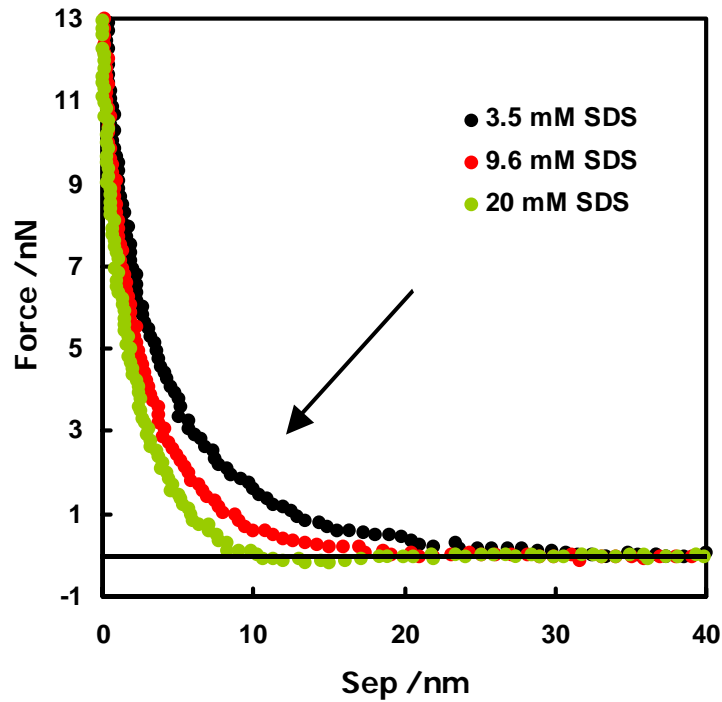


Figure 5.2 Forces between silica surfaces in ~200 ppm PEO as a function of SDS concentration.

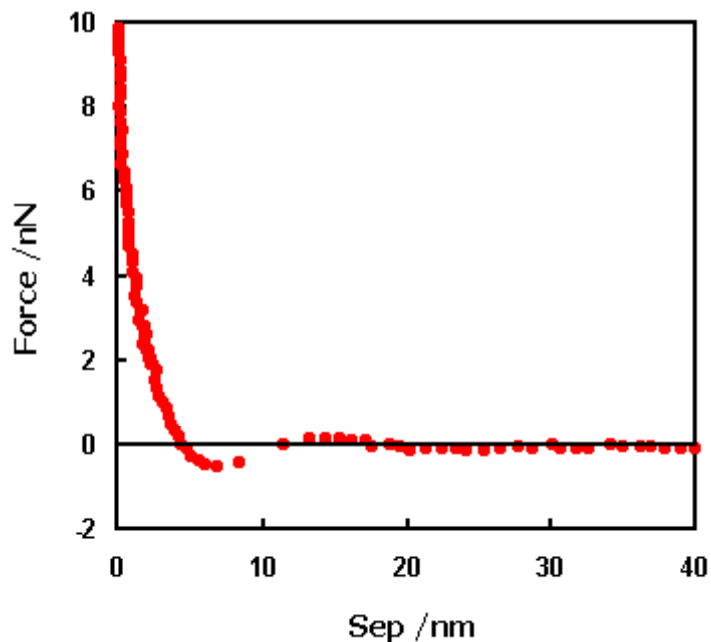


Figure 5.3 Force between silica surfaces in the presence of ~200 ppm PEO and 40 mM SDS solutions. The repulsion below ~ 5nm is probably due to the confinement of PEO or PEO/SDS complex between the two surfaces.

Table 5.1 gives the measured decay lengths of the repulsive forces in PEO/SDS solutions and the measured decay lengths of the forces in SDS solutions from Chapter 2. The presence of PEO has only a small effect on the decay length at 9.6 mM SDS and no effect at 3.5 and 20 mM SDS.

Table 5.1 Comparison of decay lengths in the presence of ~200 ppm PEO as a function of SDS concentration with measured decay lengths in SDS only solutions.

| [SDS] (mM) | Decay Length (nm) | Debye Length (nm) |
|---------------|----------------------|----------------------|
| 3.5 | 6.13 ± 0.05 | 5.9 ± 0.2 |
| 9.6 | 4.5 ± 0.5 | 3.7 ± 0.1 |
| 20 | 3.5 ± 0.5 | 3.57 ± 0.02 |

5.5. Conclusions

Experiments with AFM showed no proof of the adsorption of a PEO/SDS complex on the silica-water interface. This may be due to the inability of the AFM to resolve the features on the surface especially if the PEO has loops and tails that are covered with SDS micelles. Probably, while imaging, the tip distorts these feature or they are so extended into the solution that it is not possible to image them with this technique. It would be better if the tip were kept at a specific distance than at a specific force. In the future, this may be achieved through the use of TIRM-AFM technique. Force measurements also do not show many interesting features. The force shows an exponential repulsion. The main evidence for adsorption at pH=6 comes from depletion forces at high surfactant concentrations.

CHAPTER 6: SURFACTANT ADSORPTION ON HYDROPHOBIC SURFACES: EFFECT OF SURFACE CRYSTALLINITY

6.1. Introduction

Surfactants have a broad range of applications from the detergent and pesticide industry to biochemical research. Most of these applications rely on the surfactants to adsorb on hydrophobic surfaces. For example, surfactants used in weed killers adsorb onto the hydrophobic leaves of the plant to make them wettable by water and therefore increase the area exposed to the pesticide in solution. In protein research, protein-surfactant interactions play an important role and these interactions are mainly governed by the adsorption of surfactants onto the hydrophobic moieties on the protein.

Earlier work aiming at understanding the interactions between surfactants and hydrophobic surfaces mainly focus on surfactant adsorption isotherms on natural hydrophobic surfaces, like graphite and carbon-black,^{1,2,3} and on model hydrophobic surfaces, like self-assembled monolayers (SAM) of alkanethiols on gold.^{4,5} However, these studies do not give information about the microstructure of the adsorbed surfactants. Surfactants are known to form aggregates on surfaces above a critical aggregation concentration, c_{ac} , similar to the critical micelle concentration in the bulk solution. With the aid of atomic force microscopy for imaging at the solid-liquid interface,^{6,7,8,9} these surface aggregates are readily observed. In this study, the aggregation behavior of a range of surfactants on hydrophobic surfaces is investigated with the use of an AFM.

¹ Parfitt, G. D.; Willis, E. *J. Phys. Chem.* **1964**, *68*, 1780–1786.

² Corkill, J. M.; Goodman, J. F.; Tate, J. R. *Trans. Faraday Soc.* **1966**, *62*, 979–986.

³ Findeneegg, G. H.; Pasucha, B.; Strunk, H. *Colloids Surf.* **1988**, *37*, 223–233.

⁴ Sigal, G. B.; Mrksich, M.; Whitesides, G. M. *Langmuir* **1997**, *13*, 2749–2755.

⁵ Sigal, G.B.; Mrksich, M.; Whitesides, G. M. *J. Am. Chem. Soc.* **1998**, *120*, 3464–3473.

⁶ Wanless, E. J.; Ducker, W. A. *J. Phys. Chem.* **1996**, *100*, 3207–3214.

⁷ Liu, J.-F. ; Ducker, W. A. *J. Phys. Chem. B* **1999**, *103*, 8558–8567.

⁸ Warr, G.G. *Current Opinion in Colloid & Interface Science* **2000**, *5*, 88–94.

⁹ Svitova, T.; Hill, R. M.; Radke, C. J. *Colloids Surf., A* **2001**, *183*, 607–620.

Wanless and Ducker⁶ have imaged SDS aggregates on graphite with AFM. They have observed hemicylinders of SDS lying parallel to the crystal axis of the graphite. Previously, Manne et al.¹⁰ have also observed hemicylinders of CTAB on graphite. A nonionic surfactant, C₁₂E₈, also forms hemicylinders on graphite^{11,12} but a flat sheet on hydrophobic silica.¹¹ Grant et al.¹³ have used self-assembled monolayers (SAM) of alkanethiol adsorbed on gold to study the structure of C₁₂E₈ surfactants on hydrophobic surfaces. They have not observed any features on these hydrophobic surfaces, meaning that C₁₂E₈ adsorbs as a flat sheet on this surface. From these experiments, it can be seen that the head-group of the surfactant and the structure of the solid surface (surface crystallinity) plays an important role in the morphology of adsorbed surfactants.

In this work, the effect of the head-group of the surfactant and the effect of the surface crystallinity are studied on the adsorbed morphology of surfactants. I am using surfactants with sulfate, trimethylammonium and ethoxy head groups. The control of surface crystallinity is achieved through the production of SAMs with different chain lengths. For C_nH_{2n+1} thiolate monolayers on gold, it is known that at room temperature for n>12, the alkyl chains are crystalline and for n<12, the chains are amorphous.¹⁴ I assume that the disorder in SAMs formed from short alkyl chains also makes the surface amorphous. My hypothesis is that crystalline surfaces may template a more ordered structure for surfactant aggregates than amorphous surfaces. Here, I report on adsorption to C₈ and C₁₆ SAMs.

Theoretical work by Johnson and Nagarajan¹⁵ shows that there should be a variety of surfactant aggregate morphologies on hydrophobic surfaces when they are adsorbed from solutions above the cac and below the cmc; hemispheres, hemicylinders, finite disks, and infinite lamella. The variety of surfactant aggregate morphologies arises because the chemical potential of the surfactant changes below the cmc of the surfactant. Therefore this range of chemical potentials may lead to various different equilibrium surface aggregate

¹⁰ Manne, S.; Gaub, H.E. *Science*, **1995**, *270*, 1480–1482.

¹¹ Grant, L.M.; Tiberg, F.; Ducker, W.A. *J. Phys. Chem. B*, **1998**, *102*, 4288–4294.

¹² Patrick, H.N.; Warr, G.G.; Manne, S.; Aksay, I.A. *Langmuir* 1997, *13*, 4349–4356.

¹³ Grant, L.M.; Ederth, T.; Tiberg, F. *Langmuir*, **2000**, *16*, 2285–2291.

¹⁴ Porter, M. D.; Bright, T. B.; Allara, D. L.; Chidsey, C. E. D. *J. Am. Chem. Soc.* **1987**, *109*, 3559–3568.

¹⁵ Johnson, R. A.; Nagarajan, R. *Colloids Surf., A* **2000**, *167*, 21–36.

structures. Following this theoretical study, I have imaged alkanethiol SAM surfaces as a function of surfactant concentration up to the cmc.

6.2. Experimental Section

6.2.1. Materials and Solutions

SDS (Sigma, St. Louis, MO) was purified according to the procedure described in Section 2.2.1. C₁₆TAB(Sigma, St. Louis, MO) was purified by recrystallization from acetone/water. C₁₂E₈ (gift from Fredrich Tiberg) was used as received. Octanethiol (Sigma, St. Louis, MO) was used as received. Hexadecanethiol (Sigma, St. Louis, MO) was purified by vacuum distillation. Alkanethiol solutions were prepared with 200 proof ethanol. Surfactant solutions were prepared with nanopure water (EASYpure UV, Barnstead Thermolyne Corp., Dubuque, IA) The cantilevers were the same as those used for imaging in Section 3.2.

6.2.2. AFM Measurements

Imaging and force measurements were performed with an AFM (Molecular Imaging, Phoenix, AZ). The gold samples were prepared by sputtering a 60 nm gold layer on mica sheets (20 x 20 x 1 mm), then H₂ flame annealing and immediately immersing the annealed mica surface in the respective 1 mM alkanethiol solution. The substrates were left in solution for 18–30 hours and then rinsed with ethanol (sometimes left in ethanol overnight to remove the physisorbed layers), dried with N₂ and put into the liquid cell of the AFM. The cell was immersed in water initially, the SAM surface in the presence of water was imaged and a smooth region of ~200 x 200 nm was found to do the imaging measurements in surfactant solutions. The force between the silicon tip and the SAM surface was also measured. Surfactant solutions were then injected with increasing concentration; 0.2 x cmc, 0.5 x cmc, cmc and sometimes 0.75 x cmc and 2 x cmc. Images were taken and force measurements were done.

6.3. Results and Discussion

Images of gold surfaces with C₈ and C₁₆ SAM in water are featureless on a 200 x 200 nm scale. The presence of C₁₆TAB, SDS and C₁₂E₈ solutions does not change the

surface morphology for either the C_{16} or the C_8 SAM. This shows either that the surfactants adsorb as a flat sheet or that AFM is not able to resolve well structures like finite disks or hemispheres (hemicylinders have been successfully imaged in previous studies).^{6,10} If the structure of the surfactant aggregates are in the form of a sheet or a disk, this is probably because of the high interaction energy between the hydrophobic surface and water.

Previously, Manne et al.¹⁶ and Ducker et al.¹¹ have determined the shapes of surfactant aggregates on hydrophobized silica. These hydrophobic surfaces are amorphous, so their results are comparable to my results with C_8 SAM surfaces. My results differ from those of Manne et al., who have reported hemispheres for the adsorption structures of cationic, anionic, zwitterionic and nonionic 12-carbon chain surfactants on hydrophobized silica surfaces. However, Ducker et al. have reported flat layers of $C_{12}E_8$ surfactants, which is similar to my observations.

Forces measured between the silicon tip and the C_8 SAM and C_{16} SAM surfaces are all attractive in water. Figure 6.1 shows the force curves in the C_{16} TAB solutions. All surfactants have similar trends in force profiles as a function of surfactant concentration, therefore forces in the presence of SDS and $C_{12}E_8$ solutions are not shown here.

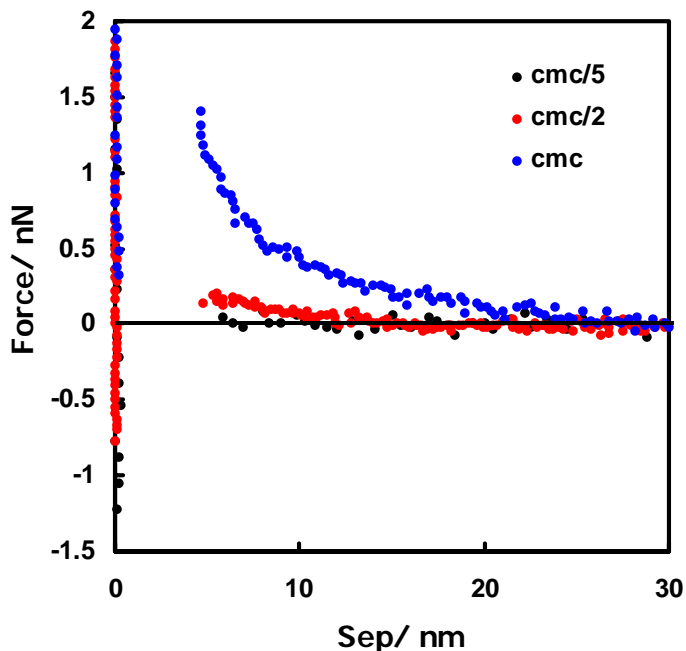


Figure 6.1 Forces between a silicon tip and a C_8 SAM surface in the presence of CTAB as a function of concentration.

¹⁶ Wolgemuth, J.L.; Workman, R.K.; Manne, S. *Langmuir*, **2000**, *16*, 3077–3081.

The force gets more repulsive as the concentration of the surfactant is increased with respect to the cmc. In the case of $C_{16}TAB$ and SDS, this is probably because of the charging of the hydrophobic surface with surfactant adsorption, leading to a repulsive electrostatic force. $C_{16}TAB$ may also adsorb onto the negatively charged silicon tip. In the case of $C_{12}E_8$, which has a nonionic headgroup, the repulsion probably arises due to the electrostatic force between the negatively charged silicon tip and the neutral hydrophilic surface created by the adsorption of $C_{12}E_8$. Figure 6.2 shows the comparison of repulsive forces measured in CTAB, SDS and $C_{12}E_8$ solutions at the cmc. The separation, where the surfaces jump-in to each other, is higher for $C_{16}TAB$ than it is for SDS and $C_{12}E_8$, which have similar jump-in distances. This is expected as both SDS and $C_{12}E_8$ have 12-carbon chains, whereas the $C_{16}TAB$ has a 16-carbon chain. The magnitude of the repulsive force is higher for the charged surfactants, SDS and $C_{16}TAB$, than the uncharged surfactant, $C_{12}E_8$.

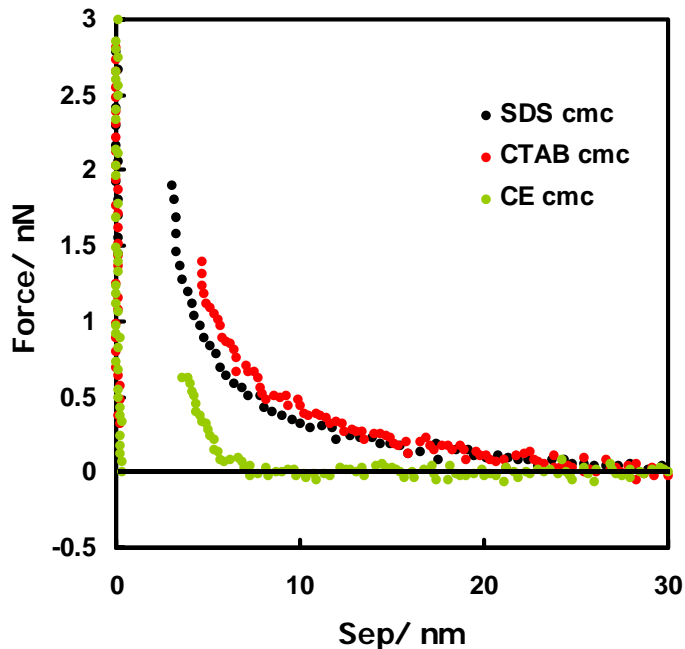


Figure 6.2 Comparison of forces between a silicon tip and a C_8 SAM surface in the presence of SDS, $C_{16}TAB$ and $C_{12}E_8$ at the cmc.

6.4. Conclusions

My studies show that neither the surface crystallinity nor the surfactant head group ($-\text{OSO}_3^-$, $-\text{N}^+(\text{CH}_3)_3$, $-(\text{OCH}_2\text{CH}_2)_8\text{OH}$) or the concentration has any effect on the surface aggregate structure on hydrophobic SAM surfaces; it seems to be a flat sheet. In the future, more studies can be done to further investigate this system: Gold balls (See Section 3.2.2) can be used as the substrate for SAM preparation for imaging experiments with Digital Instruments AFM, which has better resolution for imaging. Also, measurements can be performed with a more wide range of concentrations, especially in the range of 0.5 x cmc and cmc, where the force is repulsive, offering a good force profile for imaging aggregates on surfaces.

CHAPTER 7: SURFACE CONFINEMENT EFFECTS ON SURFACTANT ADSORPTION

7.1. Introduction

In recent years, there has been a major thrust to pattern surfaces on the nanometer scale. This thrust has two objectives: 1) to create higher density information storage and, 2) to discover and utilize properties of materials that are different when at least one length-scale is reduced to nanometer dimensions. Throughout this thesis, I have examined matter that has a nanometer length-scale normal to an interface. In this chapter, I try to investigate the effect of confining the size in the other two dimensions. Specifically, I examine adsorbed surfactant structure on surfaces that are patterned on a nanometer scale.

As described in Chapter 1, much is known about how the aggregation of surfactants is affected by the nature of the solid. Here, I create nanometer scale patterns of chemical heterogeneity on a surface, and examine whether the adsorbed structure is sensitive to the lateral dimensions of the pattern. (See Figure 7.1.) The heterogeneity is created by the nanografting technique.¹ A SAM surface is prepared by adsorption of an alkanethiol with an -OH functional group (the background) (OH-SAM). A -COOH functional group heterogeneity (COOH-SAM) is created on this surface by the nanografting technique. The adsorption of a positively charged surfactant, C₁₄TAB, is studied on these surfaces.

¹ Xu, S.; Liu, G. *Langmuir*, **1997**, *13*, 127–129.

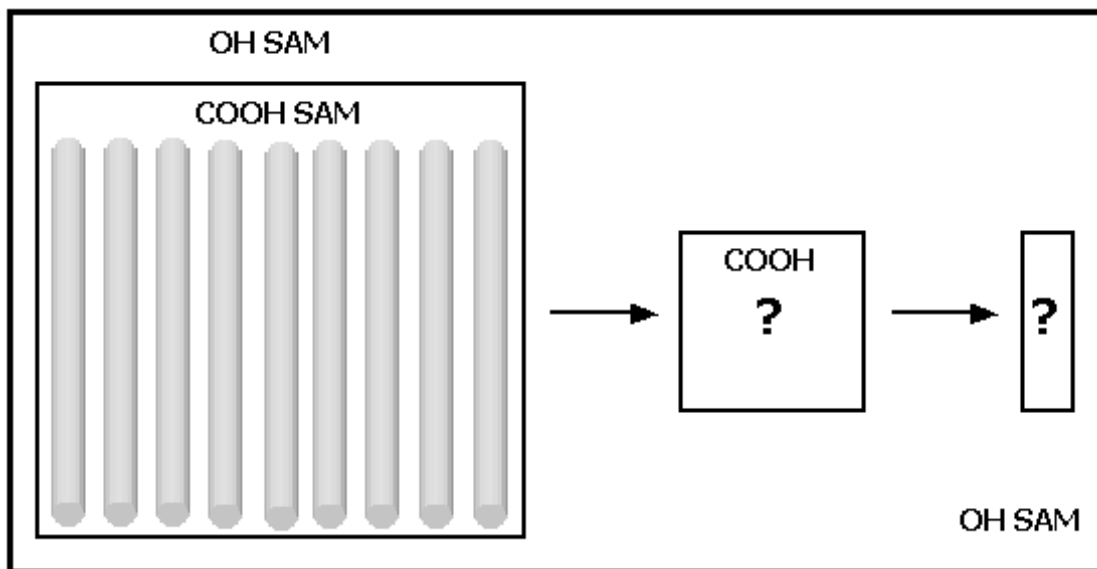


Figure 7.1 Is organization of surfactants a function of patch dimension?

7.2. Experimental Section

7.2.1. Materials and Solutions

C_{14} TAB (Sigma, St. Louis, MO) was purified by recrystallization from acetone. 1-mercapto-undecanol (Sigma-Aldrich, St. Louis, MO) and 1-mercapto-undecanoic acid (Sigma-Aldrich, St. Louis, MO) were used as received. 1-mercapto-undecanol solutions were prepared with 200 proof ethanol. 1-mercapto-undecanoic acid solutions were prepared with 10% acetic acid/ ethanol to reduce the physisorbed thiol molecules on SAM surfaces. Surfactant solutions were prepared with nanopure water (EASYpure UV, Barnstead Thermolyne Corp., Dubuque, IA). Ultrasharp silicon nitride cantilevers (Park Scientific Instruments) with a force constant of 0.5 N m^{-1} were used for both imaging and patterning.

7.2.2. AFM Measurements

Imaging measurements were performed with an AFM (Digital Instruments (Veeco), Santa Barbara, CA). The gold samples were prepared as explained in Section

3.3.2. The substrates were left in solution for 18-30 hours and then rinsed with ethanol, dried with N₂ and put into the liquid cell of the AFM. For C₁₄TAB adsorption experiments on OH-SAM and COOH-SAM, the cell was immersed in water initially, the SAM surface in the presence of water was imaged and a smooth region of ~200 x 200 nm was found to do the imaging measurements in surfactant solutions. C₁₄TAB solution of 14 mM was then injected and images were taken. In a separate experiment, the patterned surfaces were prepared with a lithographic method: The AFM cell was immersed in ethanol initially, the OH-SAM surface in ethanol was imaged and a smooth region of 3 x 3 μ was found to perform the lithography. The filling solution of 1-mercapto-undecanoic acid was then injected into the liquid cell and the region, where the heterogeneity would be introduced, was imaged at a high force. The cell was then rinsed with ethanol and imaged in ethanol to check the success of lithography. After the creation of patches on the surfaces, the cell was rinsed with water and imaged. Surfactant solution at 14 mM was then injected and images were taken.

7.3. Results and Discussion

7.3.1. C₁₄TAB Adsorption on COOH-SAM and OH-SAM

The water-COOH-SAM interface was found to be featureless, which showed that COOH-SAM was homogenous. After the injection of 14 mM C₁₄TAB, AFM images showed the formation of cylinders on COOH-SAM as it can be seen from Figure 7.2. The cylinders are not very long (30–50 nm) and seem to follow the steps of the gold underneath. Images in the presence of C₁₄TAB on OH-SAM are featureless and therefore not shown here.

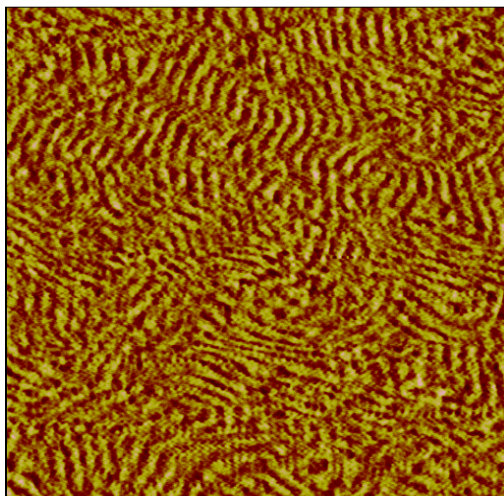


Figure 7.2a 185-nm AFM deflection image of the interface between COOH-SAM and 14 mM C₁₄TAB solution.

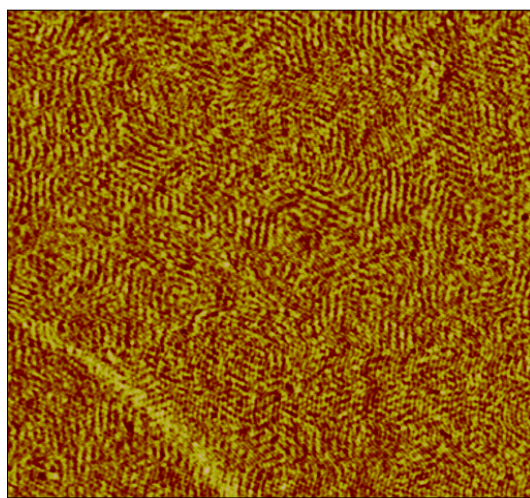


Figure 7.2b 385-nm AFM deflection image of the interface between COOH-SAM and 14 mM C₁₄TAB solution.

7.3.2. Lithography and C₁₄TAB Adsorption on the Heterogeneous SAM

A homogenous OH-SAM was prepared and COOH-SAM patterns with dimensions of 200 nm x 200 nm and 20 nm x 200 nm were made on the film. Figure 7.3 shows patches of COOH-SAM in a background of OH-SAM in ethanol. The light regions represent the presence of a repulsive force between the negatively charged tip and the negatively charged COOH-SAM.

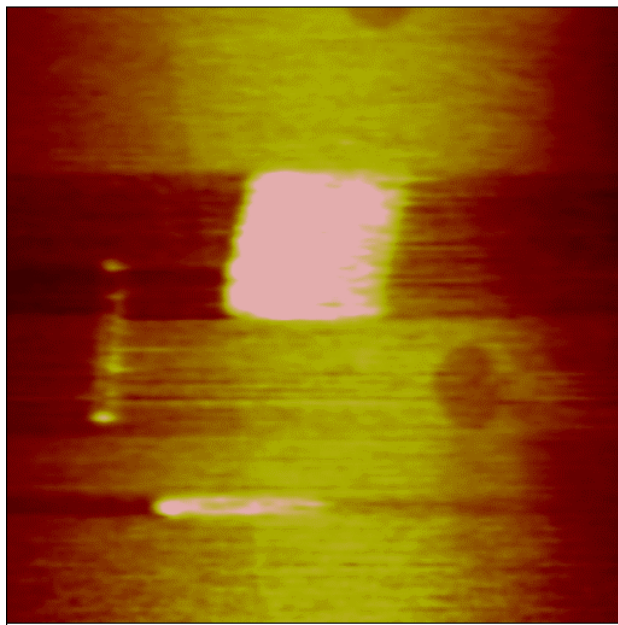


Figure 7.3 890-nm AFM height image of the patterned surface in ethanol.

The patches of COOH-SAM were imaged in water and then in 14 mM C₁₄TAB solutions, but no cylinders were observed in the presence of the surfactant solution. This was not expected. Recall that the C₁₄TAB forms short cylinders on a homogenous COOH-SAM surface. The lack of cylinders in the imaged patch of COOH-SAM could be due to one of two possibilities: a) The COOH-SAM created by lithography is different from the COOH-SAM created by lithography and therefore produces a different adsorbed surfactant structure or b) the AFM tip does not have the same resolution after performing the lithography.

To examine (b) I performed a control experiment in which I patterned a COOH-SAM within a COOH-SAM. I have prepared a homogenous COOH-SAM and nanografted patches of COOH-SAM on this surface. The patterned surface was not significantly different from the one in Figure 7.3; that is the nanografted region is different from the surrounding region, even when it contains the same thiolate molecule. This shows that the structure of the COOH-SAM changes when it is prepared by this lithographic technique. I have also tried to image this surface in the presence of 14 mM C₁₄TAB solution. No cylinders were observed on the background COOH-SAM, which suggests that the tip has also actually become dull after lithography.

7.4. Conclusions

The C₁₄TAB forms cylinders on a homogenous COOH-SAM surface. COOH-SAM patterned surfaces are created with a lithographic method on OH-SAMs. After lithography, no cylinders are observed on the COOH-SAM. AFM imaging shows that the COOH patches are different from COOH-SAM surfaces produced through solution adsorption. The AFM tip is also probably more blunt after making the COOH patches. In order to continue to study the effect of lateral dimensions of surface-heterogeneity on surfactant adsorption, a new method for producing nanopatterns on surfaces needs to be found.

VITA

Ayşen Tulpar was born on November 9, 1976 in Istanbul, Turkey. She finished Kadiköy Anatolian High School, Istanbul, Turkey in 1994 and received her Bachelor of Science degree in Chemistry from Koç University, Istanbul, Turkey in 1998. She started her graduate studies at Virginia Polytechnic Institute and State University Chemistry Department under the direction of Professor William Ducker in the Fall of 1998. As a graduate teaching assistant, she taught junior and senior physical chemistry laboratories for three years, general chemistry laboratories three semesters. She received the graduate teaching award in Spring 2001, and the graduate service award in 2002.